UCAM
UNIVERSIDAD CATÓLICA DE MURCIA

ESCUELA INTERNACIONAL DE DOCTORADO
Programa de Doctorado en Ciencias de la Salud

Potencial aplicación de la biocerámica de silicofosfato cálcico "Fase A de Nurse" en Ingeniería de Tejido Óseo. Estudios *in vitro* e *in vivo*.

Autor:
Rubén Rabadán Ros

Directores:
Dr. D. Luis Meseguer Olmo
Dra. Dña. Piedad N. de Aza Moya
Dr. D. Salvador D. Aznar Cervantes

Murcia, Enero de 2018

UCAM
UNIVERSIDAD CATÓLICA DE MURCIA

ESCUELA INTERNACIONAL DE DOCTORADO
Programa de Doctorado en Ciencias de la Salud

Potencial aplicación de la biocerámica de silicofosfato cálcico "Fase A de Nurse" en Ingeniería de Tejido Óseo. Estudios *in vitro* e *in vivo*.

Autor:
Rubén Rabadán Ros

Directores:
Dr. D. Luis Meseguer Olmo
Dra. Dña. Piedad N. de Aza Moya
Dr. D. Salvador D. Aznar Cervantes

Murcia, Enero de 2018

UCAM
UNIVERSIDAD CATÓLICA
DE MURCIA

AUTORIZACIÓN DE LO/S DIRECTOR/ES DE LA TESIS

PARA SU PRESENTACIÓN

El Dr. D. Luis Ramón Meseguer Olmo, la Dra. Dña. Piedad N. de Aza Moya y el Dr. D. Salvador Aznar Cervantes como Directores[1] de la Tesis Doctoral titulada "Potencial aplicación de la biocerámica de silicofosfato cálcico "Fase A de Nurse" en Íngeniería de Tejido Óseo. Estudios *in vitro* e *in vivo*" realizada por D. Rubén Rabadán Ros en el Departamento de Ciencias de la Salud, **autoriza su presentación a trámite** dado que reúne las condiciones necesarias para su defensa.

LO QUE FIRMO, PARA DAR CUMPLIMIENTO A LOS REALES DECRETOS 99/2011, 1393/2007, 56/2005 Y 778/98, EN MURCIA A 8 DE ENERO DE 2018.

[1] Si la Tesis está dirigida por más de un Director tienen que constar y firmar ambos.

UCAM EIDUCAM Escuela Internacional de Doctorado

Organización de la Tesis

La Tesis Doctoral que se presenta adopta el formato de compendio de trabajos previamente publicados. En ella se realiza una síntesis de conceptos y ensayos *in vitro* e *in vivo* que sustentan los trabajos publicados. Este tipo presentación es acorde con la normativa vigente de la Escuela Internacional de Doctorado de la Universidad Católica San Antonio de Murcia. A continuación, se citan las referencias completas de dichos artículos:

ARTÍCULO 1

Rabadan-Ros, R., Mazón, P., Serena, S., Sainz, M. A., Meseguer-Olmo, L., & De Aza, P. N. **In vitro behaviour of Nurse's A ss-phase: A new calcium silicophosphate ceramic.** *Journal of the European Ceramic Society*, 2017, *37*(8), 2943-2952. DOI: 10.1016/j.jeurceramsoc.2017.03.014

Factor de impacto (JCR): 3.411; Categoría: Material Science, Ceramics; Clasificación: 1/26 (Q1); Fecha de publicación: 2017

ARTÍCULO 2

Rabadan-Ros, R., Aznar-Cervantes, S., Mazón, P., Ros-Tarraga, P., De Aza, P. N., & Meseguer-Olmo, L. **Nurse's A-phase material enhance adhesion, growth and differentiation of human bone marrow-derived stromal mesenchymal stem cells**. *Materials*, 2017, *10*(4), 347-361. DOI: 10.3390/ma10040347

Factor de impacto (JCR): 2.654; Categoría: Material Science, Multidisciplinary; Clasificación: 82/275 (Q2); Fecha de publicación: 2017

ARTÍCULO 3

Rabadan-Ros, R., Revilla-Nuin, B., Mazón, P., Aznar-Cervantes, S., Ros-Tarraga, P., De Aza, P. N., & Meseguer-Olmo, L. **Impact of a porous Si-Ca-P monophasic ceramic on variation of osteogenesis-related gene expression of adult human mesenchymal stem cells**. *Applied Sciences*, 2018, 8 (1), 46-58. DOI: 10.3390/app8010046

Factor de impacto (JCR): 1.679 (2016); Categoría: Physics, Applied; Clasificación: 75/147 (Q3) (2016); Fecha de publicación: 2018

ARTÍCULO 4

Rabadan-Ros, R., Velásquez, P. A., Meseguer-Olmo, L., & De Aza, P. N. **Morphological and structural study of a novel porous nurse's A ceramic with osteoconductive properties for tissue engineering.** *Materials*, 2016, *9*(6), 474-487. DOI: 10.3390/ma9060474

Factor de impacto (JCR): 2.654; Categoría: Material Science, Multidisciplinary; Clasificación: 82/275 (Q2); Fecha de publicación: 2016

AGRADECIMIENTOS

A través de estas líneas quisiera expresar mi más sincero agradecimiento a todas aquellas personas que, en mayor o menor medida, me han ayudado a lo largo de estos 3 años y han formado parte de esta tesis de uno u otro modo.

Puede que no se percatara de ello pero, desde el primer instante, Luis Meseguer Olmo ha sabido, de un modo espontáneo, transmitirme toda la pasión, ilusión y amor que profesa a la medicina y a la ciencia. No sabría como agradecerle la oportunidad que me brindó al invitarme a formar parte de su grupo de investigación en la Universidad Católica San Antonio de Murcia, pasar a ser mi jefe y director de Tesis, y encauzarme de nuevo en este apasionante mundo de la investigación. Por sus incontables horas dedicadas en mi formación y en el desarrollo de este trabajo se ha convertido por méritos propios en una figura que recordaré el resto de mis días, y espero sea ejemplo para todas las personas que se han cruzado o se cruzarán en su camino como lo ha sido para mí.

Junto a Luis, mis codirectores, Piedad N. de Aza y. Salvador David Aznar Cervantes, han permitido que esta Tesis sea una realidad. Piedad, siempre amable y disponible, paciente y dispuesta, tratando de conectar dos mundos tan dispares y, al mismo tiempo, tan íntimamente ligados como la Ingeniería de Biomateriales y la Biología. Salva, codirector además de amigo, ha sido una fuente constante de inspiración, ejemplo de trabajo, humildad y sacrificio, todo ello adornado con una personalidad dinámica y carismática con la capacidad de motivar y suscitar la admiración de todo aquel que le conoce. Estoy seguro que todos sus esfuerzos por elevar a los más altos estándares de calidad las investigaciones sericícolas en Murcia serán fuertemente recompensados en el futuro.

El destino ha puesto a numerosas personas en mi camino, pero si me preguntasen quién ha sido mi compañera de fatigas durante estos años sin duda se llamaría Patricia Ros Tárraga. Hemos conseguido, con la ayuda de José Antonio Acosta, superar nuestros miedos, mareos y desvanecimientos en el quirófano. Muchas horas entre pipetas y frascos de cultivo nos han permitido crecer, no solo como científicos, también como personas.

¿Pero quién me iba a decir que de una compañera de catas en la Universidad de Murcia obtendría una amistad? La fortuna hizo que Ana Pagán regresase de nuevo a mi vida. Gracias a ella conocí a Luis y ha sido un ejemplo y una guía permanente a fin de ser más meticuloso, limpio y organizado en el laboratorio. Pero, sobre todo, ha hecho que mi estancia en IMIDA sea siempre divertida. Reconocer del mismo modo la ayuda que me han brindado el resto de integrantes de IMIDA, a José Luis Cenis Anadón por abrirnos las puertas del centro y acogernos junto a su grupo de investigación, a Abel Lozano Pérez por su ayuda desinteresada en el aprendizaje y manejo de nuevas técnicas, y a Daniel Cervantes por su colaboración en las tareas cotidianas del laboratorio.

No podría olvidar a todas aquellas personas que han contribuido con su conocimiento y experiencia en la consecución de los resultados de muchos de los experimentos aquí expuestos. Patricia Mazón, experta en Ciencia de los Materiales de la UMH; María Josefa Yánez Gascón, jefa del servicio de microscopía de la UCAM; Antonia Bernabeu Esclapez, jefa de sección de cultivo de tejidos en el SACE; Beatriz Revilla Nuin, experta en Biología Molecular del Hospital Virgen de la Arrixaca; y Carlos Martínez, experto en Histopatología

Animal del Hospital Virgen de la Arrixaca. A todos ellos, gracias. Del mismo modo, mencionar a todos los integrantes del Vicerrectorado de Investigación de la UCAM, encabezado por María Estrella Núñez Delicado, y, especialmente por su paciencia y servicialidad, a Mª Carmen Hernández Iniesta y María Elena Martínez Molina.

Sin duda, todos los valores que nos inculca nuestra familia son los que nos forman como personas. De una buena familia siempre saldrán personas buenas, pero, por encima de todo, gracias a mi familia soy una persona feliz. Gracias a mis hermanos, Miguel y Antonio, a mis abuelos, y, sobre todo, gracias a mamá y papá por todos sus esfuerzos, que sé que han sido muchos, para conseguir que todos sus hijos tuviésemos la oportunidad de recibir una buena educación y alcanzar nuestros sueños.

Por último, quisiera agradecer, de un modo muy especial, el amor y el apoyo incondicional que me ha mostrado Belén durante todos los años que caminamos juntos.

"Por muy larga que sea la tormenta,

el sol vuelve a brillar entre las nubes"

Khalil Gibrán (1883-1931)

ÍNDICE GENERAL

Siglas y abreviaturas

Las abreviaturas se han reseñado por orden alfabético

*ah*MSCs	Células madre humanas adultas de la médula ósea
ALP	Fosfatasa alcalina
AL_2O_3	Alúmina
AR-s	*Alizarin Red Solution*
BSP	Sialoproteína ósea
Ca	Calcio
$CaCO_3$	Carbonato cálcico
$CaHPO_4$	Fosfato dicálcico
CaP	Fosfato cálcico, $Ca(PO_4)_2$
CD	Marcador de superficie / Antígeno de membrana
CHA	Carbohidroxiapaita, $Ca_5(PO_4)_3(COH)$
Cl	Cloro
Col I	Colágeno tipo I
Col V	Colágeno tipo V
CO_3^{2-}	Carbonatos
CS	Silicato cálcico, $CaSiO_4$
C_2S	Silicato dicálcico, Ca_2SiO_4
DAS	Difracción de Electrones en el Área Seleccionada
DMEM	Medio de Cultivo Eagle Modificado de Dulbecco
EDX	Microanálisis de Energía Dispersiva de Rayos X

F	Flúor
FESEM	Microscopía Electrónica de Barrido de Emisión de Campo
GM	Medio de crecimiento
HA	Hidroxiapatita, $Ca_5(PO_4)_3(OH)$
HADC	Hidroxiapatito deficiente en calcio
HE	Hematoxilina-eosina
HS	Heparán sulfato
ICP-MS	Espectrometría de Masas con Plasma Acoplado Inductivamente
MEB	Microscopía Electrónica de Barrido
MET	Microscopía Electrónica de Transmisión
MEx	Matriz extracelular
Mg	Magnesio
MFA	Microscopía de Fuerza Atómica
Na	Sodio
OM	Medio osteogénico
OPN	Osteopontina
OCN	Osteocalcina
ON	Osteonectina
P	Fósforo
PCR	Reacción en cadena de la polimerasa
PET	Polietileno
PGA	Ácido poliglicólico

PMMA	Polimetilmetacrilato
PLA	Ácido poliláctico
PO_4^{3-}	Fosfatos
qRT-PCR	Reacción en cadena de la polimerasa (PCR) cuantitativa-transcripción inversa
RUNX2	Factor de transcripción Runx-2: *Runt-related transcription factor 2*
SFA	Suero fisiológico artificial / Suero simulado humano
Si	Silicio
SiO_2	Óxido de silicio
TCP	Fosfato tricálcico, $Ca_3(PO_4)_2$
ZrO_2	Zirconio

1. PREFACIO

1. PREFACIO

En las últimas décadas se ha producido un incremento en la incidencia de problemas relacionados con la degeneración ósea y articular. El aumento de la expectativa de vida de la sociedad y el envejecimiento progresivo de la población está ligado al incremento de afecciones articulares degenerativas que requieren mayoritariamente de sustitución protésica y sus correspondientes recambios con el paso del tiempo. Además, factores externos, como los traumatismos de alta energía cinética como consecuencia de accidentes de tráfico, nos enfrentan a múltiples y complejas fracturas esqueléticas asociadas a perdida de tejido óseo. Se calcula que, en países desarrollados, el 50% de los enfermos crónicos con más de 50 años sufren problemas osteoarticulares, estimándose que esta cantidad se doblará para el año 2020 (1, 2).

Es por ello, que especialidades médico-quirúrgicas como la Traumatología y Cirugía Ortopédica en general y la Cirugía oncológica requieren de grandes técnicas de reconstrucción y del empleo de materiales para conseguir una óptima regeneración ósea (3). Por este motivo, uno de los retos más importantes en la actualidad en el campo de la biomedicina es obtener biomateriales capaces de promover activamente y de modo eficaz la regeneración o sustitución ósea, de forma que puedan restablecer su función. De este modo, los biomateriales allanan el camino hacia un envejecimiento saludable y aumentan la calidad de vida de la población.

El trasplante de hueso del propio individuo es el material de elección para el tratamiento de las soluciones de continuidad del hueso. El empleo del autoinjerto óseo esponjoso, conocido como "*gold standard*", es probadamente el mejor procedimiento para ello, sin embargo, presenta grandes inconvenientes como la limitada disponibilidad de tejido óseo y la potencial morbilidad para el paciente (4). Los aloinjertos óseos (injerto entre individuos de la misma especie) presentan mayor disponibilidad pero aumentan el riesgo de transmisión de enfermedades al receptor.

Teniendo presente las limitaciones descritas para los injertos óseos, varios grupos de investigadores han centrado sus esfuerzos durante estas dos últimas décadas en el desarrollo, formulación y síntesis de diversos tipos de biomateriales que pretenden mimetizar al hueso desde el punto de vista biológico al tiempo que proporcione un entramado estructural que le confiera suficientes propiedades mecánicas para ser capaces de suplir el uso de los injertos óseos. Las cerámicas de fosfatos de calcio se sitúan entre los biomateriales de mayor interés (5), con estructuras cristalinas o amorfas, que poseen bioactividad y osteoconductividad, entendidas como la capacidad de unirse íntimamente al tejido óseo vivo y de permitir o guiar su crecimiento de forma multidireccional después de su implantación.

En nuestro grupo, se ha investigado la preparación de materiales de fosfato cálcico con sustituciones iónicas para fomentar la formación de tejido óseo y acentuar la velocidad de reabsorción, siendo objeto de estudio en el presente

trabajo de tesis la ***Potencial aplicación de la biocerámica de silicofosfato cálcico "Fase A de Nurse" en Ingeniería de Tejido Óseo***.

2. INTRODUCCIÓN

2. INTRODUCCIÓN

2.1 Antecedentes

La reconstrucción de defectos óseos como consecuencia de traumatismos complejos, infecciones graves, malformaciones esqueléticas o resecciones tumorales continúa siendo un desafío en numerosas disciplinas quirúrgicas como Cirugía Ortopédica y Traumatológica, Cirugía Oral y Maxilo-facial, y Neurocirugía, entre otras (6).

Durante siglos se ha estudiado la posibilidad de realizar la sustitución del tejido óseo, remontándose los primeros conocimientos a la Edad de Bronce, cuando se realizaron rellenos de defectos en cráneos mediante autoinjertos (7). Sin embargo, ha sido durante el transcurso del último siglo cuando la reconstrucción de defectos óseos ha progresado de forma vertiginosa. Esto se ha debido al desarrollo de nuevas tecnologías, así como al avance continuo que ha experimentando el conocimiento científico, haciendo posible la extensión de la aplicabilidad de una amplia gama de materiales, tanto naturales como sintéticos, en muchos campos de la medicina moderna.

2.2 El tejido óseo

El tejido óseo es el principal componente del esqueleto. Sus funciones más importantes son servir de soporte estructural, alojar la médula ósea hematopoyética y proteger los órganos blandos vitales. Sin embargo, los huesos no solo son estructuras de soporte y protección, también actúan como depósito de

calcio, fosfato y otros iones, siendo un tejido dinámico que está en constante proceso de renovación o remodelación (8).

2.2.1. Características generales del tejido óseo

El hueso es un órgano constituido por tejido adiposo, tejido hematopoyético, vasos sanguíneos, nervios y tejido óseo. El tejido óseo es un tejido conjuntivo especializado formado por una matriz extracelular (MEx) altamente mineralizada con un análogo del mineral natural hidroxiapatita (HA) [Ca_{10} $(PO_4)_6(OH)_2$], que se encuentra presente como un cristal plano de 20-80 nm de largo y 2 a 5 nm de espesor y confiere al hueso su dureza característica (8). Las impurezas presentes tales como carbonatos (CO_3^{2-}), flúor (F^-) y cloro (Cl^-) pueden reemplazar los grupos fosfato (PO_4^{3-}) e hidroxilos (OH^-) ocasionando alteraciones en ciertas propiedades físicas del cristal como, por ejemplo, la solubilidad. Por otra parte, el hueso posee un revestimiento interno (endostio) y externo (periostio), constituido por tejido conjuntivo con células osteogénicas y una amplia red de vasos que lo nutren de forma centrífuga al mismo tiempo que suministran células para su crecimiento y regeneración (8, 9).

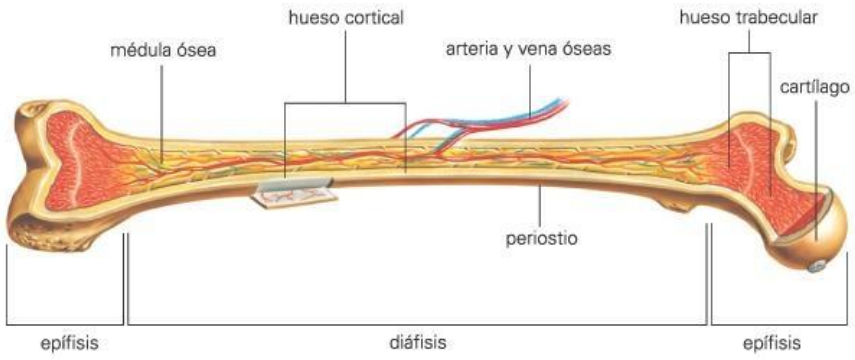

Figura 1. Estructura y divisiones del hueso (10).

2.2.2. Organización del tejido óseo

a. Fase inorgánica

La matriz ósea tiene una gran resistencia y estabilidad, y está formada por componentes inorgánicos y orgánicos. El componente inorgánico se constituye por una alta concentración de iones calcio (Ca^{2+}) y fósforo (P^{3-}) y, en menor medida, sodio (Na^{+}) y magnesio (Mg^{2+}), sirviendo de reservorio de iones en el organismo y proporcionando al tejido óseo la mayor parte de su rigidez y resistencia (11).

b. Fase orgánica

La fase orgánica de la MEx del hueso desempeña una amplia variedad de funciones, determinando su estructura y propiedades mecánicas del mismo. Está constituida por un 90 % de colágeno tipo I (Col I) y en menor medida colágeno tipo V (Col V). El 10% restante está formado por otros constituyentes proteicos no colágenicos minoritarios tal como glucosaminoglucanos (hialuronato, condroitinsulfato y queratansulfato), glicoproteínas (osteocalcina [OCN], osteonectina [ON] y osteopontina [OPN]), y diferentes tipos de sialoproteínas óseas. Estos componentes orgánicos del tejido son de gran relevancia ya que participan en la organización de la matriz, la mineralización del hueso y establecen un feed-back que regula el comportamiento de las células (8).

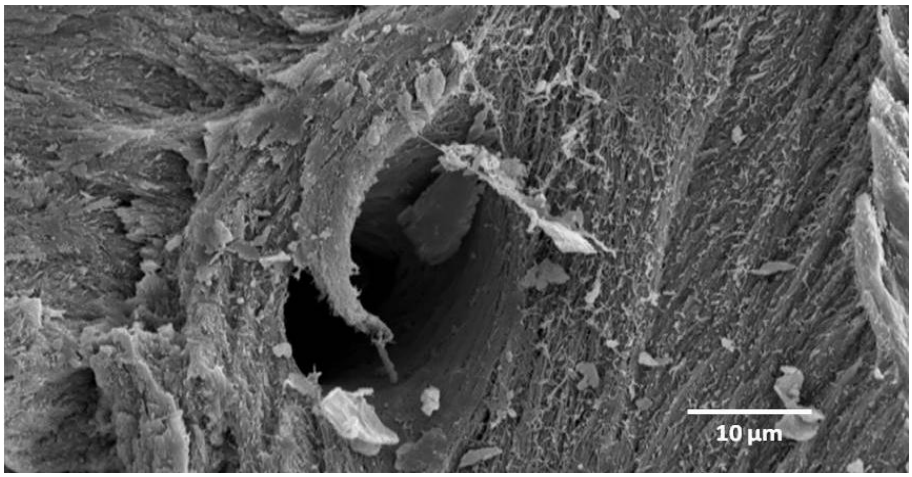

Figura 2. Microfotografía obtenida de un espécimen del estudio mediante microscopía electrónica de barrido (MEB). Detalle de una trabécula ósea en la que se observa la distribución espacial de las fibras de colágeno (Magnificación: barra 10 µm).

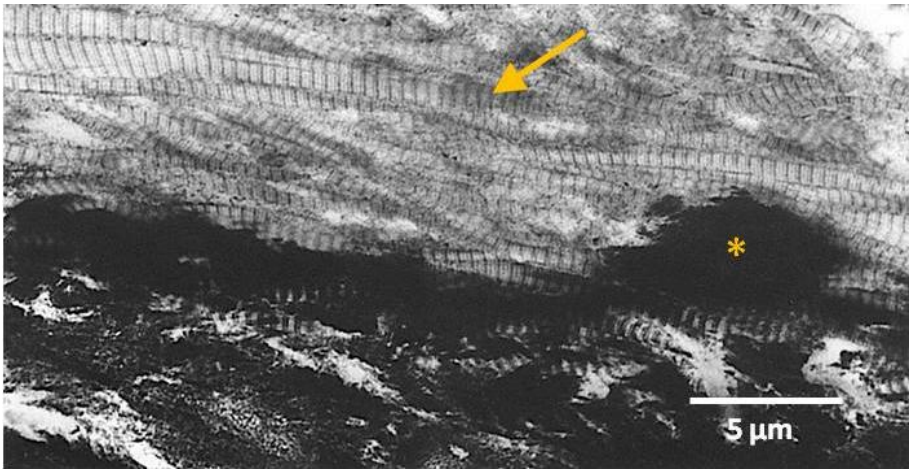

Figura 3. Microfotografía obtenida de un espécimen del estudio mediante microscopía electrónica de transmisión (MET). Presencia de fibras de Col I del hueso en el que se detalla el aspecto típico estriado de las mismas (Flecha) y material electronodenso correspondiente a un frente de mineralización originado por depósitos de cristales de HA (asterisco) (Magnificación: barra 5 µm).

2.2.3 Morfología celular ósea

Los principales tipos de células que podemos encontrar en el hueso son: osteocitos, osteoblastos y osteoclastos. Los **osteocitos** se localizan en las lagunas osteocíticas (osteoplastos), que están distribuidas concéntricamente alrededor de la luz central de la osteona y entre sus láminas. Éstos representan el 90% de las células óseas del esqueleto maduro y tienen como función principal ayudar a la regulación de la concentración de calcio en la sangre, así como la eventual secreción de una nueva matriz extracelular.

Los **osteoblastos** se encuentran en la superficie de los huesos en crecimiento y, cuando están activos, sintetizan osteoide, que es la porción orgánica sin mineralizar de la matriz ósea que se forma con anterioridad a la maduración del tejido óseo. Son los responsables de la síntesis y secreción de la fase orgánica no mineralizada de la matriz ósea, produciendo Col I y glucoproteínas (12). Los osteoblastos activos llegan a rodearse de matriz mineralizada y dar lugar a los osteocitos, ambas células poseen extensas prolongaciones citoplasmáticas que facilitan el contacto entre ellas y con osteocitos adyacentes a través de los canalículos.

Los **osteoclastos** son células multinucleadas encargadas de la resorción del hueso y se caracterizan por su gran tamaño (20-200 μm) y la presencia un gran número de mitocondrias y lisosomas en su citoplasma. Tienen su origen en células precursoras hematopoyéticas (estirpe macrofágica-monocítica) que dan lugar a los monocitos y macrófagos. Se encuentran en los lugares de reabsorción del hueso o lagunas de Howship (8, 9).

Por otro lado, las **células madre mesenquimales osteoprogenitoras** residen en el endostio, periostio y médula ósea. Éstas son células indiferenciadas multipotenciales con la capacidad de proliferar (autorenovarse) y de diferenciarse en otro tipo celular de fenotipo osteoblástico cuando son estimuladas y el microambiente en donde se encuentran es el óptimo.

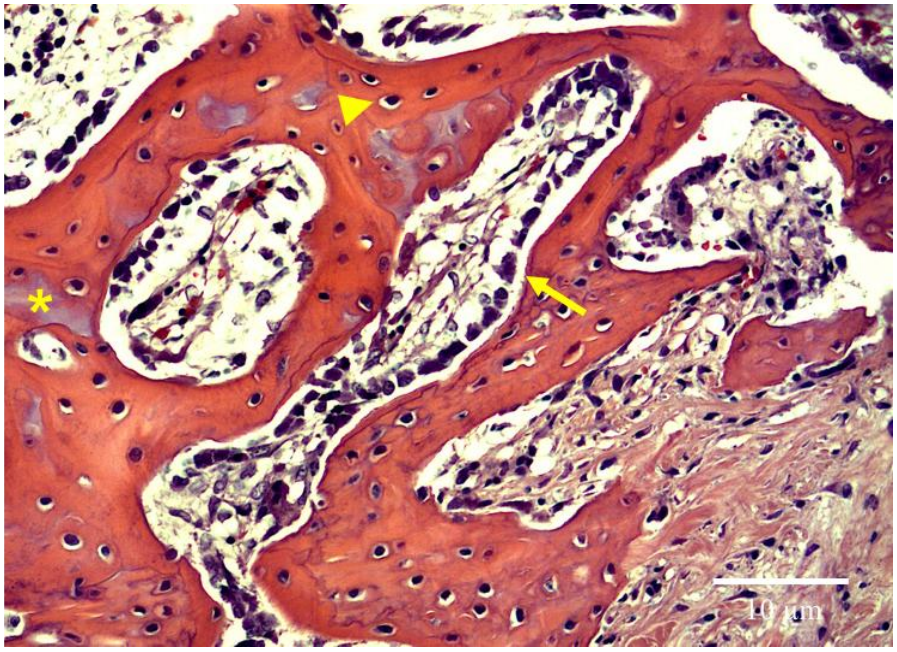

Figura 4. Microfotografía óptica representativa de un los espécimen del estudio en la que se observa: Ribete de osteoblastos (flecha) sobre la superficie de trabéculas óseas; múltiples osteocitos ocupando sus osteoplatos o lagunas osteocíticas (cabeza de flecha) y matriz ostoide en fase de mineralización (asterisco) (Hematoxilina-Eosina (H-E), Magnificación barra 10 µm).

2.2.4 Remodelación ósea

El hueso sufre un proceso de renovación constante en el que se alternan ciclos de destrucción del hueso (resorción ósea) y creación o reemplazo de ese

hueso destruido por hueso nuevo (formación ósea). A esto se le conoce como remodelación ósea. Es un proceso equilibrado; es decir, al final de cada ciclo permanece la misma cantidad de hueso que al inicio.

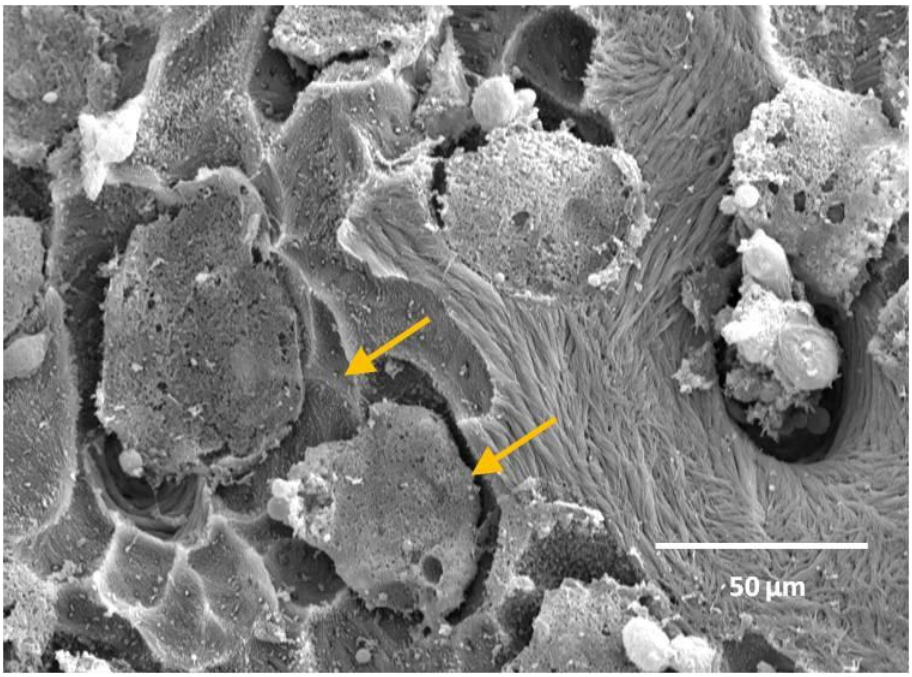

Figura 5. Microfotografia mediante MEB de un espécimen del estudio en la que se detallan con precisión la presencia de osteoclastos y lagunas de Howship (Flechas) (Magnificación: barra 50 µm).

La **remodelación ósea** se lleva a cabo mediante la acción sucesiva de los osteoclastos y los osteoblastos en un punto concreto de la superficie. Para destruir la matriz ósea, los osteoclastos se unen a la superficie del hueso, formando un espacio cerrado entre la célula y el hueso. A la vez, sus endosomas contienen bombas de protones de membrana que migran a la zona celular más cercana al hueso y se insertan en la membrana; esto provoca que disminuya el pH en el

espacio existente entre el osteoclasto y el hueso, solubilizando la fase mineral del mismo.

Para degradar la fase orgánica del hueso, los osteoclastos secretan hidrolasas ácidas y fagocitan fragmentos de matriz, que van degradándose en las vacuolas citoplasmáticas (13). De este modo, los osteoclastos excavan el hueso originando las lagunas de Howship (Figura 5).

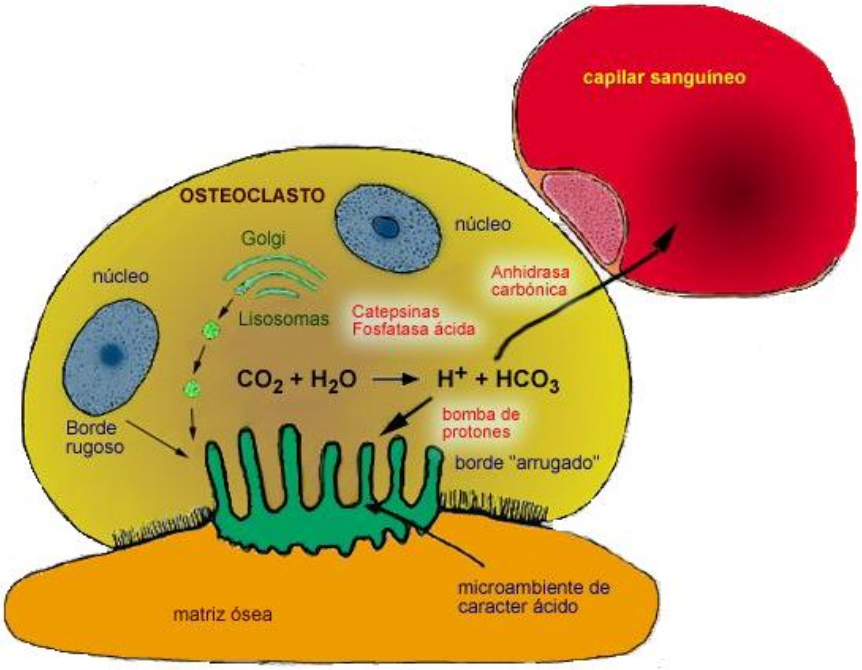

Figura 6. Esquema simplificado del proceso de resorción ósea realizado por el osteoclasto (14).

La aposición del hueso nuevo se lleva a cabo por capas sucesivas. Los osteoblastos, atraídos por las sustancias liberadas (TGF-β, entre otras) desde el hueso excavado previamente por los osteoclastos, rellenan la zona depositando

inicialmente una matriz orgánica desmineralizada u osteoide. La **mineralización** de esta matriz se produce tras un tiempo de maduración, denominado tiempo de desfase de la mineralización. Este período suele durar unos 10 días aproximadamente y se realiza por capas, siguiendo el mismo orden que la aposición ósea. La zona de transición entre el hueso mineralizado y el que no lo está constituye el "frente de mineralización". A medida que avanza la mineralización, la fase sólida de fosfato cálcico inicial (brushita) va a dar paso a una HA poco cristalizada con un cociente molar calcio/fósforo bastante bajo. Con el transcurso del tiempo y a medida que se completa la maduración ósea, aumenta la estructura cristalina y el cociente calcio/fósforo de la HA llega a alcanzar una Ca/P próxima a 1.6.

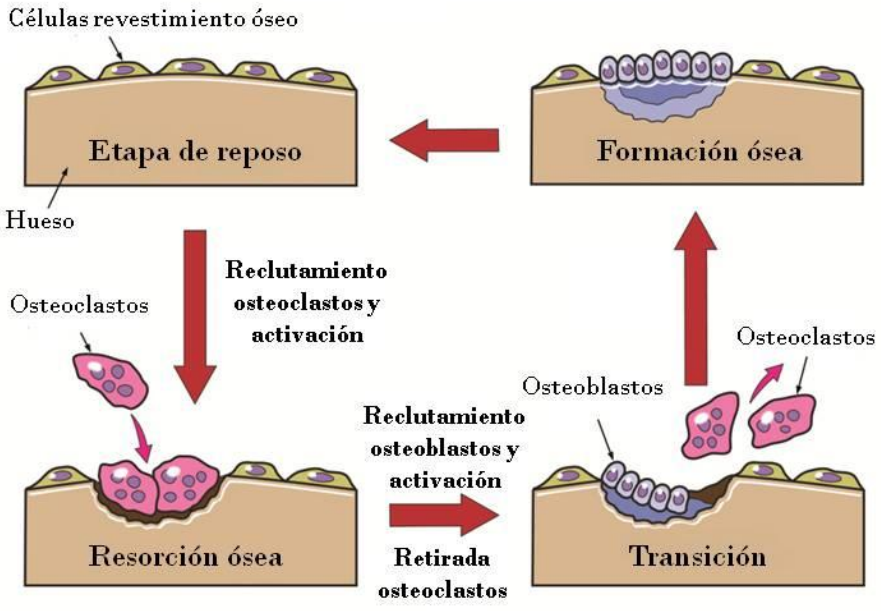

Figura 7. Imagen representativa del mecanismo de remodelación ósea llevada a cabo por osteoclastos y osteoblastos [Imagen adaptada de (15)].

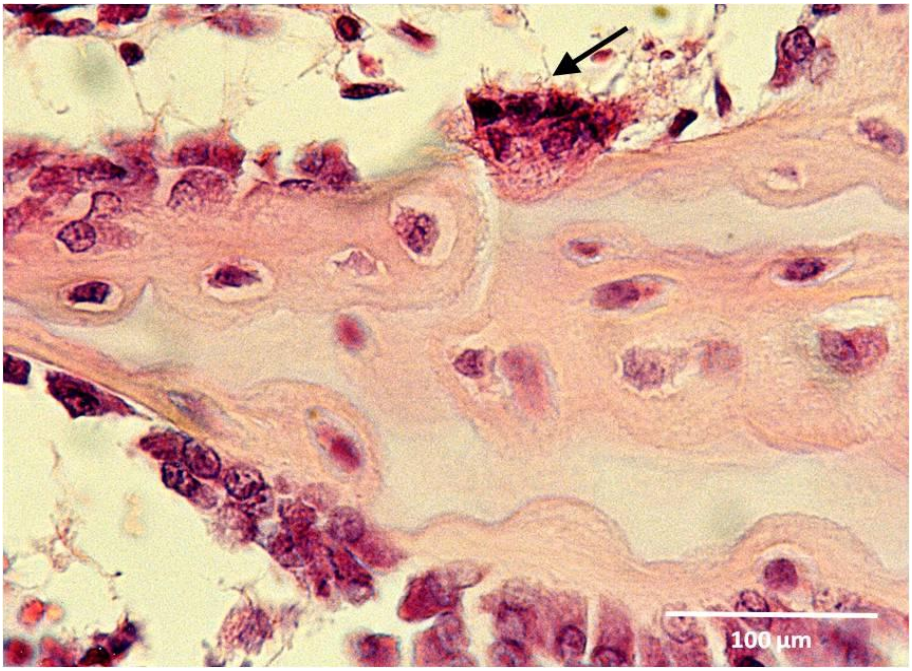

Figura 8. Imagen histológica de un espécimen del estudio correspondiente a una trabécula ósea con ribete de osteoblastos en la periferia y osteoclasto (flecha) (H-E, Magnificación: barra 100 µm).

2.2.5. Estructura histológica del hueso

Desde el punto de vista histológico se distinguen dos tipos de hueso: **Reticular** o inmaduro (Woben) y **laminar** o maduro. Este último, dependiendo de su densidad ósea, puede clasificarse en hueso compacto y hueso esponjoso.

El hueso compacto se caracteriza por presentar una porosidad muy baja en torno al 10%. Éste constituye aproximadamente el 80% del esqueleto adulto y contiene en su interior a la médula ósea hematopoyética. Se organiza en columnas óseas cilíndricas y paralelas al eje mayor del hueso constituidas por capas concéntricas dispuestas alrededor de un canal central (canal de Havers) que

contiene vasos sanguíneos, linfáticos y nervios, constituyendo así una osteona, unidad funcional del tejido óseo.

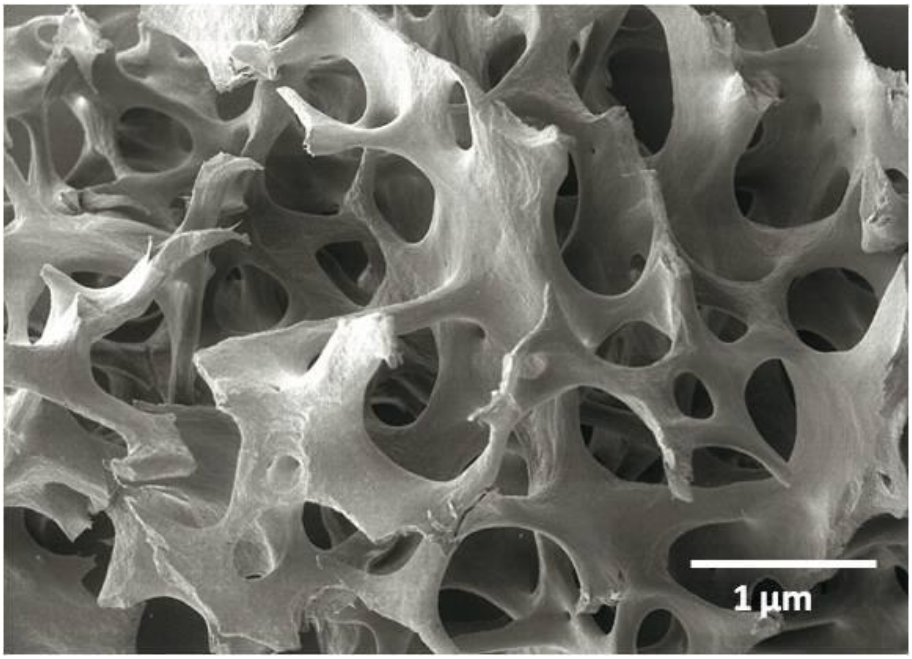

Figura 9. Microfotografía obtenida mediante MEB de tejido óseo esponjoso donde se pueden apreciar la disposición 3D de las trabéculas óseas delimitando los poros (Magnificación: barra 1mm) [Imagen cedida por Luis Meseguer Olmo].

El **hueso esponjoso** presenta una porosidad que oscila del 50 al 90%. Está compuesto por un entramado tridimensional de trabéculas óseas separadas por espacios laberínticos comunicados que alojan en su interior a la médula ósea hematopoyética. Las células en las trabéculas se disponen en su superficie, pudiendo estar influenciadas por las células de la médula ósea, a diferencia de lo que ocurre en el hueso compacto donde la mayoría de las células están completamente rodeadas de matriz ósea. Es por ello que el hueso esponjoso tiene

una tasa metabólica y de remodelación más elevada que el hueso compacto. Al ser la resistencia a la compresión proporcional a la densidad, ésta es diez veces mayor por unidad de volumen en el hueso compacto que en el esponjoso (16).

Por otro lado, es característico que la orientación de las fibras de colágeno varíe con el tipo de hueso. De este modo, en el hueso reticular, primario o inmaduro que forma el esqueleto del embrión las fibras de colágeno se disponen irregularmente. Tiene una tasa metabólica superior a la del hueso laminar, y más osteocitos. Además, debido al alto contenido celular y de agua, es más flexible y elástico. Salvo ciertas excepciones, como son los tendones, ligamentos y suturas craneales, el hueso inmaduro raramente está presente en el esqueleto humano a partir de los 5 años de edad. Sin embargo, también puede aparecer en respuesta a lesiones óseas (8). Por el contrario, el hueso secundario, laminar o maduro, presenta las fibras de colágeno organizadas en láminas que pueden permanecer paralelas las unas a las otras o disponerse en capas concéntricas en torno a los conductos por los que discurren los vasos sanguíneos, constituyendo los denominados sistemas de Havers. Estos sistemas están interconectados a lo largo de su trayecto mediante canales de menos diámetro, denominados canales de Volkmann.

2.3 Injertos óseos

Tradicionalmente y hasta el día de hoy, las lesiones óseas que conllevan una pérdida de sustancia ósea, se tratan mediante cirugía reconstructiva

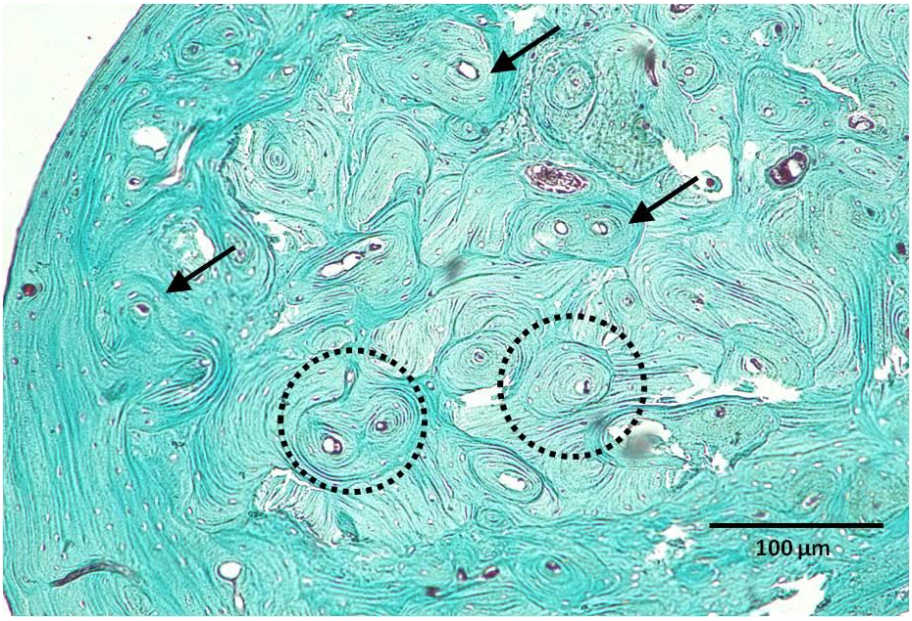

Figura 10. Microfotografía de un espécimen del estudio de tejido óseo compacto donde se pueden apreciar las osteonas (círculos) y los canales de Havers (flechas) (Tricromico de Masson, Magnificación: barra 100 µm).

implantando injertos óseos autólogos, alogénicos o xenogénicos (17). El injerto de hueso autólogo o **autoinjerto**, obtenido del propio paciente, es ampliamente reconocido como el más efectivo y ha sido elegido clásicamente por los cirujanos ortopédicos para el tratamiento de defectos óseos. Es considerado el "*gold standard*" (18, 19) debido a que cumple con los tres elementos fundamentales necesarios para que se lleve a cabo la regeneración ósea, también conocidos como la *triada de la regeneración ósea*: [1] Presenta una estructura porosa abierta con una disposición tridimensional que permite su colonización por tejido óseo neoformado (**osteoconducción**), [2] posee proteínas no colágenas presentes en la matriz ósea extracelular que actúan de forma autocrina y paracrina como factores

inductores, estimulando la migración y proliferación de células madre adultas osteoprogenitoras de médula ósea (*ah*MSCs), así como su diferenciación a osteoblastos (**osteoinducción**) y [3] aporta numerosas células madre mesenquimales precursoras de osteoblastos y osteoblastos maduros (**osteogenicidad**).

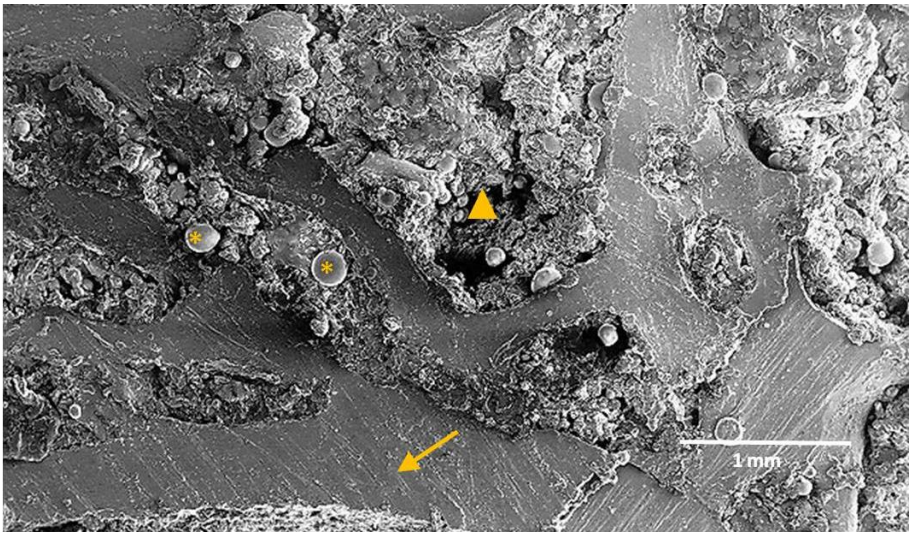

Figura 11. Microfotografía obtenida mediante MEB de una sección ósea (injerto óseo) en el que se observa tejido óseo compacto (flecha), médula ósea (punta de fecha) y *ah*MSCs (asteriscos) (Magnificación: barra 1 mm) [Imagen cedida por Luis Meseguer Olmo].

A pesar de ello, el uso de injertos óseos autólogos conlleva desventajas relacionadas con la morbilidad de la zona dadora, tales como dolor postoperatorio, sangrado, riesgo de infección, cantidad limitada de tejido óseo y necesidad de sacrificar estructuras normales, motivos por los que se continúa restringiendo su aplicación (20).

Las ventajas de los **aloinjertos** (donante de la misma especie que el receptor) y xenoinjertos (donante de distinta especie que el receptor) sobre los autoinjertos están en relación a su fácil disponibilidad, ausencia de morbilidad de la zona dadora, menor tiempo quirúrgico, menor sangrado y la capacidad de reconstrucción de grandes pérdidas óseas. Por contra, su capacidad osteoconductora y osteoinductora es menor respecto al autoinjerto (4). A ello se suma una posible respuesta inmune y rechazo del implante además de su relación con la posibilidad real de transmisión de enfermedades como VIH o hepatitis B. En el caso de los aloinjertos, el empleo de la liofilización como método de conservación disminuye las propiedades mecánicas del injerto óseo, al contrario que la congelación.

Tabla 1. Características de los autoinjertos y los aloinjertos (21).

INJERTO ÓSEO	Resistencia estructural	Osteoconducción	Osteoinducción	Osteogénesis
AUTOINJERTO				
Esponjoso	No	+++	+++	+++
Cortical	+++	++	++	++
ALOINJERTO				
Esponjoso				
Congelado	No	++	+	No
Liofilizado	No	++	+	No
Cortical				
Congelado	+++	+	No	No
Liofilizado	+	+	No	No

2.4 Ingeniería de Tejidos

2.4.1 Evolución de los biomateriales utilizados en regeneración ósea

En las últimas décadas, se han desarrollado diferentes métodos y materiales biocompatibles como alternativa al uso de los injertos óseos. Estos materiales, de origen natural o sintético, resultan en muchas ocasiones una opción útil para la reparación de defectos óseos dependiendo de su extensión, localización y edad del paciente.

Para tratar de comprender la evolución de los biomateriales y su aplicación en la clínica de los últimos 60 años, podemos clasificarlos en tres generaciones. Cada generación representa una evolución en los requisitos y las propiedades de los materiales involucrados, pero cada nueva generación no anula necesariamente el uso de las anteriores (22).

Los materiales de **primera generación** fueron diseñados y desarrollados por primera vez con el único requisito de sustituir el tejido dañado (23). Por tanto, los materiales de primera generación son inertes, no interaccionando con el tejido receptor. A fin de reducir al mínimo la reacción a un cuerpo extraño el organismo forma una capsula de tejido fibroso que lo aísla del medio en donde está implantado. En este grupo se incluyen todos los materiales metálicos como las aleaciones de cromo-cobalto, el acero inoxidable, el titanio y sus aleaciones, polímeros con distintas aplicaciones como el nylon, la silicona, los poliésteres, el ácido poliglicólico (PGA), el ácido poliláctico (PLA), el polietileno (PET) y el

polimetilmetacrilato (PMMA) y algunas cerámicas como la alúmina (Al_2O_3), y el zirconio (ZrO_2).

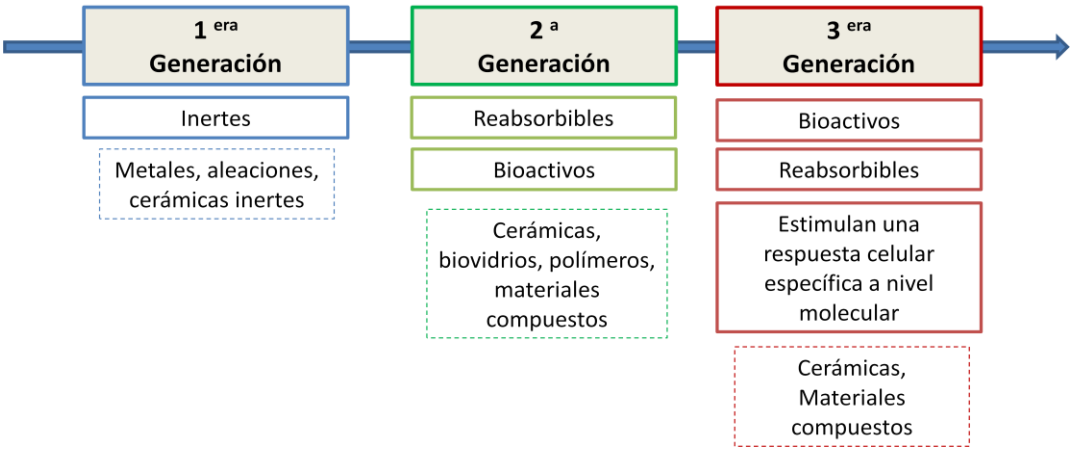

Figura 12. Cronograma de las tres generaciones de biomateriales de regeneración ósea.

Los materiales de **segunda generación** se caracterizan por ser bioactivos y/o biodegradables y tienen la función de reparar el tejido dañado. Son materiales que han desarrollado la capacidad de interactuar con el entorno biológico, bien a través de una unión química entre el material y el hueso, a fin de conseguir una respuesta del mismo que facilite la unión del material al tejido humano, o bien a través de un mecanismo de degradación donde el material es progresivamente disuelto y el tejido que lo rodea lo sustituye y se regenera (22). Dentro de este grupo se incluyen las cerámicas propiamente dichas, los vidrios bioactivos y las vitrocerámicas, además de algunos polímeros y combinaciones de metales con cerámicas. La HA, el fosfato tricálcico (TCP) ($Ca_3(PO_4)_2$) y sus derivados son los biomateriales más utilizados.

Los materiales de **tercera generación**, además de ser bioactivos y bioabsorbibles, son capaces de estimular una respuesta celular específica a nivel molecular en el tejido receptor (24) dado que su función es regenerar el tejido dañado. Consisten en estructuras porosas tridimensionales que estimulan la invasión, adhesión y proliferación celular, con superficies con secuencias peptídicas que imitan a la matriz extracelular para estimular respuestas celulares específicas (25). Las biocerámicas de segunda generación son empleadas como materiales de partida para fabricar las de tercera generación, para lo que es necesaria la búsqueda de nuevos métodos de conformado a temperatura ambiente de piezas porosas, denominadas andamios o *scaffolds* (término anglosajón), empleándose como sustratos en el campo de la ingería tisular.

2.4.2 Características de los biomateriales

La **Ingeniería de Tejidos** es un campo de investigación emergente profundamente multidisciplinar que requiere y concentra los conocimientos de diferentes ramas de la Ciencia, como la Biología, la Química, la Ingeniería y la Medicina. El objetivo de la Ingeniería de Tejidos es el desarrollo de compuestos biológicos y biomateriales implantables en el organismo, con intención de reparar, mantener o mejorar la función de órganos y tejidos. En ella se combina el uso de andamios, células y moléculas biológicamente activas con el fin de conseguir la reconstrucción del hueso, cuando de regeneración ósea se trata, evitando la necesidad de utilizar injertos óseos. En este sentido, los biomateriales constituyen una parte integral de la ingeniería de tejidos destinados a proporcionar un marco

arquitectónico que recuerda o imita a la matriz extracelular natural con el fin de estimular el crecimiento celular y la eventual regeneración del tejido.

Conceptualmente, los biomateriales son materiales biocompatibles que pueden definirse como *una sustancia que ha sido diseñada para tomar una forma que, sola o como parte de un sistema complejo, se usa para dirigir, mediante el control de las interacciones con componentes de sistemas vivos, el curso de cualquier procedimiento terapéutico o diagnóstico, en humanos o medicina veterinaria (26).*

Todos los materiales implantados en un tejido vivo provocan una respuesta diferente en el tejido huésped. Esta respuesta ocurre en la interfase implante-tejido. Dependiendo del tipo de respuesta del huésped, se clasifican en (1) **bioinertes**, generándose tejido fibroso alrededor del mismo; (2) **bioactivos**, cuando provocan una reacción química que da lugar a una unión interfacial entre el tejido y el implante y (3) **biodegradables**, cuando el biomaterial se disuelve o reabsorbe y es reemplazado por el tejido circundante (23).

El desarrollo de nuevos materiales biocompatibles como son las biocerámicas de fosfato cálcico (CaP) constituye una prometedora alternativa a la hora de reemplazar o regenerar partes del sistema esquelético evitando el uso de injertos óseos (27). Con este fin, la Ingeniería de Tejidos utiliza andamios tridimensionales, los cuales deben ser osteoconductores (28), biocompatibles, bioactivos y reabsorbibles, mostrar propiedades mecánicas similares a las del hueso natural donde se vayan a implantar y, al mismo tiempo, deben poseer la capacidad de estimular la proliferación de *ah*MSCs y su diferenciación a

osteoblastos, que serán en definitiva los encargados de producir MEx mineralizada (29).

Tabla 2. Interacciones implante-tejido (30).

REACCIÓN	CONSECUENCIA
TÓXICA	Necrosis
INERTE	Encapsulación fibrosa
BIOACTIVA	Unión química interfacial
SOLUBLE	Sustitución

2.4.3 Las células madre y su implicación en la Ingeniería de Tejidos

Una célula madre se define como aquella que tiene: (1) capacidad de autorrenovación o de formar durante su división al menos una copia idéntica de la célula inicial, con las mismas características y propiedades biológicas, (2) capacidad de diferenciación hacia una (o varias) células maduras con función especializada y (3) capacidad de proliferación a largo plazo (31).

La médula ósea integra un *pool* de células progenitoras hematopoyéticas, vasculares, estromales y mesenquimales. La capacidad de reparar partes del sistema esquelético se debe a la facultad que poseen las *ah*MSCs de diferenciarse en células de linaje mesodérmico como osteoblastos, condrocitos, adipocitos o miocitos, entre otras (32, 33). Cuando son cultivadas *in vitro* suponen una población heterogénea de células de aspecto fibroblástico y morfología fusiforme.

En la actualidad no se conoce ningún marcador específico que defina a las *ah*MSCs. Por este motivo, y para evitar la dificultad a la hora de comparar diferentes trabajos sobre las *ah*MSCs, la sociedad internacional de terapia celular (ISCT, del inglés —Internacional Society for Cellular Therapy) propone unos criterios mínimos para definir una *ah*MSC (34):

- Las *ah*MSCs deben tener capacidad de adherencia al plástico cuando se mantienen en condiciones estándar de cultivo y mostrar capacidad de diferenciarse in vitro hacia osteoblastos, adipocitos y condrocitos.

- Deben expresar determinados marcadores o antígenos de membrana (cluster de diferenciación) (CD105, CD73 y CD 90) y no expresar otros marcadores específicos de diversas líneas hematopoyéticas como CD45 (panleucocitario), CD34 (células progenitoras hematopoyéticas), CD14 o CD11b (monocitos), CD79 alfa o CD19 (linfocitos B) ni expresar moléculas de clase II del complejo mayor de histocompatibilidad mayor (HLA-DR)

Las células madre tienen el potencial de mejorar el rendimiento de los sustitutos óseos y son el foco de atención de investigaciones (35, 36). Por todas estas razones, los cultivos celulares de *ah*MSCs resultan ser un método útil para estudiar las interacciones que tienen lugar en la interfaz célula-material que constituyen los scaffolds destinados a la ingeniería del tejido óseo.

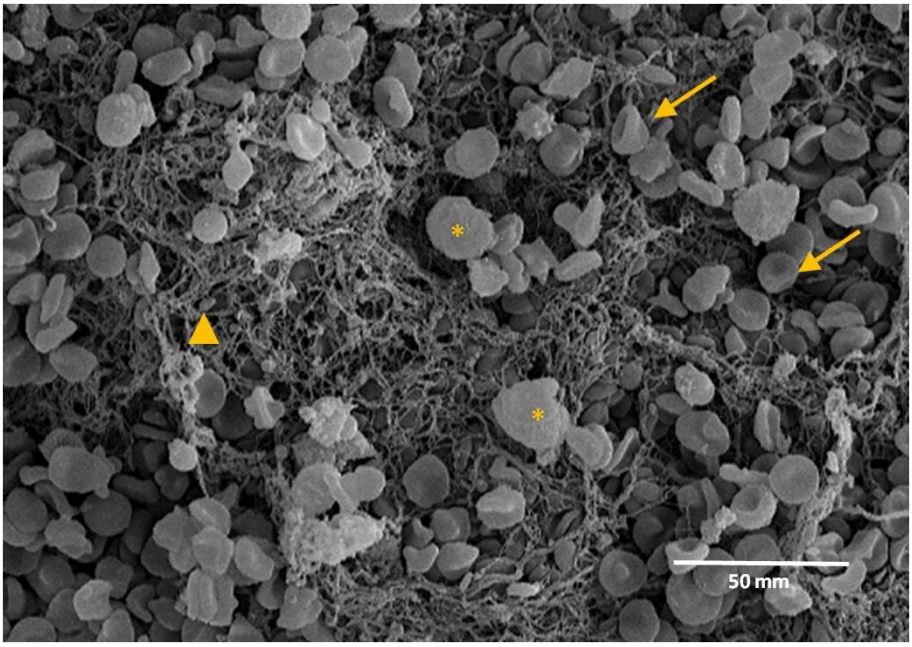

Figura 13. Microfotografía obtenida con MEB de una muestra de medula ósea procedente de un espécimen incluido en el estudio y en la que destacan los diferentes tipos celulares. Glóbulos rojos (flecha), plaquetas (cabeza de flecha), linfocitos (asterisco) dispuestos sobre una red de fibrina (Magnificación: barra 50 μm).

2.5 Biocerámicas basadas en fosfatos cálcicos

2.5.1 Hidroxiapatita y fosfato tricálcico

Las biocerámicas basadas en CaP se comenzaron a emplear en el campo de la medicina ya en 1890 con la intención de estimular la regeneración ósea. Sin embargo, no fue hasta 1920 cuando Albee et al (37) obtuvieron resultados favorables en los que se demostraba la capacidad osteoconductora del TCP. Aun así, el verdadero impulso de los materiales basados en fosfatos cálcicos tuvo lugar más adelante, en los años setenta y ochenta, cuando se descubrió la capacidad de

la HA y el Bioglass de guiar la formación de hueso neoformado a partir de una unión superficial directa material-hueso (38-40).

Las biocerámicas basadas en CaP con aplicaciones clínicas constituyeron desde ese momento, un campo muy interesante de investigación para el desarrollo y producción de implantes biocerámicos, empleándose en la actualidad prácticamente en todas las zonas del sistema esquelético.

Los sustitutos óseos cerámicos más comunes incluyen biocerámicas basadas en CaP como son la HA, el β-TCP, los vitrocerámicos y los biovidrios. Estos materiales presentan una composición y una estructura similar a la fase mineral del hueso, son biocompatibles, osteoconductores y capaces de formar una interfase con una unión fuerte con el hueso vivo (41). Una de las características más importantes que podemos aportarles a las biocerámicas reside en la porosidad. Debe poseer una elevada porosidad formada por poros abiertos e interconectados, con una elevada razón área/volumen. Debe ser tal que permita la colonización celular y la vascularización del material, a partir del tejido circundante (42). La relevancia de la porosidad de un andamio y del tamaño del poro se debe a la similitud con respecto a la estructura nativa porosa del hueso. En primer lugar, la porosidad y el tamaño del poro afectan a la adhesión celular, que consecuentemente influye en la distribución y la migración celular (43, 44). Además, la porosidad afecta a las características mecánicas del scaffold (resistencia), hecho importante especialmente para aquellas biocerámicas destinadas a la regeneración de huesos sometidos a cargas mecánicas.

El tamaño ideal del poro de una cerámica debería imitar al del hueso esponjoso: la macroporosidad proporciona un substrato adecuado para que se lleve a cabo la colonización celular y vascular del material, mientras que, la microporosidad permite la circulación inicial de los fluidos corporales desde el primer momento de su implantación en el lecho receptor (45). Se ha comprobado que el tamaño de los poros para el crecimiento óseo en los implantes porosos debe oscilar entre 100 y 450 μm (46, 47). Además, el diámetro de la interconexión entre poros condiciona el tipo de tejido que crece en el implante, y se considera que debe ser mayor de 100 μm para que se regenere hueso mineralizado, entre 40 y 100 μm para el crecimiento de formas osteoides y entre 10 y 40 μm para la formación de tejido fibrovascular.

Tanto la HA como el β-TCP son altamente biocompatibles, pero difieren en la respuesta biológica que generan en el sitio de implantación. Mientras que la HA se mantiene permanente en el tiempo, el TCP se reabsorbe a medida que el hueso nuevo crece, proceso conocido como *creeping substitution* (48). La capa superficial del TCP incrementa la unión con el hueso adyacente, al que se une directamente, lo que estimula la reabsorción por los osteoclastos y la formación de hueso nuevo "in situ" por los osteoblastos (23) . Las cerámicas recién implantadas carecen de las características mecánicas del hueso, pero tras su incorporación, la matriz ósea desmineralizada (osteoide) se dispone directamente sobre la superficie de la cerámica, seguidamente esta se mineraliza y el hueso neoformado comienza a remodelarse hasta adquirir las propiedades y características del tejido óseo en donde se ha implantado (18).

Entre los sustitutos óseos sintéticos de tipo cerámico, el β-TCP ha demostrado ser un material reabsorbible y osteoconductor (49, 50). Durante décadas, ha sido utilizado ampliamente para la reparación de pequeños defectos óseos, comprobándose que es un material en el que los osteoblastos y las *ah*MSCs son capaces de proliferar, proporcionando una matriz adecuada para la formación ósea (50-53).

2.5.2 Materiales cerámicos compuestos

Los sustitutos óseos cerámicos basados en CaP pueden ser usados de forma individual o en combinación con otras cerámicas o compuestos como proteínas o polímeros (PLA o el PGA) (54, 55). Se ha demostrado que los fosfatos cálcicos bifásicos compuestos por β-TCP y HA en proporción variable presentan ventajas favoreciendo la bioactividad y la biodegradación controlada *in vivo* (56), pudiendo usarse como vectores o carriers para diferentes tipos de moléculas con fines terapéuticos. Estos compuestos se integran directamente en el tejido óseo del huésped mediante la mineralización de la superficie, formando una capa de HA, facilitando la adhesión de proteínas contenidas en los fluidos biológicos en la superficie del material y, consecuentemente, promoviendo la adhesión celular gracias a las integrinas de la membrana celular, así como, la proliferación y la diferenciación osteogénica de las *ah*MSCs.

2.5.3 Silicato dicálcico

La estimulación ósea de las biocerámicas puede verse mejorada mediante la incorporación de determinados iones a su composición química. Muchas investigaciones se han centrado en la preparación y caracterización de biomateriales añadiendo iones como Silicio (Si), Calcio (Ca), Magnesio (Mg) o Zinc (Zn). Los iones Si o Ca procedentes de biomateriales basados en silicatos cálcicos pueden desempeñar un papel importante en el crecimiento celular (57). Se cree que el Si juega un papel importante en los procesos de mineralización del hueso alrededor del implante, en concreto como estimulador de dichos procesos (58). Entre otras características, presenta la propiedad de ser necesario para la síntesis de glicosaminoglicanos, así como la propiedad de ser un ingrediente fundamental del colágeno (59). También es necesario para la formación y crecimiento del hueso y se le atribuye gran importancia en la síntesis de células osteoblásticas, fruto del efecto causado por el ácido ortosilícico (60). Aunque no se conocen con exactitud los efectos del silicio en la actividad genética, parece ser que los silicatos solubles e iones de Ca procedentes de vidrios bioactivos tienden a crear hueso, debido a esa posible activación genética inducida por el silicio. También se ha demostrado recientemente que la disolución de iones Si, Ca y P procedentes de vidrios bioactivos activan los genes y controlan el ciclo de vida de los osteoblastos (61).

Estudios recientes han demostrado el potencial del silicato dicálcico ($2CaOSiO_2$-C_2S) para ser utilizado como biomaterial. Se ha comprobado que el silicio tiene efecto sobre la diferenciación osteoblástica y, por tanto, la

mineralización del hueso (62, 63). Las cerámicas de C_2S permiten la adhesión de las *ah*MSCs así como su propagación y colonización de toda su superficie. Además, el C_2S puede unirse espontáneamente al hueso vivo, sin formar un tejido fibroso alrededor del mismo, debido a la formación de una capa de apatita en su superficie similar a la del hueso (64). Estos hallazgos indican que la cerámica C_2S es biocompatible y además muestra buenas propiedades mecánicas, por lo que podría considerarse un potencial sustituto óseo (64, 65).

2.6 Biomateriales en el Sistema Ca_2SiO_4- $Ca_3(PO_4)_2$

2.6.1 Silicofosfatos cálcicos

Los biomateriales de silicofosfatos cálcicos son considerados candidatos muy interesantes para su posible aplicación en el campo de la regeneración ósea ya que aportan silicio al medio biológico e inducen una respuesta osteogénica de las *ah*MSCs (57, 66, 67).

El diagrama de fases C_2S - TCP presenta dos compuestos intermedios estables a temperatura ambiente: la silicocarnotita (Ca_2SiO_4-$Ca_3(PO_4)_2$) con una relación molar C_2S - TCP 1/1 y la fase A de Nurse $2Ca_2SiO_4$ – $Ca_3(PO_4)_2$, con un relación molar C_2S - TCP 2/1.

La silicocarnotita es un silicofosfato de calcio con estructura de carnotita, aunque algunos autores indican que su estructura es más parecida a la del hidroxiapatito debido a la pérdida de todo el –OH de la red de HA y su sustitución por SiO_4, considerando de esta forma a la silicocarnotita como una

mezcla de una apatita deshidratada sustituida con silicio y oxiapatita(68). La fase A de Nurse posee una red cristalina hexagonal simple de tipo A2XO4 = ABXO4, en los que un octavo de los cationes de la estructura hexagonal no están ocupados (69).

2.6.2 Fase A de Nurse

La primera referencia bibliográfica que se tiene de la fase A de Nurse data de 1959 cuando Nurse y col[49] estudiaron las relaciones de compatibilidad del sistema binario C_2S –TCP. Posteriormente este diagrama de fases ha sido estudiado y revisado por Fix y col. (70) en 1969 y, más recientemente, por Rubio y col. (71) (fig. 12), por Martínez y col. (72) y Ros-Tárraga y col (73). Como resultado de dichas revisiones la Fase A de Nurse ha sufrido ligeras variaciones en cuanto a la extensión de su campo primario de estabilidad y a la temperatura de transformación. Según la últimas revisión del diagrama, la Fase A de Nurse transforma directamente a R_{ss} a 1397ºC ± 2ºC, presentando un campo primario de cristalización muy pequeño, entre el 48% y el 50% en peso de TCP.

En la presente tesis se parte de un material poroso de fase A de Nurse que ha sido obtenido y caracterizado recientemente en el Instituto de Bioingenería de la Universidad Miguel Hernández (IB-UMH) (74, 75). La producción del biomaterial se realiza mediante una reacción en estado sólido a partir de la mezcla estequiométrica de fosfato dicálcico ($CaHPO_4$), carbonato de calcio ($CaCO_3$) de un tamaño medio de partícula de 13,8 μm y óxido de silicio (SiO_2) con un tamaño de partícula medio <50 μm. La mezcla de los materiales es calentada a 1500 ° C

durante 3 h, enfriada con nitrógeno líquido, molida y prensada. En segundo lugar, se lleva a cabo un calentamiento a 1300 ° C durante 3 h y, finalmente, se mantiene recociendo a 1200 ° C durante 24h. Los detalles sobre la obtención y caracterización del mismo se pueden encontrar en publicaciones anteriores del grupo (74, 75).

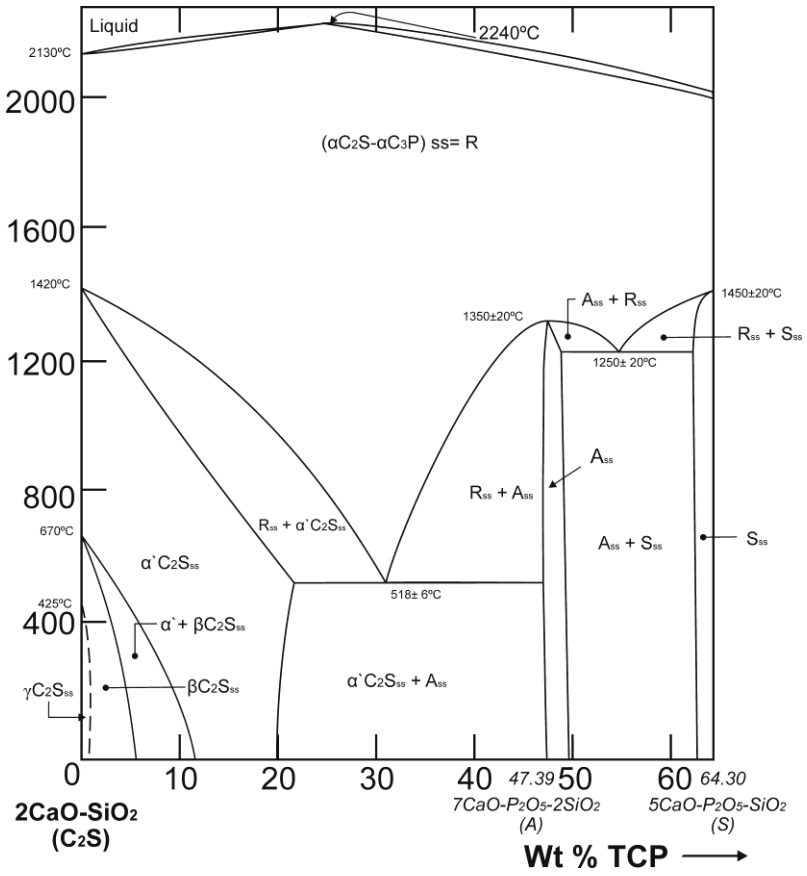

Figura 14. Diagrama de equilibrio de fases del sistema Ca_2SiO_4- $Ca_3(PO_4)$ según Rubio y col. (71) y Ros-Tárraga y col. (73).

3. HIPÓTESIS DE TRABAJO

Los biomateriales de silicofosfatos cálcicos aportan Si al medio biológico con capacidad para inducir una respuesta osteogénica. Por esta razón, hemos establecido la hipótesis de que el compuesto intermedio Fase A de Nurse, dentro del sub-sistema Fase A de Nurse – Silicocarnotita perteneciente al sistema TCP - C_2S, por sus especiales características físico-químicas es capaz de liberar iones de Si al medio después de su inmersión en SFA, y además, es competente para promover la capacidad osteoinductora de *ah*MSCs al tiempo que se reabsorbe progresivamente después de su implantación *in vivo* por un periodo de 2 meses.

4. OBJETIVOS

El objetivo general de la presente Tesis Doctoral es investigar la disposición de la cerámica monofásica "Fase A de Nurse" para crear un microambiente citocompatible óptimo que permita la adhesión de *ah*MSCs, la proliferación y la diferenciación osteogénica. Asimismo, evaluar su comportamiento tras ser implantada en un tejido vivo, con el fin de estimar su potencial uso en bioingeniería del tejido óseo en el contexto de las terapias avanzadas. Para alcanzar este objetivo principal, nos hemos propuesto los siguientes objetivos específicos:

- Estudiar la bioactividad de la cerámica Fase A de Nurse *in vitro* utilizando suero fisiológico artificial (SFA) (76) con el fin de determinar la capacidad de mineralización de la biocerámica.
- Precisar la tasa de disolución del material y liberación iónica al medio y los procesos de precipitación en la interfase de reacción en función del tiempo de inmersión en SFA.
- Evaluar *in vitro* mediante test directos (siembra celular directa sobre el material) e indirectos (extractos) la respuesta celular de una población de *ah*MSCs para corroborar que el material cumple permanentemente durante el periodo de estudio, los criterios de biocompatibilidad.
- Comprobar la capacidad de osteoinducción del material *in vitro* mediante ensayos de adhesión celular, viabilidad, proliferación y diferenciación osteogénica de *ah*MSCs en cultivo, comparándola con un control (crecimiento celular en placas de cultivo de poliestireno).

- Determinar *in vivo* los cambios experimentados por el material en el transcurso del experimento (reabsorción), así como la naturaleza de los acontecimientos biológicos que tienen lugar en la interfase biomaterial-hueso huésped (osteoconducción, osteointegración) tras la implantación intraósea en tibias de conejo durante 15, 30 y 60 días.

5. ARTÍCULO 1

Journal of the European Ceramic Society 37 (2017) 2943–2952

Contents lists available at www.sciencedirect.com

Journal of the European Ceramic Society

journal homepage: www.elsevier.com/locate/jeurceramsoc

In vitro behaviour of Nurse's A_{ss}-phase: A new calcium silicophosphate ceramic

R. Rabadan-Ros[a], P. Mazón[b], S. Serena[c], M.A. Sainz[c], L. Meseguer-Olmo[a,d], P.N. De Aza[e,*]

[a] *Grupo de Investigación en Regeneración y Reparación de Tejidos, UCAM – Universidad Católica San Antonio de Murcia, 30107 Guadalupe, Murcia, Spain*
[b] *Departamento de Materiales, Óptica y Tecnología Electrónica, Universidad Miguel Hernández, Universidad s/n, 03202 Elche, Alicante, Spain*
[c] *Departamento de Cerámica, Instituto de Cerámica y Vidrio, CSIC, 28049 Cantoblanco, Madrid, Spain*
[d] *Servicio de Cirugía Ortopédica y Traumatología del Hospital Clinico Universitario Virgen de la Arrixaca y Departamento de Ortopédia de la, UCAM – Universidad Católica San Antonio de Murcia, 30120 Murcia, Spain*
[e] *Instituto de Bioingeniería, Universidad Miguel Hernández Avda, Universidad s/n, 03202 Elche, Alicante, Spain*

ARTICLE INFO

Article history:
Received 2 November 2016
Received in revised form 24 February 2017
Accepted 4 March 2017
Available online 15 March 2017

Keywords:
Bioceramics
Calcium silicophosphates
Bioactivity
Biocompatibility
Biomedical applications

ABSTRACT

In the present study, a new single phase Si–Ca–P-based ceramic (called Nurse's A_{ss}) was obtained and its *in vitro* behaviour was explored for potential bone tissue regeneration. A porous Si–Ca–P single phase ceramic was obtained from high-temperature sintering of previously synthesised γ-dicalcium silicate and β-tricalcium phosphate. Apatite-mineralisation ability and the dissolution rate were systematically studied by immersing the material in simulated body fluid (SBF) for several time points. Massive new dense calcium deficient hydroxyapatite (CDHA) layer formation was observed at the SBF-sample interface. Adjacent to the dense CDHA layer, a porous structure developed parallel to the interface, formed by the pseudomorphic transformation of Si–Ca–P (Nurse's A_{ss}) into CDHA. The cell attachment test showed that the new material supported adult human bone marrow-derived mesenchymal stem cells (*h*MSCs) adhesion and spreading, and cells came into close contact with the ceramic surface during an extended 28-day culture. These findings indicate that the new calcium silicophosphate ceramic possesses good bioactivity and biocompatibility, and might be a promising bone graft substitute.

1. Introduction

With the world's increasing population age, the need for new bone implant materials has simultaneously increased. A successful bone implant requisite is rapid osseointegration and long-term mechanical stability. The new generation of tissue engineering scaffolds for bone regeneration should be highly bioactive, degradable and mechanically strong. There are many essential factors for tissue engineering scaffolds, among which bioactive composition [1,2], roughness [3,4] and macroporous morphology [5,6] are assumed critical for influencing the cell response.

The bone mineral fraction is the calcium–phosphate (Ca–P)-based apatite phase. For this reason, Ca–P ceramics, typically hydroxyapatite (HA) and tricalcium phosphate (TCP) ceramics, are widely used for bone tissue replacement and regeneration because of their generally good biocompatibility and similar chemical composition with biological apatite in bone tissue [7–10]. Regarding Ca–P materials that contain silicon, the role of Si is well-known in the development of healthy bone and connective tissues [11–15]. Silicon also modifies material properties and improves the biological activity of Ca–P materials that contains silicon. Thus they have been widely studied as biomaterials *per se* or associated with cells (cell–ceramic construct) for osseous repairs [16–21].

Interest in Si–Ca–P biomaterial is presently increasing because of its good bioactivity response and low cytotoxicity. In this context, Si–Ca–P (Nurse's A_{ss}) is a solid solution with an approximate composition of $7CaOP_2O_52SiO_2$, but should not be confused with the mineral of the same composition identified by Nagelshmidt in 1937 [22]. We recently synthesised a new single Si–Ca–P (Nurse's A_{ss}) phase material with a $Ca_2SiO_4/Ca_3(PO_4)_2$ molar ratio equal to 2:1 in the binary system dicalcium silicate (Ca_2SiO_4 = C2S)-tricalcium phosphate ($Ca_3(PO_4)_2$ = TCP) [23–25] by a solid-state reaction method [26,27]. However to date, studies into Nurse's A_{ss}-phase ceramic have been limited to establishing the simplest and most economical route of synthesis, and there are no reports on the *in vitro* bioactivity and biocompatibility of ceramic. So it would be

* Corresponding author.
E-mail addresses: rrabadan@ucam.edu (R. Rabadan-Ros), pmazon@umh.es (P. Mazón), serena@icv.csic.es (S. Serena), masainz@icv.csic.es (M.A. Sainz), lmeseguer.doc@gmail.com (L. Meseguer-Olmo), piedad@umh.es (P.N. De Aza).

http://dx.doi.org/10.1016/j.jeurceramsoc.2017.03.014
0955-2219/

very interesting to know the *in vitro* behaviour of this new ceramic to use a scaffolds for bone tissue engineering applications.

A method to estimate the bone-bonding potential ability of material is the simulated body fluid (SBF) method, which involves immersing materials into SBF for bone-like apatite formation on its surface. According to Kokubo et al. [28], bone-like apatite seems to activate signalling proteins and cells to start a series of events (attachment, proliferation and differentiation), which finally leads to bone formation. In other words, *in vivo* behaviour could be predicted by using the SBF method *in vitro*. Therefore, the aim of this study is to prepare a Si–Ca–P single phase ceramic by an economical route of synthesis, characterise its *in vitro* bioactivity and biocompatibility in SBF, and evaluate its ability to provide a suitable microenvironment to enhance the attachment and proliferation of adult human bone marrow-derived mesenchymal stem cells (*h*MSCs) for its use as a bone substitute or a supportive scaffold in bone tissue engineering.

2. Materials and methods

2.1. Material processing and characterisation

An Si–Ca–P (Nurse's A_{ss}) single-phase ceramic material was prepared from tricalcium phosphate and dicalcium silicate ceramics, which were used as starting materials. Details of the technique and the characterisation of the starting materials can be found in previous publications [26,27]. Briefly, a mixture of 47.39 wt% TCP and 52.61 wt% C2S was prepared. First, TCP and C2S powders were ground to an average particle size of ~30 μm, and the desired proportions of each component were weighed on an analytical balance and thoroughly mixed with PSZ-zirconia balls in a liquid medium. After drying, samples were isostatically pressed in bars at 200 MPa. The pellets obtained from the bars were put into small platinum foil crucibles, which were suspended from a platinum wire in the hot zone of an electrical furnace with an electronic temperature controller (±1 °C). Pellets were heated to 1500 °C for 3 h and were then liquid/nitrogen-quenched, ground and pressed. Second, heating at 1300 °C lasted 3 h with subsequent annealing at 1200 °C for 24 h. This combined heat treatment procedure was required to ensure that equilibrium conditions were achieved. The chemical analysis of the synthesised material as well as the X-ray diffraction (XRD), Fourier transform infrared spectroscopy (FTIR) and μ-Raman results, confirmed that the obtained material contained Nurse's A_{ss} as a single phase.

2.2. *SBF* in vitro *test*

The *in vitro* bioactivity of Nurse's A_{ss} ceramic disc was assessed by soaking samples in SBF solution, which was prepared according to the procedure described by Kokubo et al. [28]. Nurse's A_{ss} ceramic discs, which measured 10 mm in diameter and 5 mm in thickness, were cut from the bars, and then washed with pure acetone before being hanged with a nylon thread in polystyrene tubes that contained 100 ml of SBF (pH 7.25). The solution was refreshed with 25% of fresh SBF every 24 h. The solid/liquid weight ratio was equal to 0.5. The tubes with SBF and samples were incubated at 37 ± 0.5 °C in a shaking water bath for predetermined intervals. After different soaking periods that lasted from 1 day to 15 days, discs were removed from the SBF solution, gently washed 3 times with double-distilled water and dried for 24 h at room temperature.

To evaluate the dissolution rate, Nurse's A_{ss} ceramics were soaked in 100 ml Tris–HCl solution (pH 7.40) at 37 °C for 3, 5, 7, 10 and 15 days, and the solution was refreshed with 25% of fresh Tris–HCl every 24 h. Tris–HCl was selected because it does not contain inorganic ions (*e.g.*, Ca, P and Si). The weight of the disc before soaking was 0.18 g. After the set soaking time, ceramics were dried at 120 °C for 1 day, and the final weight of each sample was accurately recorded. Weight loss was expressed as the percentage of initial weight. Ten samples were used for this test.

After exposure to SBF, the surfaces and cross-sections of the samples were examined at 20 keV. Cross-sections were previously embedded in epoxy resin under vacuum and polished to 1 μm finish using a diamond paste, gently cleaned in an ultrasonic bath, and palladium-coated for SEM (SEM-Hitachi S-3500N, Ibaraki, Japan) examination and the EDS microanalysis (EDS-INCA-Oxford). The evolution of the samples was established by measuring the thickness of the layer formed on the ceramic–SBF interface by SEM.

SBF was removed after several immersion periods, and silicon, calcium, and phosphorus were determined in the removed SBF by inductively coupled plasma optical emission spectrometry (ICP-OES Perkin-Elmer Optima 2000^{TM}). For the TEM study (JEM-2010 JEOL), samples were prepared by carefully removing the reaction layer from the sample surfaces with a razor blade, and dispersing the powder on the surface of ethanol in a Petri dish. After drying, powder specimens were then collected on carbon-coated TEM copper grids (300 mesh). Electron beam transparent particles were chosen for the TEM examination by selected area diffraction (SAD), and also by EDS.

The atomic force microscopy (AFM) characterisation of samples' surface was performed in the tapping mode by a Cervantes Full Mode AFM System, equipped with a Dulcinea Control System (Nanotec Electrónica, Spain). Silicon cantilevers, with a 42 N/m force constant and a 330 kHz resonance frequency, were used. The structural characterisation of the samples' surface was also performed by confocal Raman (Witec ALPHA 300RA) with Nd:YAG laser excitation at 532 nm and a 100× objective (NA = 0.9).

2.3. In vitro *cell tests*

Adult human bone marrow-derived mesenchymal stem cells (*h*MSCs) were isolated from the bone marrow biopsy (40 ml) obtained through direct aspirations of the iliac crest from three healthy donors aged 25–40 years. They all provided informed consent and all the procedures were approved by the Institutional Ethical and Clinical Trials Committee (the V. Arrixaca University Hospital of Murcia, Spain). The isolation and culture procedures of the *h*MSCs and subcultures, and the characterisation of *h*MSCs, were processed by previously described methods [29]. For this study, only the *h*MSCs from the third passage (P3) were employed for all the experiments.

2.3.1. *Biofunctionality test*

The surface morphology of samples was analysed by SEM-EDS to evaluate the biofunctionality of the Nurse's A discs by studying cell adherence, morphology and growth on the ceramic surface. Briefly, discs were rinsed in an ultrasonic cleaner and dried a 100 °C prior to use. A tissue culture plate (Bechton Dickinson, Franklin Lakes, NJ, USA), was used as a control (hereinafter referred to as "plastic"). Prior to cell seeding, the material was sterilised by gas-plasma and conditioned by placing in DMEM with 10% FBS and incubating at 37 °C for 1 h.

After detaching *h*MSCs, viability was quantified by the trypan blue dye (Sigma–Aldrich) exclusion test. *h*MSCs were seeded onto the tops of the prepared disc-shaped Nurse's A_{ss} phase (6 mm in diameter, 3 mm high) at a density of 5×10^3 cells cm^{-2}, and were cultured for 1, 3, 7, 14, 21 and 28 days at 37 °C, 7.5% CO_2 in a humidified incubator. The medium was replaced every 3 days. After the incubation period, the cell-cultured discs or construct were/was rinsed with PBS for 10 min and fixed for 1 h with 3% glutaraldehyde in 0.1 M cacodylate buffer to then be postfixed with 1% osmium tetroxide. Next the cell-cultured construct was dehy-

drated in graded ethanol solutions (30%, 50%, 70%, 90% and 100% (v/v) in distilled water). Critical point drying was done with liquid CO_2. Finally, specimens were sputter-coated with gold and examined by a secondary image under a 15 kV field emission scanning electron microscopy (Merlin™ VP Compact, Carl Zeiss Microscopy S.L., Germany). All the analyses were performed in at least triplicate.

2.3.2. Cellular metabolic activity test

To assess the biological properties of the Nurse's A_{ss} ceramics, a metabolic activity assay was run (Alamar Blue™ assay, Invitrogen). Briefly, cells were seeded onto prepared Nurse's A phase surface discs in 48-well culture plates at a cell density of 5×10^3 cells cm^{-2}, and were allowed to adhere for 1 h. Afterwards, 1 ml of medium was added to each well, and were finally incubated under the same culture conditions as those described above. *h*MSCs were also seeded on plastic as a control. The medium was replaced every 3 days. The Alamar Blue™ assay was performed at days 1, 3, 7, 14, 21, and 28. At the end of the each culture period, the medium was discarded and wells were washed twice with PBS. Each well was filled with 200 μl of fresh medium with 10% of Alamar Blue™ and were incubated at 37 °C for 4 h. The solution in each well was transferred to a 96-well plate and fluorescence was determined directly in a Synergy MX ultraviolet visible instrument (UV–Vis) (Bio Tek Instruments Inc., Winooski, VT, USA) at a wavelength of 590 nm emission.

2.4. Statistical analysis

All the quantitative data are presented graphically as mean ± standard deviation (SD) of the experiments performed in at least triplicate. The results were analysed using a standard analysis with a Student's *t*-test. Differences were considered statistically significant when a *p*-value was below <0.05. An ANOVA was used to detect differences between group means.

3. Results

3.1. Material characterisation

Fig. 1 shows the ceramic characterisation before the *in vitro* test. Fig. 1A illustrates the polished surface of the obtained material after chemical etching (0.5% acetic acid for 2 s). The microstructure is open, with a density of 2.17 ± 0.9 g/cm^3 and elongated pores, which corresponds to the large open porosity (24.11 ± 1.2%). Sample composition was determined by a quantitative analysis by EDS at different points on the sample surface to be around 21 ± 1 wt% SiO_2, 24 ± 1 wt% CaO and 55 ± 1 wt% P_2O_5, which came close to the composition of the synthesised material determined by the chemical analysis (around 19 ± 1 wt% SiO_2, 22 ± 1 wt% CaO and 59 ± 1 wt% P_2O_5). This result indicated that the composition was homogeneous over the whole material surface.

Fig. 1B shows the XRD diffraction pattern of the obtained powder ceramic. The obvious sharp peaks and low backgrounds indicated that the ceramic was highly crystalline. It was possible to assign all the peaks to the reflections of $7CaOP_2O_52SiO_2$ (JCPD card no. 11-0676).

A summary of the microstructural parameters studied in a previous paper is shown in Table 1 to provide a better understanding of the material's microstructure. The strength values obtained for the material were relatively low due the ceramic's porosity. The results were directly related to the material's density [26,30].

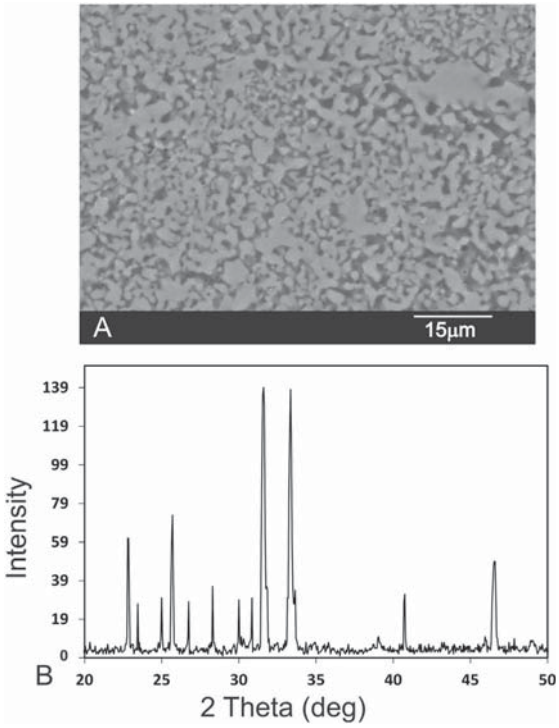

Fig. 1. (A) SEM image of the polished and chemical etched material and (B) the X-ray diffractions pattern of the synthesised ceramic material.

3.2. In vitro *bioactivity*

Figs. 2 and 3 respectively show what the specimens' surface looked like before and after SBF testing, and the cross-sections of the tested specimens. Fig. 2(B–E) depicts how the surface differed completely from the beginning of soaking (Fig. 2A). After the experiment, surfaces were covered by a layer of globular particles of about 2–3 μm in diameter (Fig. 2(B–D)), and the layer covered the entire surface of specimens after 3 days. The EDS analysis of the layers (Fig. 4) revealed Ca/P ratios to be about 2.03, which were higher than that in the HA stoichiometrics. This fact suggested that a Ca-deficient hydroxyapatite (CDHA) formed on the ceramic's surface. The higher magnification of the SEM image (Fig. 2E) revealed that agglomerates (5–6 μm) were composed of a large number of tiny worm-like crystals with a crystallite size of about 300–400 nm long (Fig. 2E).

At 24 h (Fig. 3A) a narrow and intermittent layer of precipitate layer was observed (arrows in Fig. 3A), where the surface was covered by spherical particles that formed small agglomerates in some areas (see Fig. 2B). With a longer test time, the microstructural study revealed the formation of two well-defined successive layers at the interface. A representative interface is shown in Fig. 3B and C for the specimen that was immersed for 14 days. Massive new dense CDHA layer formation (about 27.04 ± 0.05 μm in thickness) was observed at the SBF-material interface. On average the new precipitate was composed of 30.55 wt% Ca, 13.56 wt% P, 0.09 wt%

Table 1
Physical and mechanical properties of the Nurse's A phase.

Crystalline size (Sherrer Å)	Shrinkage (%)	Real density (g/cm^3)	Apparent density (g/cm^3)	Total porosity (%)	Strength (MPa)
213	30.0 ± 0.5	2.17 ± 0.7	1.57 ± 0.3	24.11 ± 1.3	0.60 ± 0.02

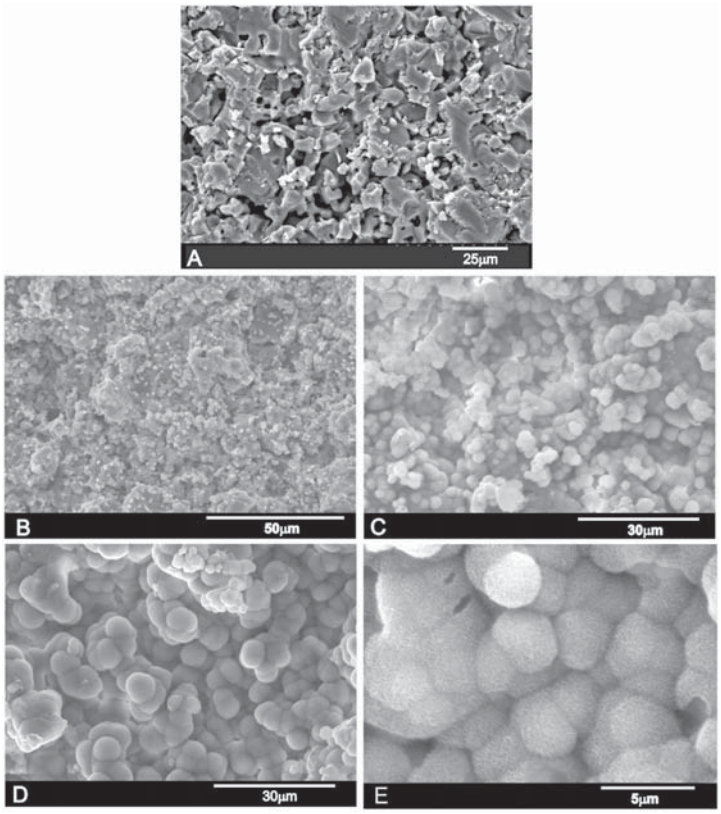

Fig. 2. SEM micrographs of the ceramic surfaces after soaking in SBF at 37 ± 0.5 °C and at different time points: (A) as sintering; (B) 1 day; (C) 7 days and (D, E) 14 days.

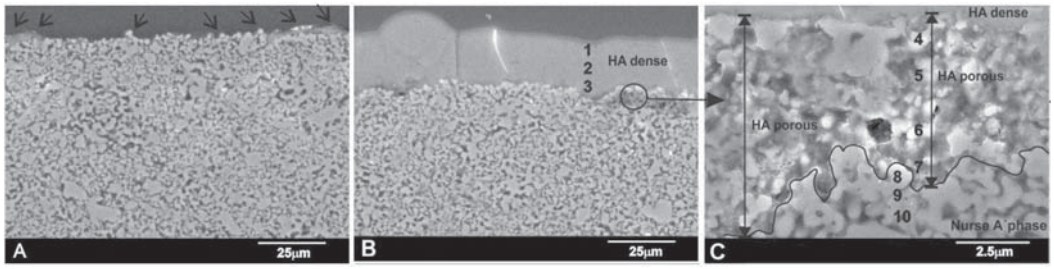

Fig. 3. View of the SEM cross-section to the bioceramic immersed in SBF for (A) 1 day; (B, C) 14 days.

Si, which was lower than the original Nurse's A material (41.6 wt% Ca, 9.68 wt% P, 8.03 wt% Si) (Fig. 5). A porous layer between the original material and the globular particles that formed the outer dense CDHA layer was in turn formed (Fig. 3C). The layer, which was about 7.3 ± 0.05 μm, had a much lower Ca/P ratio (1.74 ≤ Ca/P ≥ 2.17) than the adjacent original material had (4.29 ≤ Ca/P ≥ 4.31) (Fig. 5).

Porous layer thickness increased from day 5 (4.65 ± 0.05 μm) to day 14 (7.30 ± 0.05 μm) at a rate of 0.29 μm/day. The outer dense layer increased sharply (~2.14 μm/day) during the first 5 days of soaking to then increase slightly (~1.38 μm/day) until the end of the assay (Table 2).

Nurse's A_{ss} had a quick dissolution rate, as shown in Fig. 6A. The weight loss of Nurse's A_{ss} ceramic reached 16.8% by day 15. The changes in the concentrations of the calcium, phosphorous and sil-

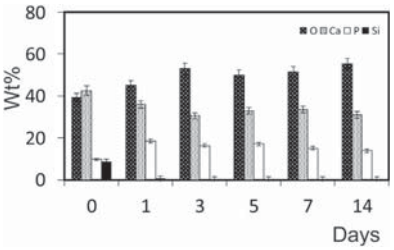

Fig. 4. EDS elemental analysis of the reaction zone after several soaking days.

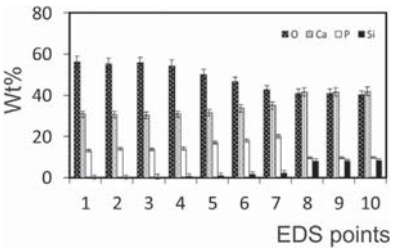

Fig. 5. EDS elemental analysis of the SEM cross-section after 14 soaking days [EDS's points of analysis are the numbers in Fig. 3].

Table 2
Thickness of the layer formed at the Nurse's A_{ss} material-SBF interfaces according to soaking time.

Days/μm	Intermediated porous layer	Outer dense layer
1	0	Intermittent
3	0	3.92 ± 0.05
5	4.65 ± 0.05	14.62 ± 0.05
7	4.98 ± 0.05	15.48 ± 0.05
9	5.01 ± 0.05	18.69 ± 0.05
11	6.43 ± 0.05	21.73 ± 0.05
13	7.13 ± 0.05	24.86 ± 0.05
14	7.30 ± 0.05	27.04 ± 0.05

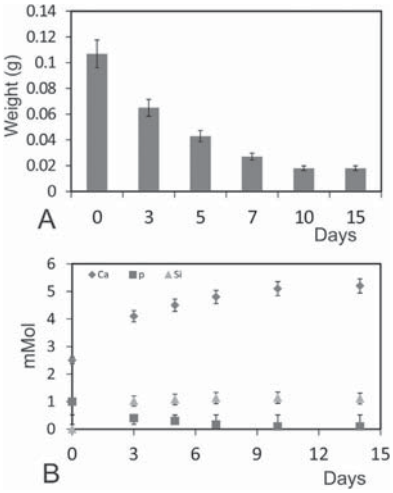

Fig. 6. (A) Weight loss (B) variation of the concentration of the calcium, phosphorus and silicon ions with immersion time in SBF at 37.0 ± 5 °C.

icon elements of SBF measured on different soaking days are shown in Fig. 6B. Nurse's A_{ss} ceramic released Si and Ca elements and removed P element from SBF. The continuous Si and Ca ion dissolution from the material contributed to increase the concentration of the Si and Ca elements in the SBF. The specific Si concentration in SBF increased from 0 to 1.14 mmol when soaked for 14 days. In addition, phosphorous element was removed from SBF and its concentration decreased from 1.0 to 0.1 mmol. After 10 soaking days, the formation rate gradually slowed down due to the depletion of the P element concentration from the SBF solution. In contrast, the Ca element concentration increased from 2.5 to 5.2 mmol.

TEM and Raman were used to examine the ultrastructure of the surface product formed after exposing the Nurse's A_{ss} sample to SBF. The TEM results (Fig. 7) for the different soaking times revealed the presence of nanocrystals with a plate-like morphology, composed mainly of Ca and P (data not shown). Individual crystals were found growing in close contact, and formed a continuous phase (Fig. 7B and C). Fig. 7A shows a TEM image of the removed reaction product from the Nurse' A ceramic soaked in SBF for 1 day. SAD in Fig. 7A shows spots correspond to the Nurse's A ceramic material. SAD in Figs. 7B and C clearly indicate on the preferential orientation of the CDHA crystals in (002) direction. A comparison with the SAD of the removed surface product from the Nurse' A ceramic soaked in SBF for 7 days in Fig. 7B indicated that the amount of CDHA crystals was significantly smaller than in 14 days sample (Fig. 7C), because de (002) arc was less prominent. The TEM and SAD results (Fig. 7B and C) were compared with information for the B-type carbo-hydroxyapatite in JCPDS (#19-272). On day 14, presence of an amorphous phase was observed (inner Fig. 7D). A slight deviation of *d* spacing from the standard carbo-hydroxyapatite d spacing was possibly due to the impurities/Si that incorporated into the carbo-hydroxyapatite structure. The results indicated the preferential orientation of the carbo-hydroxyapatite crystallites in the surface reaction product.

Fig. 8 depicts the micro-Raman spectrum of the Nurse's A_{ss} samples' surface after 1 and 14 soaking days in the spectral region of 200–1200 cm^{-1}. For comparison purposes, the Raman spectra of the pure hydroxyapatite and the Nurse's A_{ss} phase are also represented in this figure. The micro-Raman spectrum of the well-crystallised pure-hydroxyapatite presents four Raman bands associated with the internal modes of the PO_4^{3-} tetrahedral units of the hydroxyapatite structure: ν_1 mode (symmetrical stretching of the P–O bonds) at 969 cm^{-1} and ν_3 mode (antisymmetrical stretching of the P–O bonds) at 1056–1082 cm^{-1}; ν_2 mode (symmetrical bending of the O–P–O bonds) at 432 cm^{-1} and ν_4 mode (antisymmetrical bending of the O–P–O bonds) at 594 cm^{-1} [31,3236,37].

The Raman spectrum of Nurse's A_{ss} shows the overlapping of bands that correspond to both the PO_4^{3-} and SiO_4^{4-} groups in its structure; the ν_1 and ν_3 vibration modes of phosphate units mainly contribute to the bands observed around 963, 1058–1084 cm^{-1} while the ν_2 and ν_4 vibration modes contribute to narrower range wavelength bands of 218–439 cm^{-1}. The most intense silicate vibrations at 857 cm^{-1} correspond to ν_1 of the vibration mode of SiO_4^{4-}. The stretching modes of the SiO_4^{4-} units (ν_2 and ν_4) contribute to the bands observed within the narrower wavelength range around 587 and 642 cm^{-1}, respectively [33–37].

After 1 day in SBF, the width of the bands in the Raman spectrum evidenced the poor crystallinity of the phases compared to the standard hydroxyapatite and the Nurse's A_{ss} ceramic spectra. Bands can be related with presence of apatite and calcium silicophosphate amorphous phases on the material surface. Presence of Nurse's A_{ss} was evidenced by the band at 854 cm^{-1}. The two very broad bands around 426–437 and 580–620, and the peak at 959 cm^{-1}, could be related to the formation of apatite on the sample surface [31,32,36–41]. After 14 days in SBF, the band at 858 cm^{-1}, assigned to Nurse's A_{ss}, still appeared in the Raman spectrum at a lower intensity. Presence of the apatite phase was supported by the displacement of the higher intensity band (959 cm^{-1}) to a wavelength closer to that observed in the hydroxyapatite standard (969 cm^{-1}). Finally, a characteristic band of the ν_1 vibration mode of CO_3^{2-} in carbonate in apatites appeared at 1090 cm^{-1}, which overlapped the PO_4^{3-} ν_3 vibration mode and evidenced the presence of carbo-apatite phases on the material's surface [42–44] and/or with the contribution of the vibration of bonds O–Si–O and O–P–O in the amorphous-like phases [36–41]. The bands around 435 and 590 were assigned to the phosphate that contained silicate glasses in relation to the vibrations in units O–P–O, which have been previously reported in the Raman spectrum of calcium–phosphate glasses [38–40]. Two very broad bands were observed at a higher wavenumber. The bands around 1038 and 1090 cm^{-1} are characteristic of the CO_3^{-2} units in the structure of the carbo-apatite

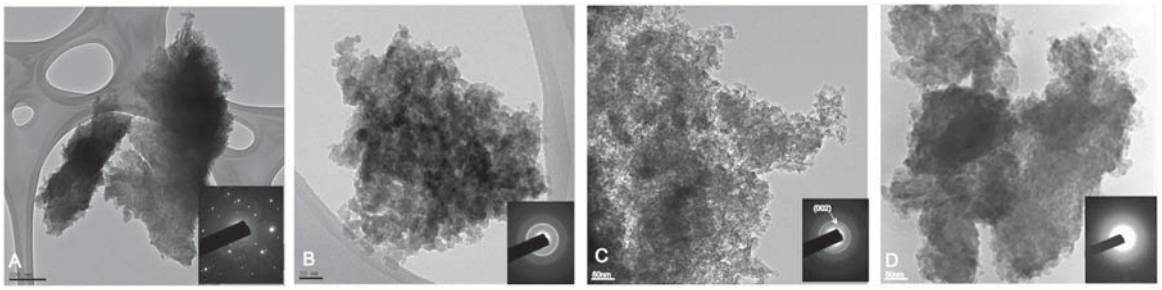

Fig. 7. TEM micrographs and SAD of the surface product from the exposure of the ceramic to SBF for different times. (A) 1 day, (B) 7 days, (C) 14 days and (D) amorphous phase.

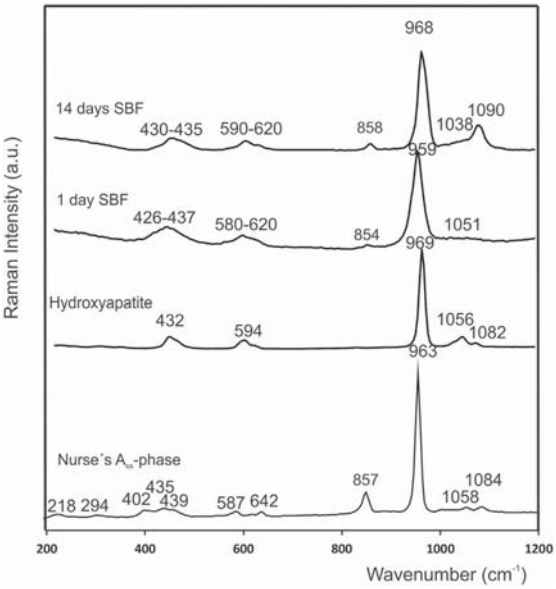

Fig. 8. Micro-Raman spectrum of the samples' surface of Nurse's A_{ss} after 1 day and 14 days in SBF in the spectral region, 200–1200 cm^{-1}. In order to compare, the Raman spectra of the pure-hydroxyapatite and Nurse's A_{ss} powders are also represented in this figure.

phases [31,32], although vibrations related to the asymmetrical stretching modes of groups Si–O–Si have also been reported in this region [34,35]. The vibrations of groups $–PO_3$ and $–PO_2$ in the phosphate amorphous phases could also contribute to this broadband between 1000 and 1300 cm^{-1} [41].

3D-topographic images with different scan sizes obtained by the AFM of the samples' surface after different soaking times are observed in Figs. 9–11 , which also present the typical roughness profiles. The AFM image of the Nurse's A_{ss} sample soaked in SBF for 1 day is found in Fig. 9. This figure shows the topography of the new small precipitates on the surface (Fig. 9A and C) along with its typical roughness profiles (Fig. 9B and D). After 1 day, the agglomerates of the precipitates appeared in the limited regions of the material surface. Fig. 9A corresponds to a region with scarce precipitation, where the initial dissolution–precipitation process stages which took place on the surface are observed. Small precipitates of 30–50 nm intermittently covered the sample's surface (Fig. 9A and C). The roughness profiles evidenced the flatness of the surface formed by an amorphous-like phase (Fig. 9B) (roughness $\sim 2.4 \pm 0.5$ nm) and the small size and smoothness of the particles of precipitates (Fig. 9D) (roughness 0.6 ± 0.2 nm).

After 7 days, rounded agglomerates of ~2–3 μm in size, and typically <800 nm high (Fig. 10A and B), covered by new nano-precipitates (~150–300 nm width and <20 nm high) were observed where precipitation was extensive (Fig. 10C and D). A major increase in surface roughness was evidenced by the roughness profiles compared to the Nurse's A_{ss} sample on day 1 in SBF (Fig. 9C and D). According to the SEM images (Fig. 2), coarse rounded-shape precipitates of ~6–7 μm were seen on the sample's surface after 14 days in SBF. AFM evidenced that a film of new nano-precipitates (~150–300 nm in size) covered the surface of some of these round agglomerates (Fig. 11C and D).

In line with these results, after immersion in SBF for 14 days, only the typical absorption bands in the Raman spectrum related to the carbo-hydroxyapatite and calcium-silicophosphate-amorphous phases were noticed, which evidenced the high transformation of the Nurse's A_{ss} phase in these areas.

3.3. Cell adhesion and proliferation assays

The morphological images obtained by SEM of the *h*MSCs that adhered to and spread on the Nurse's A discs after incubation under standard conditions at all the time points (from 24 h to 28 days) are representatively shown in Fig. 12A–D. In general, cell appearance changed with time in culture, and in such a way that they appeared to completely spread over and well adhere to the whole Nurse's A disc surfaces at the last examined time point (28 days). *h*MSCs underwent morphological changes to stabilise the cell–material interface of Nurse's A ceramic.

Adhesion was enhanced by multiple cytoplasmic digitations (filopodias) that spread across the material's surface to increase the contact area with the surface material. During the first 24 h of incubation (Fig. 10A), the majority of cells cultured in the material exhibited a round-shaped morphology. On incubation day 7 (Fig. 12B), the cells on the examined Nurse's A ceramic discs spread well, presented a similar morphology, and some cells adhered either individually or in small groups (Fig. 12C) and spread across the material's surface. On days 14 and 21, cells came into close contact with the material's surface, appeared well spread, and exhibited a polygonal morphology, with thin filopodia extensions that either extended along the ceramic surface or connected to neighbouring cells. Cell coverage on incubation day 21 was greater than on day 14. No other differences were observed between these time points. After 28 days of incubation, the density of cultured cells increased in the Nurse's A discs to form a confluent layer and came into contact with each other through lamellipodia, with markedly decreased intercellular spaces. At this end time point, no signs of cytotoxicity (debris, small cell size, sloughed cells, *etc.*) were observed. Hence the cytoplasm of cells spread completely

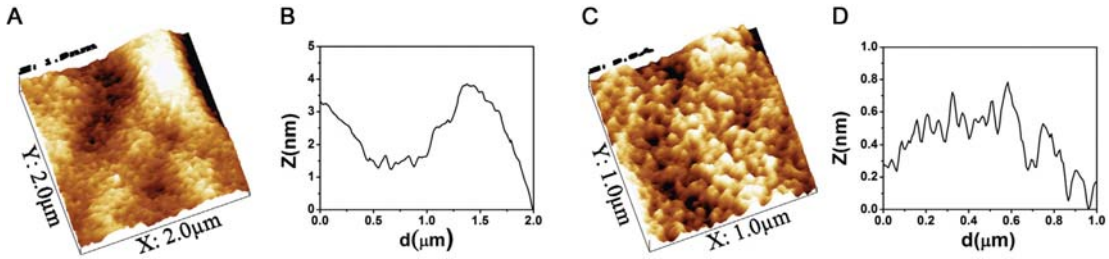

Fig. 9. AFM topographic images of Nurse's A soaked in SBF for 1 day. (A) 2 μm × 2 μm scan size and (B) the typical roughness profile. (C) 1 μm × 1 μm scan size and (D) the typical roughness profile.

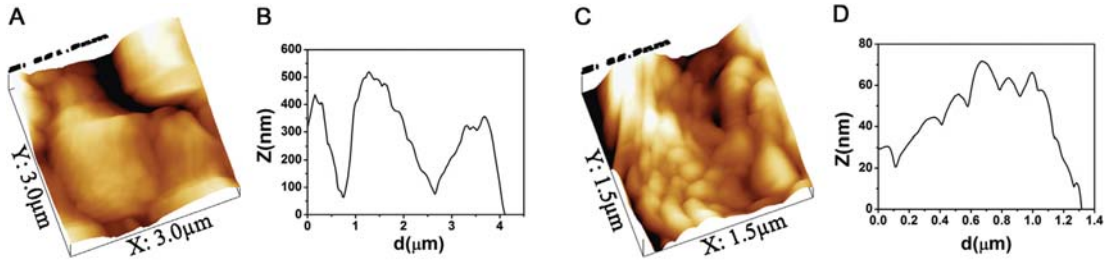

Fig. 10. AFM topographic images of Nurse's A soaked in SBF for 7 days. (A) 3 μm × 3 μm scan size and (B) the typical roughness profiles of regions with micro-precipitates. (C) 1.5 μm × 1.5 μm scan size and (D) the typical roughness profile of new nano-precipitates.

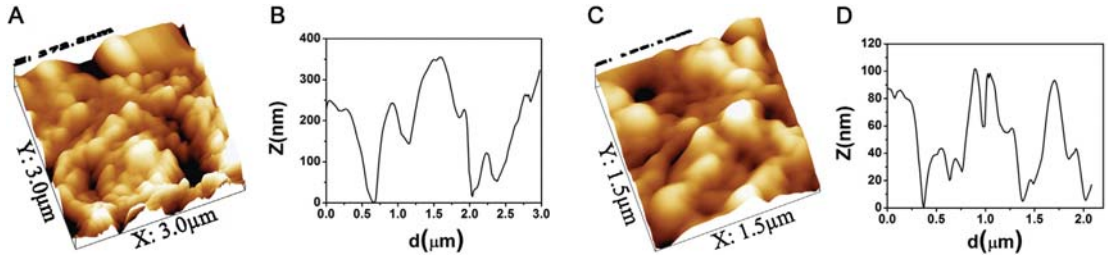

Fig. 11. AFM topographic images of Nurse's A soaked in SBF for 14 days. (A) 3 μm × 3 μm scan size of round-shaped precipitates and (B) the typical roughness profile of smooth particles. (C) 1.5 μm × 1.5 μm scan size of a region with agglomerates and (D) the typical roughness profile of new agglomerates.

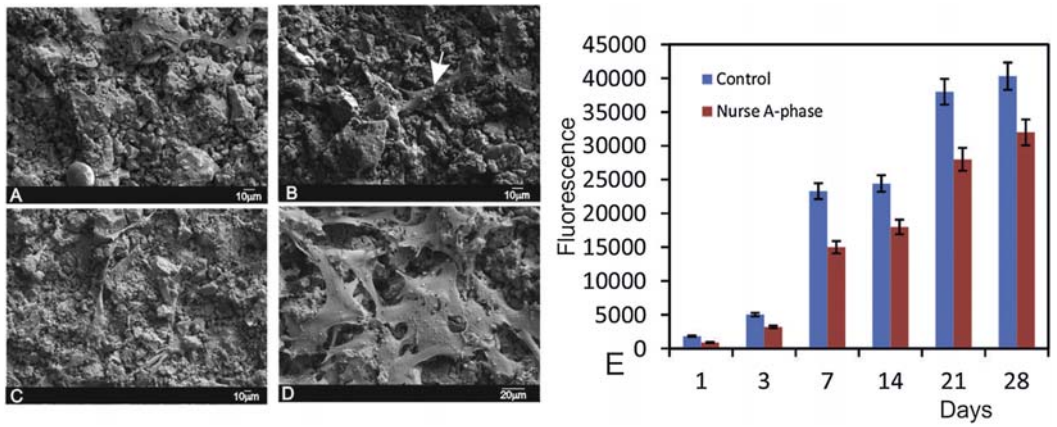

Fig. 12. SEM images of the *h*MSCs-A cultured under standard conditions on Nurse's A_{ss} ceramic surface at (A) 24 h, (B) 7 days (C) 14 days (D) 28 days, and (C) the proliferation rate of *h*MSCs seeded and cultures on ceramics and plastic at the all the time points. Data represent mean ± SD [*($p < 0.05$)].

and came into close contact with the ceramic, while the filopodia progressively projected (Fig. 12D). This scenario indicates that the ceramic firmly supported the adhesion and spreading of *h*MSCs.

Cell metabolic activity measurements confirmed the SEM observations (Fig. 12E). The Alamar Blue™ assay revealed that cell proliferation gradually increased with culture time, and that the percentage of metabolic activity was significantly higher in the cells plated and grown on plastic (control group) than those seeded directly on the Nurse' A_{ss} discs surface ($p < 0.05$).

4. Discussion

In vitro studies are usual docketed and standardised procedures (ISO-10993-5) [45] as a preliminary assay to assess the biofunctionality-biocompatibility of novel bioactive ceramics. Likewise, the bone marrow cell culture system seems useful for studying the interactions that occur at the cell-interface of implants to be used for bone tissue engineering.

In the present work, we examined the effect of the physical and chemical characteristics of a novel Si–Ca–P single-phase ceramic called Nurse' A_{ss} on its *in vitro* behaviour in both an inorganic medium (SBF) and a primary culture of adult human bone marrow-derived MSCs. The intention was to evaluate its potential use as a bone substitute for filling bone defects, or as a substrate or scaffold for tissue engineering and the subsequent clinical application in bone tissue reconstruction. Therefore, the proliferation of *h*MSCs was also evaluated in this study.

Bearing in mind the mechanism process proposed by several authors [16,19,46,47] to explain the bioactive response of calcium silico-phosphate ceramics and the experimental results obtained herein, the reaction of Nurse's A_{ss} in SBF can be described as a dissolution/precipitation process. Table 2 and Figs. 3 and 4 revealed the preferential dissolution process of Nurse's A_{ss}, while the precipitation of a new phase on the ceramic's surface was evidenced by SEM, AFM and Raman spectroscopy. The SEM observations of the sample after soaking in SBF and Table 2 prove that the process took place not only on the material's surface (Fig. 2), but also in the material's internal pores (Fig. 3). The AFM results indicated that the precipitation process began with the formation of nanometric rounded-shape particles in an amorphous-like matrix. Subsequently, these precipitates progressed to round-shaped particles with a granulate structure that finally covered the whole ceramic surface. Precipitates were identified by TEM, and by Raman as the carbo-hydroxyapatite and the Ca–Si–P–O–H amorphous phase. The SAD study performed in TEM (Fig. 7A–C) showed that the apatite phase was composed of nanocrystals with a plate-like morphology. When the specimen was appropriately oriented, SAD often displayed (002) and (210) arcs, which indicates the preferential orientation of the apatite crystals in the layer (inner of Fig. 7B and C), as well as the presence of a Ca–Si–P–O–H amorphous phase (inner of Fig. 7D).

The reactions of Nurse's A ceramic that came into contact with SBF are summarised in the following steps:

(a) Rapid exchange of H_3O^+/H^+ ions from the solutions and formation of $Si–OH^+$ at the material surface interface.
(b) Dissolution of Nurse's A in SBF with the release of SiO_4^{4-}, HPO_4^{2-} and Ca^{2+} (Fig. 6A):

$$Ca_7(PO_4)_2(SiO_4)_2 + 2H_2O \rightarrow 2SiO_4^{4-} + 2HPO_4^{2-} + 7Ca^{2+} + 2OH^-.$$

Only slight variations in the release of Si, Ca and P ions were observed (Fig. 6B). Therefore, ions should be retained on the Nurse's A_{ss} surface.

(c.) Repolymerisation of the silanol groups that led to the formation of an SiO_2-rich amorphous-like phase in limited regions of the material surface, as observed by TEM and AFM (Figs. 7D and 9).
(d.) Afterwards, the $3HPO_4^{2-}$ and Ca^{2+} groups migrated (Fig. 6B) to the surface through the SiO_2-rich (Fig. 7D) and rounded particles of Ca–P-rich precipitates (Fig. 2) and, which are immersed in the amorphous-like phase after short soaking times (Fig. 9). Presence of the SiO_2-rich phase induced hydroxyapatite nucleation, so this phase grew: $3HPO_4^{2-} + 5Ca^{2+} + H_2O \rightarrow Ca_5(PO_4)_3OH + 4H^+$ (Fig. 3).
(e.) Finally, crystallisation of amorphous $CaO–P_2O_5$ by incorporating OH^- or $CO_3^=$ from the solution, and through the reaction of the SBF phosphate ions with excess calcium ions released to SBF from the Nurse's A_{ss} surface that came into contact with SBF took place (Fig. 6). As a result, the material surface was covered by precipitates (Figs. 2, 3, 10, 11) of carbo-hydroxyapatite and the Ca–Si–P–O–H amorphous phase, as revealed by the μ-Raman and TEM results.

Considering all the possible reactions in the dissolution of Nurse's A_{ss}, another apatite-like precipitation reaction could occur:

$$(6-x)HPO_4^{2-} + ySiO_4^{4-} + 10Ca^{2+} + 8OH^- \rightarrow Ca_{10-x}(HPO_4)_x(PO_4)_{6-y}(SiO_4)_y(OH)_{2-x} + 6H_2O$$

The silicate ions released by Nurse's A_{ss} material can produce silicon-HA. The SEM-EDS data suggest a small quantity of silicon substitution in the apatite phase according to Figs. 4 and 5.

The reaction started on the Nurse's A_{ss} surface, and progressed deeply into the material in the confined pores as Nurse's A_{ss} ceramic dissolved. Once apatite nuclei formed on the surface of the porous layer, they grew spontaneously by consuming the calcium and phosphate elements from the surrounding SBF solution.

The results showed that the morphology generated in SBF was controlled by Nurse's A_{ss} phase' solubility, which brought about changes to surface chemistry and surface topography. This mechanism led to the "*in situ*" formation of a porous interconnected silicon-apatite structure, which is expected to promote bone growth if Nurse's A_{ss} ceramic is implanted into bone defects. [5,6]. It is important to note that the apatite-like formation in Nurse's A_{ss} ceramic under *in vitro* conditions was really a substitute HA. As previously reported [48], the mechanism of incorporating Si into the hydroxyapatite structure is complex and involves hydroxyl vacancies and phosphate-silicate vacancies due to a carbonate-involving mechanism. Hence the resulting apatite phase should be the Si-carbohydroxyapatite phase.

The mechanism described herein to explain the behaviour of Nurse's A_{ss} under *in vitro* conditions was also supported by the $SiO_2–CaO–P_2O_5–H_2O$ phase diagram [37,49–51]. According to the isopletal section of the $SiO_2–CaO–P_2O_5–H_2O$ phase diagram (Fig. 13), Nurse's A_{ss} was unstable when water was present, and the phases that resulted from its hydration were calcium silicate hydrated (C–H–S), portlandite ($Ca(OH)_2$) and hydroxyapatite for Ca_2SiO_4-rich Nurse's A_{ss}, and hydroxyapatite, and a $SiO_2–CaO–H_2O$-gel phase for $Ca_3(PO_4)_2$-rich Nurse's A_{ss}. The formation of amorphous phases during the hydration and dissolution of calcium silicates has been widely studied [32,48–50]. Ca/Si hydration leads to non-crystalline calcium silicate hydrated phases of variable composition. At Ca/Si molar ratios around 1.5–1.8, the

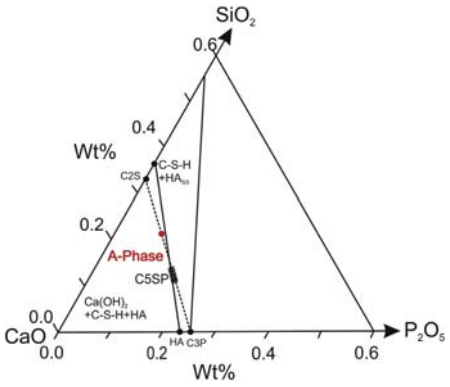

Fig. 13. Redraw of the projection on the $CaO–SiO_2–P_2O_5$ ternary part of the $CaO–SiO_2–P_2O_5–H_2O$ quaternary system [45–47]. (C–S–H: $(CaO)_{1.7}–SiO_2–H_2O_x–(CaO)_{0.8}–SiO_2–H_2O_x$; HA_{ss}: $(CaO)_{(10-x)}(HPO_4)_x(PO_4)_{(6-x)}(OH)_{(2-x)}(0<x>1)$; HA: hydroxyapatite $Ca_{10}(PO_4)_6(OH)_2$; C5SP: silicocarnotite $Ca_5(PO_4)_2SiO_4$: A-Phase: Nurse's A phase $Ca_7(PO_4)_2(SiO_2)_2$: C3P: tricacium phosphate $Ca_3(PO_4)_2$; C2S: dicalcium silicate–Ca_2SiO_4.

hydration of calcium silicates leads to calcium silicate hydrated phases (C–H–S) and $Ca(OH)_2$, while hydrated calcium silicate (C–H–S) appear at a higher Ca/Si molar ratio. It is well-known that the results of the hydration of calcium phosphate phases produce hydroxyapatite. The phases found in the presented Nurse's A_{ss} material after the *in vitro* experiments corresponded to that expected of the hydration of $Ca_3(PO_4)_2$-rich Nurse's A_{ss}.

From a biological perspective, and regarding the morphology of the cells grown on Nurse's A_{ss} ceramic, cells underwent their morphological changes to stabilise the cell–biomaterial interface. Cells also spread and established close contacts with ceramics by adapting a flattened morphology and showing filopodia that anchored cells to the bioactive Nurse's A_{ss} ceramic surface from day 3 in culture. Cells were able to produce small mineral deposits of calcium phosphate in both the extracellular matrix core and proximities of cells (arrow in Fig. 12B). This effect has also been observed with other bioactive ceramic types [52–54]. The amount of coverage of the hydroxyapatite-like layer is a cell adhesion- and proliferation-related factor. For this reason, the results about the proliferation and growth of the *h*MSCs on Nurse's A ceramic after 28 days of incubation indicated that the distribution of cells over specimens was homogeneous, they were well attached and uniformly colonised, and formed a monolayer on the ceramic surface. One of the possible reasons could be that the dissolution of Nurse's A ceramic lead to high concentrations of the Ca, inorganic PO_4, and Si ions in the extracellular environment, which promotes cell proliferation. The hydroxyapatite-like layer has positive effects by absorbing proteins from the FBS content in the culture medium [55]. This indicates that the Nurse's A_{ss} ceramic developed herein is biocompatible, and has a high colonisation and a consistent proliferation rate ($p < 0.05$) over the entire 28-day cultivation period (Fig. 12D).

In vitro cell–material interaction is a useful criterion to evaluate the biocompatibility of new biomaterials [56–59]. The present study indicates that Nurse's A_{ss} ceramic supports *h*MSCs cells proliferation. Cells came into close contact with the ceramic. This cell behaviour suggests that the Nurse's A_{ss} material's surface is non-irritant and does not affect structural cell integrity. Cells appeared flat and exhibited an intact well-defined polygonal morphology with cytoplasmic extensions (filopodia) and cell membrane integrity. Preservation of cytoplasmic extensions is important because they allow a vital three-dimensional network within bone. Such results suggest the possibility of Nurse's A_{ss} ceramic providing a suitable microenvironment for cell survival when compared with plastic.

5. Conclusions

Porous Si–Ca–P monophasic bioceramics were successfully prepared by solid-state sintering, and proved bioactive, biodegradable and biocompatible. The new porous Nurse's A_{ss} ceramic presents high reactivity in SBF, with the formation of two well-differentiated Si-carbohydroxyapatite areas; one formed by alteration of the material giving rise to the solution of Nurse's A_{ss} into SBF and subsequent formation of Si-carbohydroxyapatite inside the material and the other, in the last stages of the experiments by deposition of Si-carbohydroxyapatite onto the ceramic surface. The layer formed at the beginning of the reaction has a porous morphology, while that formed at the end of the reaction has a dense morphology. The Nurse's A_{ss} evaluated herein provides a favourable microenvironment for the adhesion, spread and proliferation of *h*MSCs, which improves with culture time.

In view of the results, Nurse's A_{ss} ceramic should be an effective substrate promoter of bone tissue regeneration, and one suitable for bone tissue bioengineering. Future performance should be done using standard biomaterials, such as Si-HA or Si-TCP.

Acknowledgments

Part of this work has been supported by Spanish Ministry of Economy and Competitiveness (MINECO) contract grant numbers: MAT2013-48426-C2-1-R and MAT2013-48426-C2-2-R.

References

[1] J.R. Jones, New trends in bioactive scaffolds: the importance of nanostructure, J. Eur. Ceram. Soc. 29 (2009) 1275–1281.
[2] P.N. De Aza, F. Guitian, S. De Aza, F.J. Valle, Analytical control of wollastonite for biomedical applications by use of AAS and ICP-OES, Analyst 123 (1998) 681–685.
[3] D.D. Deligianni, N.D. Katsala, P.G. Koutsoukos, Y.F. Missirlis, Effect of surface roughness of hydroxyapatite on human bone marrow cell adhesion, proliferation, differentiation and detachment strength, Biomaterials 22 (1) (2001) 87–96.
[4] P. Mazon, D. Garcia-Bernal, L. Meseguer-Olmo, P.N. De Aza, Human mesenchymal stem cell viability, proliferation and differentiation potential in response to ceramic chemistry and surface roughness, Ceram. Int. 41 (2015) 6631–6644.
[5] P.N. De Aza, J.E. Mate-Sanchez de Val, C. Baudin, C. Perez Albacete-Martínez, A. Armijo Salto, J.L. Calvo-Guirado, Bone neoformation of a novel porous resorbable Si–Ca–P base ceramic with osteoconductive properties: physical and mechanical characterization, histological and histomorphometric study, Clin. Oral. Implant. Res. 27 (2016) 1368–1375.
[6] R. Rabadan-Ros, P.A. Velasquez, L. Meseguer-Olmo, P.N. De Aza, Morphological and structural study of a novel porous Nurse's A ceramic with osteoconductive properties for tissue engineering, Materials 9 (2016) 474, http://dx.doi.org/10.3390/ma9060474.
[7] J. Chevalier, L. Gremillard, Ceramics for medical applications: a picture for the next 20 years, J. Eur. Ceram. Soc. 29 (2009) 1245–1255.
[8] J.E. Maté-Sánchez de Val, P. Mazon, J.L. Calvo-Guirado, R.A. Delgado-Ruíz, M.P. Ramírez-Fernandez, N. Bruno, A. Marcus, P.N. De Aza, Comparison of three novel β-tricalcium phosphate/collagen ceramic scaffolds: an in vivo study, J. Biomed. Mater. Res. A 102A (4) (2014) 1037–1046.
[9] J.E. Maté Sánchez de Val, J.L. Calvo Guirado, G. Gomez Moreno, C. Perez Albacete-Martinez, P. Mazón, P.N. De Aza, Influence of hydroxyapatite granule size, porosity and crystallinity on tissue reaction in vivo: Part A. Synthesis, characterization of the materials and SEM analysis, Clin. Oral. Implant. Res. 27 (2016) 1331–1338.
[10] A.H. De Aza, P. Velasquez, M.I. Alemany, P. Pena, P.N. De Aza, In situ bone-like apatite formation from a Bioeutectic® ceramic in SBF dynamic flow, J. Am. Ceram. Soc. 90 (4) (2007) 1200–1207.
[11] E.M. Carlisle, Silicon: an essential element for the chick, Science 178 (1972) 619–621.
[12] E.M. Carlisle, A silicon requirement for normal skull formation in chicks, J. Nutr. 110 (1980) 352–359.
[13] E.M. Carlisle, Silicon: a possible factor in bone calcification, Science 167 (1970) 279–280.
[14] K. Schwarz, D.B. Milne, Growth-promoting effects of silicon in rats, Nature 239 (1972) 333–334.

[15] M.Y. Shie, S.J. Ding, H.C. Chang, The role of silicon in osteoblast-like cell proliferation and apoptosis, Acta Biomater. 7 (6) (2011) 2604–2614.
[16] I.R. Gibson, S. Best, W. Bonfield, Chemical characterization of silicon-substituted hydroxyapatite, J. Biomed. Mater. Res. 44 (1999) 422–428.
[17] J.W. Reid, L.K. Tuc, M. Sayer, K. Fargo, J.A. Hendry, Synthesis and characterization of single-phase silicon-substituted α-tricalcium phosphate, Biomaterials 27 (2006) 2916–2925.
[18] A. Bandyopadhyay, S. Bernard, W. Xue, S. Bose, Calcium phosphate-based resorbable ceramics: influence of MgO, ZnO, and SiO_2 dopants, J. Am. Ceram. Soc. 89 (9) (2006) 2675–2688.
[19] S.V. Dorozhkin, In vitro mineralization of silicon containing calcium phosphate bioceramics, J. Am. Ceram. Soc. 90 (1) (2007) 244–249.
[20] J.E. Mate-Sanchez de Val, J.L. Calvo-Guirado, R.A. Delgado-Ruiz, P. Ramirez-Fernandez Ma, I.M. Martinez, J.M. Granero-Marin, B. Negri, F. Chiva-Garcia, J.M. Martinez-Gonzalez, P.N. De Aza, New block graft of alpha-TCP with silicon in critical size defects in rabbits: chemical characterization, histological, histomorphometric and micro-CT study, Ceram. Int. 38 (2012) 1563–1570.
[21] P. Velasquez, Z.B. Luklinska, L. Meseguer-Olmo, J.E. Mate-Sanchez de Val, R.A. Delgado-Ruiz, J.L. Calvo-Guirado, Ma P. Ramirez-Fernandez, P.N. de Aza, α-TCP ceramic doped with dicalcium silicate for bone regeneration applications prepared by powder metallurgy method: in vitro and in vivo studies, J. Biomed. Mater. Res. A 101A (7) (2013) 1943–1954.
[22] G. Nagelschmidt, A new calcium silicophosphate, J. Chem. Soc. (1937) 865–867.
[23] W. Fix, H. Heymann, R. Heinke, Subsolidus relations in the system $2CaO{\cdot}SiO_2$–$3CaO{\cdot}P_2O_5$, J. Am. Ceram. Soc. 52 (6) (1969) 346–347.
[24] V. Rubio, M.A. de la Casa-Lillo, S. De Aza, P.N. De Aza, The system $Ca_3(PO_4)_2$–Ca_2SiO_4: the sub-system Ca_2SiO_4–$7CaOP_2O_52SiO_2$, J. Am. Ceram. Soc. 94 (12) (2011) 4459–4462.
[25] P. Ros-Tarraga, P. Mazón, L. Meseguer-Olmo, P.N. De Aza, Revising the subsystem Nurse's A – phase-silicocarnotite within the system $Ca_3(PO_4)_2$–Ca_2SiO_4, Materials 9 (2016) 322, http://dx.doi.org/10.3390/ma9050322.
[26] G.J. Lugo, P. Mazón, P.N. De Aza, Phase transitions in single phase Si–Ca–P-based ceramic under thermal treatment, J. Eur. Ceram. Soc. 35 (2015) 3693–3700.
[27] G.J. Lugo, P. Mazón, P.N. De Aza, Material processing of a new calcium silicophosphate ceramic, Ceram. Int. 42 (1) (2016) 673–680.
[28] T. Kokubo, H.M. Kim, M. Kawashita, T. Nakamura, What kinds of materials exhibit bone-bonding? in: J.E. Davies (Ed.), Bone Engineering, EM2, Toronto, Canada, 2000, pp. 190–194.
[29] P.N. De Aza, D. Garcia-Bernal, F. Gragnolini, P. Velasquez, L. Meseguer-Olmo, The effects of Ca_2SiO_4–$Ca_3(PO_4)_2$ ceramics on adult human mesenchymal stem cell viability, adhesion, proliferation, differentiation and function Mater. Sci. Eng. C 33 (2013) 4009–4020.
[30] G.J. Lugo, P. Mazón, P.N. De Aza, Nurse's A phase: synthesis and characterization in the binary system Ca_2SiO_4–$Ca_3(PO_4)_2$, J. Am. Ceram. Soc. 98 (10) (2015) 3042–3046.
[31] A. Antonakos, E. Liarokapis, T. Leventouri, Micro-Raman and FTIR studies of synthetic and natural apatites, Biomaterials 28 (2007) 3043–3054.
[32] P. Layrolle, A. Ito, T. Tateishi, Sol–gel synthesis of amorphous calcium phosphate and sintering into microporous hydroxyapatite bioceramics, J. Am. Ceram. Soc. 81 (6) (1998) 1421–1428.
[33] F.P. Glasser, E.E. Lachowski, D.E. Macphee, Compositional model for calcium silicate hydrate (C–H–S) gels, their solubility and free energies of formation, J. Am. Ceram. Soc. 70 (7) (1987) 481–485.
[34] C. Remy, B. Reynard, M. Madon, Raman spectroscopic investigations of dicalcium silicate: polymorphs and high-temperature phase transformations, J. Am. Ceram. Soc. 80 (1997) 413–423.
[35] J. Ibáñez, L. Artús, R. Cuscó, A. López, E. Menéndez, M.C. Andrade, Hydration and carbonation of monoclinic Ca_2SiO_4 and Ca_3SiO_5 studied by Raman spectroscopy, J. Raman Spectrosc. 38 (2001) 61–67.
[36] S. Serena, M.A. Sainz, A. Caballero, Single-phase silicocarnotite synthesis in the subsystem $Ca_3(PO_4)_2$–Ca_2SiO_4, Ceram. Int. 40 (6) (2014) 8245–8252.
[37] S. Serena, A. Caballero, P.N. De Aza, M.A. Sainz, New evaluation of the in vitro response of silicocarnotite monophasic material, Ceram. Int. 41 (8) (2015) 9412–9419.
[38] F. Bonino, A. Damin, V. Aina, M. Miola, E. Vernè, O. Bretcanu, S. Bordiga, A. Zecchina, C. Morterra, In situ Raman study to monitor bioactive glasses reactivity, J. Raman Spectrosc. 39 (2008) 260–264.
[39] H. Aguiar, E.L. Solla, J. Serra, P. González, B. León, F. Malz, C. Jäger, Raman and NMR study of bioactive Na_2O–MgO–CaO–P_2O_5–SiO_2 glasses, J. Non-Cryst Solids 354 (2008) 5004–5008.
[40] J. Sułowska, I. Wacławska, Z. Olejniczak, Structural studies of copper-containing multicomponent glasses from the SiO_2 P_2O_5–K_2O–CaO–MgO systems, Vib. Spectrosc. 65 (2013) 44–49.
[41] J.E. Pemberton, L. Latifzadeh, J.P. Fletcher, S.H. Risbud, Raman spectroscopy of calcium phosphate glasses with varying CaO modifier concentrations, Chem. Mater. 3 (1991) 195–200.
[42] G. Penel, G. Leroy, C. Rey, E. Bres, Micro-Raman spectral study of the PO_4 and CO_3 vibrational modes in synthetic and biological apatites, Calcif. Tissue Int. 63 (1998) 475–481.
[43] A. Krajewski, M. Mazzocchi, P.L. Buldini, A. Ravaglioli, A. Tinti, P. Taddei, C. Fagnano, Synthesis of carbonated hydroxyapatites: efficiency of the substitution and critical evaluation of analytical methods, J. Mol. Struct. 744–747 (2005) 221–228.
[44] A. Awonusi, M.D. Morris, M.M. Tecklenburg, Carbonate assignment and calibration in the Raman spectrum of apatite, Calcif. Tissue Int. 81 (1) (2007) 46–52.
[45] International Standard (ISO), Biological Evaluation of Medical Devices. Part 5. Tests for In Vitro Cytotoxicity. ISO-10993-5, 3rd ed., 2009.
[46] Z.G. Gou, J. Chang, Synthesis and in vitro bioactivity of dicalcium silicate powders, J. Eur. Ceram. Soc. 24 (1) (2004) 93–99.
[47] A. Bandyopadhyay, S. Bernard, W. Xue, S. Bose, Calcium phosphate-based resorbable ceramics: influence of MgO, ZnO, and SiO_2 dopants, J. Am. Ceram. Soc. 89 (9) (2006) 2675–2688.
[48] S. Gomes, J.M. Nedelec, E. Jallot, D. Sheptyakov, G. Renaudin, Silicon location in silicate-substituted calcium phosphate ceramics determined by neutron diffraction, Cryst. Growth Des. 11 (2011) 4017–4026.
[49] J. Hu, D.K. Agrawal, R. Roy, Investigation of hydration phases in the system CaO–SiO_2–P_2O_5–H_2O, J. Mater. Res. 3 (4) (1988) 772–780.
[50] P. Vanis, I. Odler, Hydration reactions in the system CaO–P_2O_5–SiO_2–(H_2O), J. Am. Ceram. Soc. 79 (4) (1996) 1124–1126.
[51] M.W. Barnes, M. Klimkiewicz, P.W. Brown, Hydration in the system Ca_2SiO_4–$Ca_3(PO_4)_2$ at 90 °C, J. Am. Ceram. Soc. 75 (6) (1992) 1423–1429.
[52] S.G. Dubois, E.Z. Floyd, S. Zvonic, G. Kilroy, X. Wu, S. Carling, Y.D. Halvorsen, E. Ravussin, J.M. Gimble, Isolation of human adipose-derived stem cells from biopsies and liposuction specimens, Methods Mol. Biol. 449 (2008) 69–79.
[53] P.A. Zuk, M. Zhu, H. Mizuno, J. Huang, J.W. Futrell, A.J. Katz, P. Benhaim, H.P. Lorenz, M.H. Hedrick, Multilineage cells from human adipose tissue: implications for cell-based therapies, Tissue Eng. 7 (2001) 211–226.
[54] K. Kieswetter, Z. Schwartz, T.W. Hummert, D.L. Cohran, J. Simpson, D.D. Dean, B.D. Boyan, Surface roughness modulates the local production of growth factors and kytokines by osteoblast-like MG-63 cells, J. Biomed. Mater. Res. 32 (1996) 55–63.
[55] J.H. Lee, J.H. Seo, K.M. Lee, H.S. Ryu, H.R. Baek, Fabrication and osteoblastic differentiation of human mesenchymal stem cells on novel CaO–SiO_2–P_2O_5–B_2O_3 glass ceramics, Artif. Organs 37 (7) (2013) 637–664.
[56] J.D. Ballard, L.M. Dell'Acqua-Bellavitis, R. Bizios, R.W. Siegel, Nanoparticle-decorated surfaces for the study of cell-protein–substrate interactions, Mater. Res. Soc. Sym. Proceed. 845 (2005) 339–344.
[57] P. Müller, U. Bulnheim, A. Diener, F. Luthen, M. Teller, E.D. Klinkenberg, H.G. Neumann, B. Nebe, A. Liebold, G. Steinhoff, J. Rychly, Calcium phosphate surfaces promote osteogenic differentiation of mesenchymal stem cells, J. Cell. Mol. Med. 12 (2008) 281–291.
[58] K.T. Bowers, J.C. Keller, B.A. Randolph, D.G. Wick, C.M. Michaels, Optimization of surface micromorphology for enhanced osteoblast responses in vitro, Int. J. Oral Maxillofac. Implants (1992) 7302–7310.
[59] A. El-Ghannam, P. Ducheyne, I.M. Shapiro, Effect of serum proteins on osteoblast adhesion to surface-modified bioactive glass and hydroxyapatite, J. Orthop. Res. 17 (3) (1999) 340–345.

6. ARTÍCULO 2

materials

MDPI

Article

Nurse's A-Phase Material Enhance Adhesion, Growth and Differentiation of Human Bone Marrow-Derived Stromal Mesenchymal Stem Cells

Ruben Rabadan-Ros [1,*], Salvador Aznar-Cervantes [2], Patricia Mazón [3], Patricia Ros-Tarraga [1], Piedad N. De Aza [4,†], and Luis Meseguer-Olmo [1,5,†]

1 Grupo de Regeneración y Reparación de Tejidos: Ortobiología, Biomateriales e Ingeniería de Tejidos, Universidad Católica San Antonio de Murcia (UCAM), Guadalupe, 30107 Murcia, Spain; p.ros.tarraga@gmail.com (P.R.-T.); lmeseguer.doc@gmail.com (L.M.-O.)
2 Department of Biotechnology, Instituto Murciano de Investigación y Desarrollo Agrario y Alimentario (IMIDA), La Alberca, 30150 Murcia, Spain; sdac1@um.es
3 Departamento de Materiales, Óptica y Tecnología Electrónica, Universidad Miguel Hernández, Avda. Universidad s/n, Elche, 03202 Alicante, Spain; pmazon@umh.es
4 Instituto de Bioingeniería, Universidad Miguel Hernández, Avda. Universidad s/n, Elche, 03202 Alicante, Spain; piedad@umh.es
5 Servicio de Cirugía Ortopédica y Traumatología del Hospital Clínico Universitario Virgen de la Arrixaca, 30120 Murcia, Spain
* Correspondence: rubenrabadanros@gmail.com; Tel.: +34-620-754-831
† Both authors have contributed equally to the work.

Academic Editor: Carla Renata Arciola
Received: 7 February 2017; Accepted: 23 March 2017; Published: 27 March 2017

Abstract: The purpose of this study was to evaluate the bioactivity and cell response of a well-characterized Nurse's A-phase ($7CaO{\cdot}P_2O_5{\cdot}2SiO_2$) ceramic and its effect compared to a control (tissue culture polystyrene-TCPS) on the adhesion, viability, proliferation, and osteogenic differentiation of *ah*MSCs in vitro. Cell proliferation (Alamar Blue Assay), Alizarin Red-S (AR-s) staining, alkaline phosphatase (ALP) activity, osteocalcin (OCN), and collagen I (Col I) were evaluated. Also, field emission scanning electron microscopy (FESEM) images were acquired in order to visualise the cells and the topography of the material. The proliferation of cells growing in a direct contact with the material was slower at early stages of the study because of the new environmental conditions. However, the entire surface was colonized after 28 days of culture in growth medium (GM). Osteoblastic differentiation markers were significantly enhanced in cells growing on Nurse's A phase ceramic and cultured with osteogenic medium (OM), probably due to the role of silica to stimulate the differentiation of *ah*MSCs. Moreover, calcium nodules were formed under the influence of ceramic material. Therefore, it is predicted that Nurse's A-phase ceramic would present high biocompatibility and osteoinductive properties and would be a good candidate to be used as a biomaterial for bone tissue engineering.

Keywords: TCP-C_2S Nurse's A-phase ceramic; biomaterials; adult human mesenchymal stem cells; solid state reaction; biomedical applications

1. Introduction

The replacement of lost bone tissue using biomaterials has been an accepted procedure in several surgical disciplines (orthopaedic, oral-maxillofacial, and neural surgery, among others) [1], as a consequence of the drawbacks and effectiveness observed with the use of the autologous bone grafts (widely accepted as the most efficient) and allogenic bone grafts [2]. This fact has led to the development of alternative natural and synthetic materials to obviate the need for bone grafts in the

last decades. Tissue engineering can be conceptualised as the use of materials to promote new tissue formation and it involve interactions of the cells with the material [3]. Based on this, bone tissue repair may be one of the major applications of this emergent discipline. The development of bioceramics has provided promising alternatives to replace or increase parts of the skeletal system [4]. Ceramic-based bone graft substitutes include calcium phosphate (CaP) based ceramics such as hydroxyapatite, β-tricalcium phosphate, and bioactive glasses. These materials can be used alone or in combination with other ceramics or compounds as proteins or polymers as polylactic (PLA) or poly lactic-*co*-glycolic acids (PLLA) [5,6]. They have been developed for hard tissue repair due to their biocompatibility and osteoconductivity [7].

Currently, there is a constant need for bone implant formulations with osteointegrative properties. One of the approaches to improve bone stimulating features of these biomaterials is the incorporation of bone stimulator ions into their chemical compositions. Many researches have focused on preparation and characterization of bioceramic-based materials incorporating ions as Si, Ca, Mg, or Zn. Si or Ca in calcium silicate-based materials may play an important role in cell growth on the materials [8,9]. Si is recognised because of its unique effect on osteoblastic differentiation and thus bone mineralization [10].

Bone marrow is a mixture of hematopoietic, vascular, stromal, and mesenchymal cells capable of repairing parts of the skeletal system due to the ability of mesenchymal stem cells (MSCs) to differentiate into mesodermal lineage such as osteoblasts, chondrocytes, adipocytes, miocytes, etc. [11]. Stem cells have the potential to augment the performance of current bone graft substitutes and are the focus of a great deal of ongoing research. Therefore, a bone marrow cell culture system seems to be useful in order to study interactions occurring at the cell-material interface of implants directed to bone tissue engineering.

Compositions belonging to the sub-system Nurse's A-phase-silicocarnotite within the system $Ca_3(PO_4)_2$–Ca_2SiO_4 (TCP-C_2S) are promising candidates for preparing ceramic bone implants. [12–14]. Nurse's A-phase is a solid solution with an approximate composition of $7CaO{\cdot}P_2O_5{\cdot}2SiO_2$, which has been recently synthesized at temperatures around 1550 °C in our laboratory and represents a good candidate for biomedical applications [14–17]. The major goal of the present study was to evaluate the initial response of Si-Ca-P monophasic ceramic called Nurse´s A-phase in its ability to provide a cytocompatible optimal microenvironment for *ah*MSCs to enhance the attachment, adhesion, proliferation, and osteogenic differentiation with a view to using the material for bone tissue engineering in the context of advanced therapy medicinal products (ATMP).

2. Results

2.1. Inductively Coupled Plasma (ICP)

The release and ionic concentrations of soluble Si, Ca, and P elements by dissolution of the A phase ceramics in relation to time of immersion and analysed by ICP-OES are shown in Figure 1. The results showed a significant initial increase of the calcium (Ca) concentration during the first 24 h of exposure, reaching the maximum concentration (208 mg/L) after four days of immersion. The Ca concentration started to decrease from the fourth day until the last day of the test, when the concentration is minimal. The Phosphorus concentration (P) decreased at day 1 and it was maintained in values of 5 mg/L from the first week to the final of the experiment. The Silicon (Si) concentration increased from the beginning of the experiment, reaching the maximum value of release after 21 days of immersion (148 mg/L).

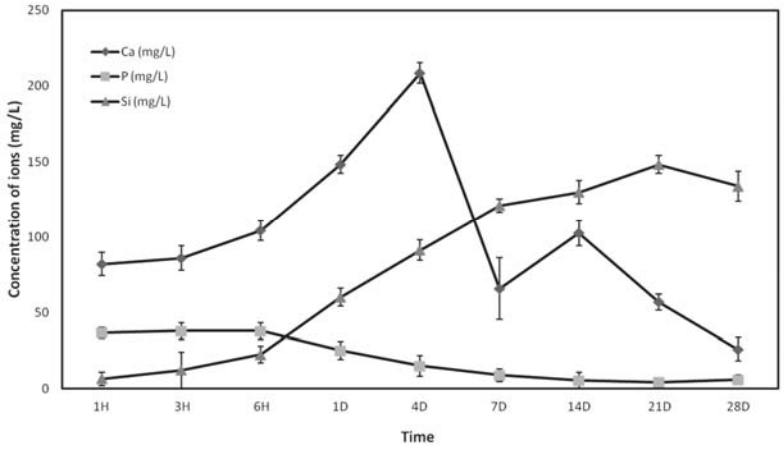

Figure 1. Changes of Si, Ca, and P concentrations of the growth medium (GM) after inmersion of Nurse's A-phase ceramic for various times.

2.2. Field Emission Scanning Electron Microscopy (FESEM).

In order to evaluate adhesion and morphology of *ah*MSCs growing on the Nurse's A-phase ceramic, the scaffolds cultured with cells were examined by FESEM at days 1, 3, 7, 14, 21, and 28 after the seeding in growth medium (GM) and just at 28 days in osteogenic differentiation medium (OM).

After 24 h in GM, *ah*MSCs seeded on the material surface were observed as individual cells (Figure 2A). Majority of them exhibited spherical or round shape (indicated by arrows), and some of them had a small central depression. The ceramic showed a granular layer composed of spicule-like structures and small nodules.

Three days after the seeding (Figure 2B), the cells showed an initial spreading, but some spherical forms still persisted as in the first day.

By day 7 (Figure 2C), all cells were stretched and they showed some thin cytoplasmatic extensions (filopodia). At this time, the presence of mineralization was also considerable. The nodules suggested the deposition of Nurse's A-phase material surface. Granules were also observed above cells, in contact with their membranes. This fact can be explained as a consequence of the formation of the nodules during the proliferation of the cells, covering the material and the cellular surfaces.

After 14 and 21 days (Figure 2D,E, respectively), *ah*MSCs seeded on the material showed a fibroblastic appearance, stretched and covering much of the surface. There were not cytotoxicity signals or morphological alterations throughout the study.

Major cell growth was observed at 28 days. The cells almost coated the whole material surface forming a monolayer and showing a greater number of interconnections. Abundant extracellular matrix expressed as fibrillar network (Figure 2G) was also observed at this time, occupying the intercellular gaps. Morphological differences were observed between cells cultivated with GM (Figure 2F) and OM (Figure 2H). The appearance of the cells treated with GM showed a fibroblastic appearance, while *ah*MSCs that grew with OM had polygonal shapes like osteoblastic cells.

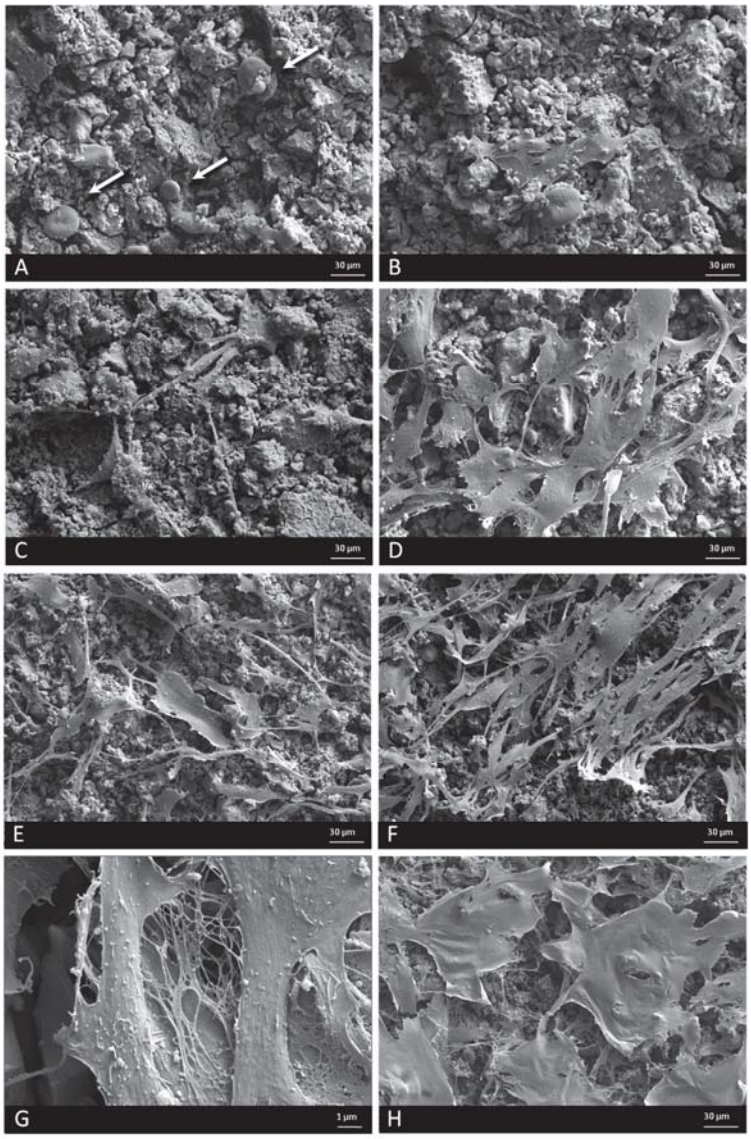

Figure 2. FESEM images of the *ah*MSCs cells grown on ceramic surfaces at 24 h (**A**) (300×) with rounded appearance (arrows), 3 days (**B**) (300×); 7 days (**C**) (300×); 14 days (**D**) (300×); 21 days (**E**) (300×); 28 days (**F**) (300×) in GM and at 28 days in osteogenic differentiation medium (OM) (**H**) (300×) and collagen bundles occupying intercellular gaps at 28 days (**G**) (3000×).

2.3. Cellular Metabolic Activity

Results of cellular metabolic activity by Alamar Blue are graphically displayed in Figure 3A. These results are shown as fluorescence arbitrary units (a.u.). *ah*MSCs cultured on Nurse's A-phase ceramic showed lower metabolic activity than control at early stages. The cells seeded on plastic (control) maintained the maximum value of metabolic activity seven days after the seeding.

A significant increase in the cellular metabolic activity was observed for cells cultured on Nurse's A-phase ceramic. By day 7, the cell metabolic activity raised but there were not significant differences (*t*-test, $p > 0.05$), 2 weeks after the seeding the cellular metabolic activity duplicated his average value (2070.80 a.u.) compared to the results obtained at seven days (882.70 a.u.). At 21 days, the metabolic activity continued growing up and it was significantly higher (*t*-test, $p < 0.05$), and by 28 days, it was registered the highest metabolic activity value for cells growing in OM (*t*-test, $p<0.05$). Remarkably, *ah*MSCs cultured on Nurse's A-phase ceramic with OM exhibited major metabolic

activity than cells cultured with GM, and there were not significant differences with control at the same experimental time (*t*-test, $p > 0.05$).

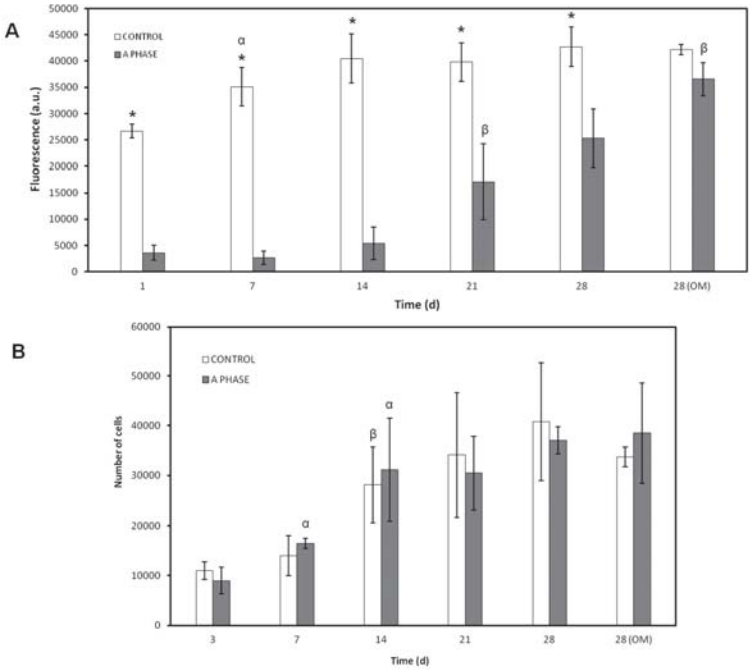

Figure 3. (**A**) Cellular metabolic activity of the cells seeded on the Nurse's A-phase scaffolds compared to cell cultures on plastic (positive controls) obtained by means of Alamar Blue Assay; (**B**) Proliferation assay of the cells seeded in indirect contact with Nurse's A-phase compared to cells growing on plastic used as control. (*) denotes significant differences ($p < 0.05$) between Nurse's A-phase and control at the same experimental time; (α) denotes significant differences ($p < 0.05$) between different experimental times obtained for control samples; (β) denotes significant differences ($p < 0.05$) between different experimental times obtained for cells growing on Nurse's A-phase scaffolds.

2.4. Proliferation Assay

As can be observed in Figure 3B, *ah*MSCs seeded in indirect contact with Nurse's A-phase and cells growing on plastic used as control were counted at different experimental times, using trypan blue staining (in order to confirm their viability), and no significant differences were found between both treatments (*t*-test, $p > 0.05$). Cells proliferated throughout the wells of the culture plates quickly, occupying the entire surface at 14 days. Once this happened, the number of cells remained constant until the end of the experiment (28 days).

2.5. Differentiation Assays

2.5.1. Alkaline Phosphatase (ALP) Activity

Results of ALP activity measurements obtained from *ah*MSCs cultured in indirect contact of Nurse's A-phase ceramics compared to plastic are graphically shown in Figure 4 as a function of optical density units (OD). The ALP activity is apparently prevented by Nurse's A-phase at early stages. In fact, from the day 7 to the day 21, its expression is always significantly lower in the cells cultured on biomaterials compared to the control (*t*-test, $p < 0.05$). The highest ALP activity is observed at 28 days coinciding with the addition of OM due to the induction of the differentiation of *ah*MSCs into osteoblasts. Contrary to the rest of the study, the cells cultured with Nurse's A-phase are significantly more active than control cells in this case (*t*-test, $p < 0.05$).

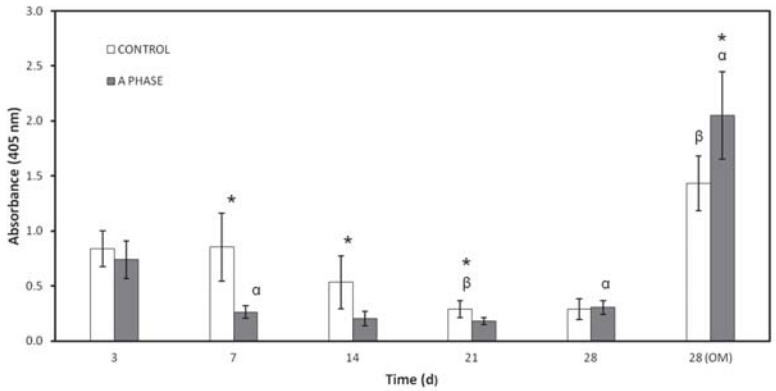

Figure 4. Alkaline phosphatase activity of the cells seeded in indirect contact with A phase compared to plastic used as control. (*) denotes significant differences ($p < 0.05$) between A phase and control at the same experimental time; (α) denotes significant differences ($p < 0.05$) between different experimental times obtained for control samples; (β) denotes significant differences ($p < 0.05$) between different experimental times obtained for cells growing on Nurse's A-phase scaffolds.

2.5.2. Alizarin Red-s (AR-s) Assay

The potential ability of cells to form calcium-rich mineralized nodules due to the presence of Nurse's A-phase ceramic discs in indirect contact with the *ah*MSCs was examined by Alizarin Red calcium staining under optical microscopy (Figure 5A) and quantified by spectrophotometry (Figure 5B).

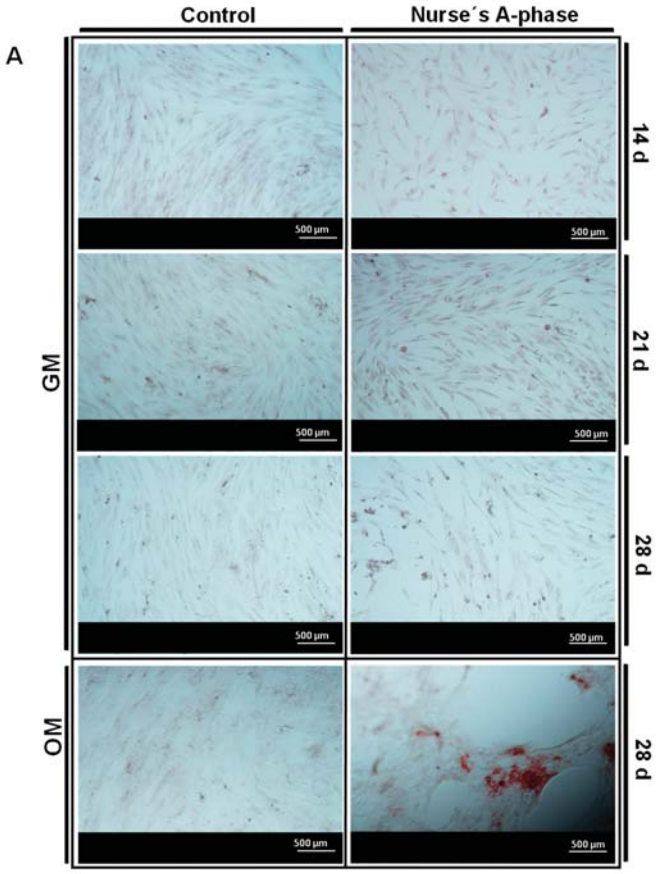

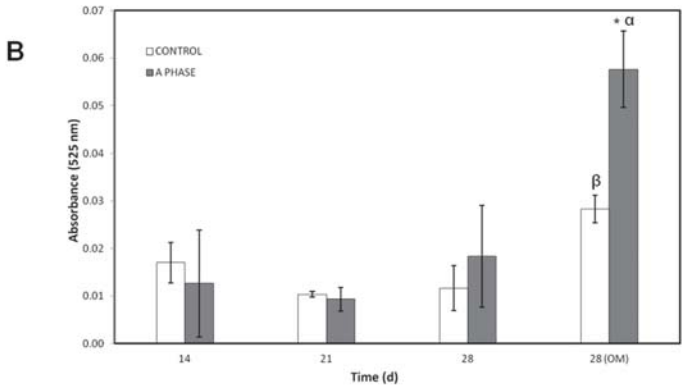

Figure 5. (**A**) AR-s images (×5 magnification) of the *ah*MSCs seeded as control in plastic and cells grown in indirect contact with Nurse's-A phase ceramic after 14 days, 21 days, 28 days with GM and 28 days in OM; (**B**) AR-s quantification of the cells seeded in indirect contact with A phase compared to control cells growing on plastic without the presence of the material. (*) denotes significant differences ($p < 0.05$) between A phase and control at the same experimental time; (α) denotes significant differences ($p < 0.05$) between different experimental times obtained for control samples; (β) denotes significant differences ($p < 0.05$) between different experimental times obtained for cells growing in indirect contact with Nurse's A-phase scaffolds.

As it is shown in Figure 5A, the control monolayers of *ah*MSCs cultured with GM and OM showed no staining. However, AR-s, *ah*MSCs growing in indirect contact with Nurse's A-phase scaffolds showed some areas clearly stained, especially intense 21 days after the seeding and until the end of the experiment. When cells were grown with OM at 28 days, the presence of the mineralized nodules dramatically increased. The quantitative examination of data obtained from this analysis confirmed the results of the visual study, with a higher value of OD in cells growing in the presence of A phase discs at 28 days, cultured with OM (*t*-test, $p < 0.05$).

2.5.3. Osteocalcin Assay

The concentration of osteocalcin (OCN) (ng/mL) released by *ah*MSCs to the culture medium was measured and is represented in Figure 6A. The cells seeded in indirect contact with Nurse's A-phase only released the OCN to the medium after 28 days of culture by means of induction with OM. However, control cells produced OCN from day 21, until the end of the experiment. There were no significant differences between growing them with OM or GM 28 days after the seeding (*t*-test, $p > 0.05$).

2.5.4. Collagen Type I Expression

Figure 6B shows immunofluorescence staining of Col I from extracellular matrix produced by *ah*MSC. The cells cultured as a control without any other stimulus than the presence of culture plastic are represented in the left column. Apparently, there were no differences between the images, and they seem to emit the same fluorescence from day 14 to day 28 (Figure 6A), even when adding OM. On the other hand, the cells seeded in indirect contact with Nurse's A-phase scaffolds (right column) showed increasing fluorescence intensity from day 14 until the end of the experiments, with the highest intensity at 28 days, regardless of the type of medium used. However, the arrangement of collagen seems to vary by acquiring rounded shapes using OM.

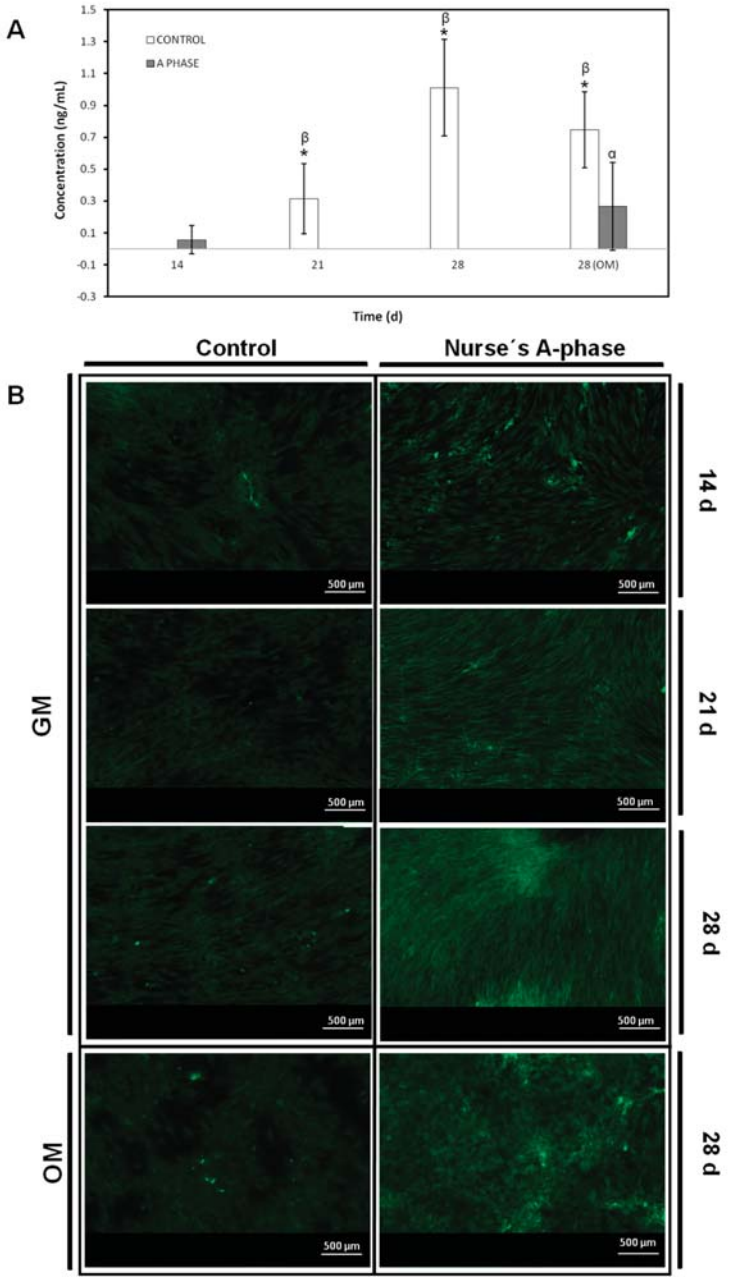

Figure 6. (**A**) Concentration of osteocalcin produced by the cells seeded in indirect contact with A-phase compared to control cells growing on plastic without the presence of the material. (*) denotes significant differences ($p < 0.05$) between A phase and control at the same experimental time; (α) denotes significant differences ($p < 0.05$) between different experimental times obtained for control samples; (β) denotes significant differences ($p < 0.05$) between different experimental times obtained for cells growing in indirect contact with Nurse's A-phase scaffolds; (**B**) Immunofluorescence staining of Collagen I images (×5 magnification) of the *ah*MSCs seeded as control in plastic and cells grown in indirect contact with Nurse's A-phase ceramic at 14 days, 21 days, and 28 days under different experimental conditions.

3. Discussion

Future biosynthetic bone substitutes based on natural and synthetic biomaterials may obviate the need for autologous bone grafts, considered today as the gold standard for bone repair [18]. Advances in tissue engineering will generate new carrier constructs that repair, regenerate, and restore tissue to its functional or physiologic state. An ideal biomaterial scaffold designed for bone tissue engineering requires osteoconductive, osteoinductive, and osteogenic properties. In addition, it must be degraded over time into non-toxic products, which can be metabolised by physiological mechanisms.

Adding inorganic elements to scaffolds could significantly improve the bioactivity of materials as previously seen with bioglass, bioceramics that contain CaO, SiO_2, and P_2O_5 or glass-ceramic [19,20]. These constructs are likely to include additional growth factors, evolving biological scaffold and incorporation of undifferentiated MSCs [21].

*ah*MSCs are commonly used to determine the responses of bone cells to biomaterials due to the fact that they are more sensitive to the action of ions delivery than the mouse or rats cells. Thus, for preclinical studies, *ah*MSCs are recommended instead of MSCs from animal origin [22]. The interaction and biological response of bone marrow–derived *ah*MSCs (proliferation and osteogenic differentiation) growing in contact with Nurse'A phase ceramics were investigated in this work.

Nurse's A material was conditioned by incubation in FBS for 1 h and 24 h prior to cell seeding because it has been indicated that the absorption of serum proteins is effective for cell proliferation [23] and cell adhesion.

In vitro studies are widely employed as preliminary tests to evaluate the biocompatibility of new materials with potential applications in biomedicine [24]. In order to evaluate the biocompatibility of Nurse's A-phase materials, we explored the attachment and growth of *ah*MSCs on scaffolds by means of FESEM. The cell proliferation was evaluated indirectly by the metabolic activity test Alamar blue and by indirect contact to evaluate the effect of ions released.

The ceramic discs cultured with *ah*MSCs examined by FESEM showed rounded globular cells on the ceramic surfaces at 24 h because they are not adhered yet. The cells were not fully adhered until day 7, when they showed the characteristic flattened polygonal shape and they were metabolically active, displaying higher values of proliferation. It has been demonstrated that levels of Ca concentrations up to 300 mg/L are cytotoxic [25], but lower concentrations are suitable for cell proliferation, differentiation, and extracellular matrix mineralization. The new biomaterial obtained, Nurse's A-phase, has a high proportion of CaO in its composition, causing the high level of Ca^{2+} ion release in the first week. Low levels of proliferation and rounded cell shape at first stages could be explained due to the high levels of calcium until day 4, when the peak of release was shown. However, the cells seeded in indirect contact with the material did not show a lower metabolic activity than the control cells, so the adaptation to the irregular and shifting surface due to ion exchange should be the most likely cause of the lower cellular activity shown by the Alamar blue assay.

After this adaptation period, the cells showed normal fibroblastic morphology, finally occupying the entire surface of the material and showing levels of metabolic activity similar to the control cells, indicating that Nurse's A-phase material is not cytotoxic and is highly biocompatible, favouring cell proliferation. From day 21 in culture, an abundant extracellular matrix with aspect of network was synthetized on the surface of all samples in the presence of the A phase materials. In fact, the intercellular gaps were occupied by that network fibrillar material. FESEM images of *ah*MSCs at 28 days cultured with OM displayed polygonal shapes typical for *ah*MSCs undergoing osteogenic differentiation, whereas cells cultured with GM at the same time showed fibroblastic pattern.

The combination of *ah*MSCs and biomaterials is a very important issue for tissue engineering and biomedicine. Thus, an evaluation of the osteogenic differentiation of *ah*MSCs on ceramics by ALP activity assay and calcium deposits staining is crucial. In adult MSCs, a high level of ALP is associated with the process of differentiation rather than with stemness. It is well known that ALP is considered an osteogenic marker expressed at the beginning of *ah*MSCs differentiation but may gradually decrease as the cell differentiate, while calcium nodules formation occurs at late stages [26].

Nurse's A material clearly seems to inhibit ALP activity, maybe because of the ions released to the environment. The role of ALP in osteoblastic differentiation is to participate in the formation of calcium-phosphate crystals by the release inorganic phosphates to the solution [27]. These crystals begin to form independently from ALP activity in the case of the bioceramics, due to the self-bioactivity of the ceramics, and this may be the cause of the reduction in *ah*MSCs ALP activity. On the other hand, ALP activity increased in cells incubated with A phase materials at 28 days after adding OM, concordant with the maximum release of silicon to the medium. The release of ions may play an important role in these processes and recent studies indicate that silicon promotes cell proliferation [10], ALP expression, and mineralization without affecting the rate of bone formation or bone loss [28]. Also, it has been demonstrated that low concentrations of Ca can stimulate cell differentiation indicated through increased ALP activity, whereas higher contents of Ca tend to decrease ALP stimulation levels. Moreover, osteogenic supplements, like ascorbic acid and β-glycerophosphate, up-regulate ALP gene expression [29]. Osteogenic supplements in OM, low concentrations of Ca, and increasing levels of Si from day 21 to day 28 may create a synergistic effect on the stimulation of ALP activity.

Other evidence of osteogenic differentiation includes mineral formation of *ah*MSCs. The mineralization over time was evaluated with AR-s staining. Control cultures remained colourless and there were no stained areas at any experimental time, while the cells seeded in indirect contact with A phase ceramics showed highly stained areas during the whole experiment and more intense staining at 28 days (especially after adding the OM). Mineralization begins with hydroxyapatite formation in the matrix vesicles budding from osteoblasts. Hydroxyapatite is formed from Ca^{2+} incorporated by the annexin calcium channel and from inorganic phosphate (Pi) [27]. In this case, the release of Ca^{2+} from A phase ceramic is high. The biomaterial provides also phosphorus ions constantly to the medium since the first day and ALP is very active at day 28, contributing this way with more P ions to the hydroxyapatite formation. All these processes explain the early formation of mineralization nodules in the presence of A phase ceramics and represent a potential improvement in the field of biomaterials for bone tissue engineering.

Nearly 90% of the organic matrix of bone is collagen (mainly Col I. Osteoblasts) synthesize, package, and export the organic constituents of bone matrix including Col I and OCN. The major non-collagenous protein produced is OCN, which makes up 1% of the matrix, so Col I and OCN are often used as markers for the bone formation process. Col I synthesis is implicated in first stages of osteogenic differentiation, while OCN is produced in later phases of differentiation (mature) [30]. Ca^{2+} acts through binding to a calcium sensing receptor, inducing the expression of osteoblastic differentiation markers such as Col I and may be the factor responsible to stimulate the intense inmunofluorescence of Col I detected in *ah*MSCs grown in indirect contact with A phase ceramic since early stages. OCN showed very low values until the last measurement (28 days), the result of which may be explained due the late expression of this marker described in the bibliography.

4. Materials and Methods

4.1. Porous Nurse's A-Phase Ceramic Preparation

Porous Nurse's A-phase ceramic was obtained by a solid-state reaction to form a stoichiometric mixture of calcium hydrogen phosphate anhydrous ($CaHPO_4$; Panreac S.L.U., Barcelona, Spain), calcium carbonate ($CaCO_3$ > 99.0 wt %; Fluka-Sigma Aldrich Quimica SL, Madrid, Spain) with an average particle size of 13.8 μm, and silicon oxide (SiO_2 > 99.7 wt %; Strem Chemicals UK Ltd., Cambridge, UK) with an average particle size <50 μm, The details of the technique and the characterization of the ceramic can be found in previous publications [22–24].

Discs-shaped Nurse's A-phase samples, measuring 7 mm in diameter and 3 mm in length, were cut from the sintered bulk with a diamond saw. Finally, Nurse's A-phase discs were individually packaged and sterilized by gas-plasma (Sterrad-1005TM, ASP, Irvine, CA, USA).

4.2. Inductively Coupled Plasma Optical Emission Spectroscopy (ICP)

The concentration of calcium (Ca), silicon (Si), and phosphorus (P) ions released from the Nurse's A-phase ceramic was determined by inductively coupled plasma optical emission spectroscopy (ICP-OES, PerkinElmer Optima 2000, Waltham, MA, USA). Five Nurse's A-phase discs were placed in a 48-well plate and 1 mL of growth medium (GM) which consisted of DMEM (Dubelcco´s Modified Eagle Medium) (Sigma-Aldrich, St. Louis, MO, USA) containing 10% FBS (Fetal Bovine Serum) (Sigma-Aldrich, St. Louis, MO, USA) and 100 $g \cdot mL^{-1}$ penicillin-streptomycin (Sigma-Aldrich, St. Louis, MO, USA) was added to each well, keeping the plates in a humidified atmosphere of 95% air, 7.5% CO_2 at 37 °C. The solutions were extracted to estimate ions concentration for 1 h, 3 h, 6 h, 1 day, 4 days, 7 days, 14 days, 21 days, and 28 days and immediately replaced by fresh GM.

4.3. Isolation, Characterization and Culture of Adult Human Bone Marrow-Derived Mesenchymal Stem Cells (ahMSCs)

The isolation and characterization of undifferentiated multipotent *ah*MSCs was described previously [31]. All the procedures were approved by the Institutional Ethical and Clinical Trials Committee (V. Arrixaca University Hospital of Murcia, Murcia, Spain). Briefly, bone marrow biopsy (40 mL) was aspirated from the iliac crest of three healthy male human volunteers aged 25–40 years. Informed consents were obtained from all of them. *ah*MSCs were isolate from the bone marrow based in their propensity to adhere to the bottom of standard tissue culture flasks (Nunc, Thermo Fisher, Geel, Belgium) and cultured in GM in a humidified atmosphere of 95% air, 7.5% CO_2 at 37 °C for three weeks. Initially, the medium was changed after 48 h to remove non-adherent cell and subsequently renewed three times a week. After 10 days in primary culture, when *ah*MSCs reached 85%–90% confluent, they were detached with 0.25% solution trypsin-EDTA (Sigma-Aldrich, St. Louis, MO, USA), centrifuged at 300 rpm for 10 min and subcultured in an initial density of 5×10^3 $cell \cdot cm^{-2}$ in 75 cm^2 flasks. Cells have been characterized following the criteria of International Society of Cell Therapy (ISCT) [32] (data not shown).

After cell expansion, *ah*MSCs of passage 3 (P3) were used for all experiments.

4.4. Field Emission Scanning Electron Microscopy

Cell adherence, distribution, morphology, and proliferation of the *ah*MSCs studies were performed to investigate the biofuncionality of the material at 1, 3, 7, 14, 21, and 28 days after the seeding. *ah*MSCs were seeded onto the tops of disc-shapped Nurse's A-phase at a density of 5×10^3 $cells \cdot cm^{-2}$ placed in 48 well-plate and cultured with GM at 37 °C, 7.5% CO_2 in a humidified incubator. Some of the *ah*MSCs cell cultures were also induced to differentiate replacing the GM by MSC osteogenic differentiation medium (OM) at 21 days, which consisted of the GM supplemented with L-ascorbic acid-2-phosphate (0.2 mM; Sigma-Aldrich, St. Louis, MO, USA), dexamethasone (10 nM; Sigma), and β-glycerolphospathe (10 nM; Merck, Darmstadt, Germany). GM or OM was replaced every three days. After the incubation period, the cell-cultured disks or construct were rinsed with phosphate buffer solution (PBS) for 10 min and fixed for 1 h with 3% glutaraldehyde in 0.1 M cacodylate buffer, then were post fixed with 1% osmium tetroxide. Then, the cell-cultured constructs were thoroughly rinsed with PBS and dehydrated in a graded series of ethanol solutions (30%, 50%, 70%, 90%, and 100% *v*/*v*). The critical point drying was undertaken with liquid CO_2. Finally, specimens were sputter-coated with gold and examined by Field Emission Scanning Electron Microscopy (Merlin™ VP Compact, Carl Zeiss Microscopy S.L., Oberkochen, Germany).

4.5. Cellular Metabolic Activity

In order to evaluate the biological properties of the Nurse's A-phase material in terms of influence in the metabolic activity of the cells Alamar Blue assay was used (Alamar Blue; Invitrogen, Carlsbad, CA, USA). Metabolic activity is commonly used as an indirect measure of cell proliferation. This assay was based on the redox activity of living cell and the metabolic activity was assessed by fluorescence measurement. Briefly, cells were seeded on biomaterial disks in 48-well plates at a cell

density of 5 × 10^3 cells·cm^{-2} and incubated in the same culture conditions described above. In addition, *ah*MSCs were seeded onto tissue culture-treated polystyrene (TCPS) culture plate served as a positive control. Alamar Blue assay was performed at 1, 7, 14, 21, and 28 days after the seeding. ahMSCs were also induced to osteoblastic differentiation replacing GM by OM at 21 days. Medium was replaced every three days. At the end of the culture period, the medium was discarded and the wells were washed twice with phosphate buffer solution (PBS). Each well was filled with 200 µL of fresh medium containing 10% (*v*/*v*) of Alamar Blue reagent and were incubated at 37 °C for 4 h. The reacted dissolution was then transferred to a 96-well plate and the fluorescence measurements were determined directly in a Synergy MX ultraviolet visible (UV-Vis) (Bio Tek Instruments Inc., Winooski, VT, USA) at excitation and emission wavelengths of 560 nm and 590 nm, respectively. The assay was performed at least in triplicate. Results are reported as arbitrary units (a.u.).

4.6. Proliferation Assay

To measure cell proliferation and density in indirect contact with Nurse's A-phase, scaffolds were placed in transwell inserts in 24-well plates and *ah*MSCs were seeded at the bottom of each well at a density of 5 × 10^3 cells·cm^{-2} and incubated in GM at 37 °C in a humidified atmosphere consisting of 95% air and 7.5% CO_2. *ah*MSCs were also induced to osteoblastic differentiation by replacing GM by OM at 21 days. The trypan blue solution (0.4%) (Thermofisher Scientific, Waltham, MA, USA) is routinely used as cell staining to assess cell viability based on the concept that viable cells do not absorb waterproof dyes. Living cells were counted using a Neubauer chamber at 3, 7, 14, 21, and 28 days. Others *ah*MSCs were seeded onto plastic in order to have a positive control.

4.7. Differetiation Assays

The ability of ahMSCs to differentiate into osteoblasts was studied by alkaline phosphatase (ALP) activity, osteocalcin (OCN) and collagen type I (Col I) production, and formation of nodules of mineralization (in vitro). ALP and Col I are both initial osteogenic markers such that their value may increase in the beginning of osteogenic differentiation. OCN and mineralization are late osteogenic markers.

To carry out all these indirect studies, Nurse's A phase scaffolds were placed in transwell inserts in 24-well plates and *ah*MSCs were seeded at the bottom of the wells at a density of 5 × 10^3 cells·cm^{-2} and incubated at 37 °C in a humidified atmosphere consisting of 95% air and 7.5% CO_2.

4.7.1. Alkalne Phosphatase (ALP) Activity

ALP is an enzyme responsible for removing phosphate groups from many types of molecules. It is expressed by cells during osteogenesis and it is well established as an osteogenic differentiation marker [26]. For these studies the measurements were taken in triplicate at 3, 7, 14, 21, and 28 days after the seeding. Also, *ah*MSCs were induced to osteoblastic differentiation replacing GM by OM at 21 days. *ah*MSCs were also seeded on plastic culture plates in order to have a control of differentiation to osteoblasts without any other stimulus than the presence of OM.

ALP was measured by Quantitative Alkaline Phosphatase ES Characterization Kit (Millipore, Billerica, MA, USA). To quantify ALP activity, the cells were treated following the manufacturer's protocol and the absorbance of enzyme product was measured at 405 nm on a spectrophotometer (Bio Tek Instruments Inc., Winooski, VT, USA).

4.7.2. Alizarin Red-s (AR-s) Assay

The presence of calcium deposition or nodules of mineralization was evaluated by the specific binding of Alizarin Red (Osteogenesis Quantitation Kit, Millipore, Billerica, MA, USA) to calcium deposits. For this purpose the measurements were taken in triplicate at 14, 21 and 28 days after the seeding. *ah*MSCs were also induced to differentiate replacing GM by MSC osteogenic differentiation medium (OM) at 21 days. After culturing the cells, they were fixed 10 min with 8% paraformaldehyde and stained for 30 min at RT with Alizarin Red Stain Solution. Stained areas were

visualized using a Nikon Eclipse 50i microscope (Nikon, Melville, NY, USA), and some photographs were taken using a Nikon *DS-Fi1* digital microscope camera (Nikon, Melville, NY, USA). To quantify matrix mineralization, the samples were treated following the manufacturer's protocol and the absorbance of Alizarin Red S extracts was measured at 525 nm on a spectrophotometer (Bio Tek Instruments Inc., Winooski, VT, USA).

4.7.3. Osteocalcin (OCN) Assay

The OCN production was determined in supernatants using Osteocalcin ELISA kit (Thermofisher Scientific, Waltham, MA, USA) following the manufacturer's instructions. For this purpose, serum was removed from the culture medium five days before carrying out the determinations. The medium was collected at days 7, 14, 21, and 28 and kept at −20 °C until analysis following manufacturer's protocol. Three determinations of each simple and standard kit were carried out.

Briefly, 25 µL of medium was pipetted out into microtiter plate coated with anti-osteocalcin antibody followed by 100 µL of anti-osteocalcin labelled with HRP (horseradish peroxidase) and incubated for 2 h at room temperature. After washing with wash solution, 100 µL of chromogenic solution was added to each well for 30 min at room temperature followed by the addition of 100 µL of stopping solution into each well. The absorbance was read at 405 nm (Bio Tek Instruments Inc., Winooski, VT, USA). A calibration curve was plotted and the OCN concentration in sample was determined by interpolation from the calibration curve.

4.7.4. Collagen Type I Expression

Col I expression was tested by immunofluorescence staining at 14, 21, and 28 days. *ah*MSCs were stained after being induced to differentiate by replacing GM by OM at 21 days (28 OM). Briefly, cells were washed three times with PBS, fixed, and permeabilized with cooled Methanol–Acetone solution (1:1) at 20 °C for 10 min. Samples were then blocked with a blocking solution (0.1% TRITON, 0.3% BSA, 10% FBS in PBS 1×) for 30 min at 37 °C. Labelling was performed by incubating the primary antibody in a blocking solution at 4 °C over night. Next samples were incubated with secondary antibody in a blocking solution for 1 h at RT. Then samples were washed with deionized water and mounted. Samples were visualized using a Nikon Eclipse 50i fluorescence microscope (Nikon, Melville, NY, USA) with excitation filters of 494 nm (green, Calcein) and some photographs were taken using a Nikon *DS-Fi1* digital microscope camera (Nikon, Melville, NY, USA).

5. Calculation

Quantitative data are presented as means ± standard deviation (SD) of at least three specimens per treatment condition. *t*-student test was used for comparison between groups. A *p*-value of less than 0.05 was considered statistically significant.

6. Conclusions

This work constitutes the first step to evaluate the potential use of a novel Nurse's A-phase material as a scaffold for bone tissue engineering. The results stated in terms of biocompatibility, adhesion, and proliferation of *ah*MSCs prove that this A phase ceramic is not cytotoxic and stimulates optimal growth of the cells comparable to *ah*MSCs cultured on plastic.

The expression of the studied osteogenic markers was always more intense in cells growing under the influence of A phase materials itself, but especially when OM was included in the culture conditions. These promising results make Nurse's A material a promising candidate to be employed as a new bone graft substitute or scaffold for bone tissue engineering.

Future work will be focused on in vivo studies and improvements of the material in terms of composition, by means of the incorporation of different molecules such as growth factors or some biocompatible polymers.

Acknowledgments: Part of this work was supported by the Spanish Ministry of Economy and Competitiveness (MINECO) contract grant number: MAT2013-48426-C2-2-R.

Author Contributions: Meseguer-Olmo L. and De Aza P.N. conceived and designed the experiments; Rabadan-Ros R. and Aznar-Cervantes S. performed the experiments; Mazón P. and Ros-Tarraga P. performed the preparation of ceramics; Rabadan-Ros R., De Aza P.N. and Meseguer-Olmo L. wrote the paper. All of the authors contributed to the analyses and discussion of the results.

Conflicts of Interest: The authors declare no conflict of interest.

References

1. Henkel, J.; Woodruff, M.A.; Epari, D.R.; Steck, R.; Glatt, V.; Dickinson, I.C.; Choong, P.F.; Schuetz, M.A.; Hutmacher, D.W. Bone regeneration based on tissue engineering conceptions—A 21st century perspective. *Bone Res.* **2013**, *1*, 216–248.
2. Laurencin, C.T.; Ambrosio, A.M.; Borden, M.D.; Cooper, J.A. Tissue engineering: Orthopedic applications. *Annu. Rev. Biomed. Eng.* **1999**, *1*, 19–46.
3. Bosetti, M.; Cannas, M. The effect of bioactive glasses on bone marrow stromal cells differentiation. *Biomaterials* **2005**, *26*, 3873–3879.
4. Hench, L.L. Bioceramics: From concept to clinic. *J. Am. Ceram. Soc.* **1991**, *74*, 1487–1510.
5. Puppi, D.; Chiellini, F.; Piras, A.; Chiellini, E. Polymeric materials for bone and cartilage repair. *Prog. Polym. Sci.* **2010**, *35*, 403–440.
6. Hild, N.; Schneider, O.D.; Mohn, D.; Luechinger, N.A.; Koehler, F.M.; Hofmann, S.; Vetsch, J.R.; Thimm, B.W.; Müller, R.; Stark, W.J. Two-layer membranes of calcium phosphate/collagen/PLGA nanofibres: In vitro biomineralisation and osteogenic differentiation of human mesenchymal stem cells. *Nanoscale* **2011**, *3*, 401–409.
7. Hutmacher, D.W.; Schantz, J.T.; Lam, C.X.F.; Tan, K.C.; Lim, T.C. State of the art and future directions of scaffold-based bone engineering from a biomaterials perspective. *J. Tissue Eng. Regen. Med.* **2007**, *1*, 245–260.
8. Hoppe, A.; Güldal, N.S.; Boccaccini, A.R. A review of the biological response to ionic dissolution products from bioactive glasses and glass-ceramics. *Biomaterials* **2011**, *32*, 2757–2774.
9. Valerio, P.; Pereira, M.M.; Goes, A.M.; Leite, M.F. The effect of ionic products from bioactive glass dissolution on osteoblast proliferation and collagen production. *Biomaterials* **2004**, *25*, 2941–2948.
10. Shie, M.Y.; Ding, S.J.; Chang, H.C. The role of silicon in osteoblast-like cell proliferation and apoptosis. *Acta Biomater.* **2011**, *7*, 2604–2614.
11. Bruder, S.P.; Jaiswal, N.; Haynesworth, S.E. Growth kinetics, self-renewal, and the osteogenic potential of purified human mesenchymal stem cells during extensive subcultivation and following cryopreservation. *J. Cell. Biochem.* **1997**, *64*, 278–294.
12. De Aza, P.N.; Mate-Sanchez de Val, J.E.; Baudin, C.; Perez Albacete-Martínez, C.; Armijo Salto, A.; Calvo-Guirado, J.L. Bone neoformation of a novel porous resorbable Si-Ca-P-based ceramic with osteoconductive properties: Physical and mechanical characterization, histological and histomorphometric study. *Clin. Oral Implants Res.* **2016**, *27*, 1368–1375.
13. Ros-Tárraga, P.; Mazón, P.; Rodríguez, M.A.; Meseguer-Olmo, L.; De Aza, P.N. Novel resorbable and osteoconductive calcium silicophosphate scaffold induced bone formation. *Materials* **2016**, *9*, doi:10.3390/ma9090785.
14. Rabadan-Ros, R.; Velásquez, P.A.; Meseguer-Olmo, L.; De Aza, P.N. Morphological and structural study of a novel porous nurse's a ceramic with osteoconductive properties for tissue engineering. *Materials* **2016**, *9*, doi:10.3390/ma9060474.
15. Lugo, G.; Mazón, P.; De Aza, P. Phase transitions in single phase Si–Ca–P-based ceramic under thermal treatment. *J. Eur. Ceram. Soc.* **2015**, *35*, 3693–3700.
16. Lugo, G.J.; Mazón, P.; Baudin, C.; De Aza, P.N. Nurse's A-phase: Synthesis and characterization in the binary system Ca_2SiO_4–$Ca_3(PO_4)_2$. *J. Am. Ceram. Soc.* **2015**, *98*, 3042–3046.
17. Lugo, G.J.; Mazón, P.; Piedad, N. Material processing of a new calcium silicophosphate ceramic. *Ceram. Int.* **2016**, *42*, 673–680.
18. Kolk, A.; Handschel, J.; Drescher, W.; Rothamel, D.; Kloss, F.; Blessmann, M.; Heiland, M.; Wolff, K.D.; Smeets, R. Current trends and future perspectives of bone substitute materials—From space holders to innovative biomaterials. *J. Cranio Maxillofac. Surg.* **2012**, *40*, 706–718.

19. Taherkhani, S.; Moztarzadeh, F. Influence of strontium on the structure and biological properties of sol–gel-derived mesoporous bioactive glass (mbg) powder. *J. Sol Gel Sci. Technol.* **2016**, *78*, 539–549.
20. García-Páez, I.H.; Carrodeguas, R.G.; Antonio, H.; Baudín, C.; Pena, P. Effect of mg and Si co-substitution on microstructure and strength of tricalcium phosphate ceramics. *J. Mech. Behav. Biomed. Mater.* **2014**, *30*, 1–15.
21. Giannoudis, P.V.; Dinopoulos, H.; Tsiridis, E. Bone substitutes: An update. *Injury* **2005**, *36*, S20–S27.
22. Moreau, J.L.; Xu, H.H. Mesenchymal stem cell proliferation and differentiation on an injectable calcium phosphate–chitosan composite scaffold. *Biomaterials* **2009**, *30*, 2675–2682.
23. Puleo, D.; Nanci, A. Understanding and controlling the bone–implant interface. *Biomaterials* **1999**, *20*, 2311–2321.
24. Kirkpatrick, C.; Bittinger, F.; Wagner, M.; Köhler, H.; Van Kooten, T.; Klein, C.; Otto, M. Current trends in biocompatibility testing. *Proce. Inst. Mech. Eng. Part H J. Eng. Med.* **1998**, *212*, 75–84.
25. Malaval, L.; Liu, F.; Roche, P.; Aubin, J.E. Kinetics of osteoprogenitor proliferation and osteoblast differentiation in vitro. *J. Cell. Biochem.* **1999**, *74*, 616–627.
26. Golub, E.E.; Boesze-Battaglia, K. The role of alkaline phosphatase in mineralization. *Curr. Opin. Orthop.* **2007**, *18*, 444–448.
27. Orimo, H. The mechanism of mineralization and the role of alkaline phosphatase in health and disease. *J. Nippon Med. Sch.* **2010**, *77*, 4–12.
28. Dong, M.; Jiao, G.; Liu, H.; Wu, W.; Li, S.; Wang, Q.; Xu, D.; Li, X.; Liu, H.; Chen, Y. Biological silicon stimulates collagen type 1 and osteocalcin synthesis in human osteoblast-like cells through the BMP-2/Smad/RUNX2 signaling pathway. *Biol. Trace Elem. Res.* **2016**, *173*, 306–315.
29. Cheng, S.L.; Yang, J.W.; Rifas, L.; Zhang, S.F.; Avioli, L.V. Differentiation of human bone marrow osteogenic stromal cells in vitro: Induction of the osteoblast phenotype by dexamethasone. *Endocrinology* **1994**, *134*, 277–286.
30. Kular, J.K.; Basu, S.; Sharma, R.I. The extracellular matrix: Structure, composition, age-related differences, tools for analysis and applications for tissue engineering. *J. Tiss. Eng.* **2014**, *5*, doi:10.1177/2041731414557112.
31. De Aza, P.N.; García-Bernal, D.; Cragnolini, F.; Velasquez, P.; Meseguer-Olmo, L. The effects of Ca_2SiO_4–$Ca_3(PO_4)_2$ ceramics on adult human mesenchymal stem cell viability, adhesion, proliferation, differentiation and function. *Mater. Sci. Eng. C Mater. Biol. Appl.* **2013**, *33*, 4009–4020.
32. Dominici, M.; Le Blanc, K.; Mueller, I.; Slaper-Cortenbach, I.; Marini, F.; Krause, D.; Deans, R.; Keating, A.; Prockop, D.; Horwitz, E. Minimal criteria for defining multipotent mesenchymal stromal cells. The international society for cellular therapy position statement. *Cytotherapy* **2006**, *8*, 315–317.

7. ARTÍCULO 3

applied sciences

MDPI

Article

Impact of a Porous Si-Ca-P Monophasic Ceramic on Variation of Osteogenesis-Related Gene Expression of Adult Human Mesenchymal Stem Cells

Rabadan-Ros Ruben [1,*], Revilla-Nuin Beatriz [2], Mazón Patricia [3], Aznar-Cervantes Salvador [4], Ros-Tarraga Patricia [1], De Aza Piedad N. [5] and Meseguer-Olmo Luis [1]

1 Tissue Regeneration and Repair Group: Orthobiology, Biomaterials and Tissue Engineering, UCAM-San Antonio Catholic University of Murcia, Guadalupe, 30107 Murcia, Spain; p.ros.tarraga@gmail.com (R.-T.P.); lmeseguer.doc@gmail.com (M.-O.L.)

2 Genomic Unit, Biomedical Research Institute of Murcia (IMIB-Arrixaca-UMU), University Clinical Hospital "Virgen de la Arrixaca", University of Murcia, El Palmar, 30120 Murcia, Spain; brevilla_nuin@yahoo.es

3 Department of Materials, Optics and Electronic Technology, Miguel Hernández University, Avda. Universidad s/n, Elche, 03202 Alicante, Spain; pmazon@umh.es

4 Department of Biotechnology, Instituto Murciano de Investigación y Desarrollo Agrario y Alimentario (IMIDA), La Alberca, 30150 Murcia, Spain; sdac1@um.es

5 Institute of Bioengineering, Miguel Hernández University, Avda. Universidad s/n, Elche, 03202 Alicante, Spain; piedad@umh.es

* Corresponding author: rubenrabadanros@gmail.com; Tel.: +34-620-754-831

Received: 4 December 2017; Accepted: 21 December 2017; Published: 1 January 2018

Abstract: This work evaluates in vitro the influence of a new biocompatible porous Si-Ca-P monophasic ($7CaO{\cdot}P_2O_5{\cdot}2SiO_2$) ceramic on the cellular metabolic activity, morphology and osteogenic differentiation of adult human mesenchymal stem cells (*ah*MSCs) cultured in basal growth medium and under osteogenic inductive medium. Alamar Blue Assay and FESEM were carried out in order to monitor the cell proliferation and the shape of the cells growing on the Si-Ca-P monophasic ceramic during the study period. The osteogenic differentiation of *ah*MSCs was investigated by means of immunofluorescent staining (osteocalcin, osteopontin, heparan sulphate and collagen type I expression), quantitative reverse transcription polymerase chain reaction (qRT-PCR) (integrin-binding sialoprotein, osteocalcin, alkaline phosphatase, osteopontin, osteonectin, runt-related transcription factor 2 and collagen type I) and expression of surface markers (CD73, CD90 and CD105). We could check osteogenic differentiation in *ah*MSCs growing under the influence of Si-Ca-P monophasic ceramics itself, but especially when growth medium was replaced by osteogenic medium in the culture conditions. These results allowed us to conclude that the new Si-Ca-P monophasic scaffold greatly enhanced *ah*MSCs proliferation and osteogenic differentiation; therefore, it may be considered to be employed as a new bone graft substitute or scaffold for bone tissue engineering.

Keywords: bioceramics; Si-Ca-P based materials; mesenchymal stem cells; osteogenic differentiation; tissue engineering

1. Introduction

Tissue engineering can be conceptualized as the use of a combination of cells, materials, and biochemical and physicochemical factors to improve or replace biological tissues [1]. Based on this, bone tissue repair-regeneration has been the focus and may be one the major applications of this discipline. A great number of strategies have been evolved over the past decades towards engineering tissue replacements, but the most common approach implies the use of reabsorbable synthetic materials

as scaffolds acting as a 3D-framework for cell growth in vitro. An ideal synthetic matrix for bone regeneration should fulfill some requirements as being bioactive and reabsorbed at medium term, displaying mechanical characteristics similar to bone tissue and, at the same time, possessing the ability to enhance cell proliferation while supporting tissue specific differentiation [2].

Among various biomaterials, calcium phosphate-based ceramics (CaP) play a critical role as scaffold in bone tissue engineering. Previously, from 1960 to 1970, these materials have been widely used to repair bone defects because of their properties of biocompatibility, safety, unlimited availability, high cost-effectiveness ratio and similarity to mineral fraction of the bone [3]. CaP ceramics can be used alone or in combination with other ceramics or compounds as proteins or polymers [4,5]. The biphasic CaP ceramics have some advantages over simple-phase ceramics by presenting favourable bioactivity and controllable biodegradation in vivo [6]. Besides, they can be used as a vector for therapeutic molecules. Alternatively, it has been demonstrated that they integrate directly in host bone tissue through formation of an apatite interface layer [7]. CaP ceramics can promote osteogenic cellular activities, mineral deposition and bone formation. Furthermore, the mineralization of the surface of these ceramics to form the apatite layer may facilitate quick protein fixing on the surface and consequently, promote cell adhesion, proliferation and osteogenic differentiation. For this reason, the surface mineralization prior to implantation by means of the use of simulated body fluid (SBF) may increase the bioactivity to improve the osteointegration with the host bone [8].

The incorporation of specific ions into the chemical composition of bioceramics is expected to improve bone stimulating features. Silicon (Si) in CaP-based materials may play an important role in cell growth on the materials [9,10]. Si is recognised because of its unique effect on osteoblastic differentiation and thus bone mineralization [11].

Consequently, we have focused our attention on synthesizing a novel porous Si-Ca-P monophasic ceramic (SCP-c) by means of a solid-state reaction that was able to induce calcium deficient hydroxyapatite mineralization in simulated body fluid through the formation of two well differentiated Si-Carbonate-Hydroxyapatite layers [12]. Moreover, its properties of degradability and stimulation of bone tissue formation [13] indicated that the ceramic material possesses osteoconductive in vivo properties. The traditional in vitro techniques evidenced the biocompatibility of the SCP-c and its potential ability to stimulate osteogenic differentiation [14]. However, little has been studied in depth about the impact on the osteogenic differentiation of a primary adult human mesenchymal stem cells (*ah*MSCs) culture. In order to ensure that this new biomaterial induces *ah*MSCs differentiation to osteoblasts and to know the route by which it acts, in this work we have investigated and monitored the expression of genetic markers involved in the osteogenic differentiation of *ah*MSCs as well as the expression of different proteins of the extracellular matrix and surface markers (surface antigens) to give greater consistency to our results.

2. Materials and Methods

2.1. Preparation of Porous Si-Ca-P Monophasic Ceramic (SCP-c)

SCP-c powder was synthetized in our laboratory, according to a previously described processing method [3]. For specific information related to its mechanical behavior and physicochemical characterization, please consult the following publications [15,16]. The ceramic was synthetized from commercial-grade calcium hydrogen phosphate anhydrous ($CaHPO_4$; Panreac S.L.U., Barcelona, Spain), calcium carbonate ($CaCO_3$ > 99.0 wt %; Fluka-Sigma Aldrich Quimica SL, Madrid, Spain) with an average particle size of 13.8 µm, and silicon oxide (SiO_2 > 99.7 wt %; Strem Chemicals UK Ltd., Cambridge, UK) with an average particle size <50 µm. We can briefly describe the process of obtaining the porous Si-Ca-P material as a solid state reaction from the above-mentioned stoichiometric products that were homogenized, milled and isostatically preset, followed by a thermal treatment at 1300 °C/3 h and annealing at 1200 °C/24 h.

For the present investigation, SCP-c was cut in disc shapes of 7 mm in diameter and 3 mm in length, and gas-plasma was used for sterilization (Sterrad-1005TM, ASP, Irvine, CA, USA). Immediately before its use, each disk was placed in a well of a 24-well plate containing fetal bovine serum (FBS) (Sigma, St. Louis, MO, USA) and incubated at 37 °C for 1 h in a cell culture incubator to favour cell adhesion to the surface of the material. After that, disks were dried under dry heat at the same temperature.

2.2. Isolation, Characterization and Primary Culture of Adult Human Bone Marrow-Derived Mesenchymal Stem Cells (ahMSCs)

*ah*MSCs were isolated as previously described [17] and characterized following the criteria of International Society of Cell Therapy (ISCT) [18] (data not shown).

After cell expansion, *ah*MSCs of passage 3 (P3) were prepared for use in all subsequent experiments. For examination of attachment and proliferation assays, cells were seeded onto the top of disc-shaped SCP-c at a density of 5×10^3 cells·cm^{-2} in a 48-well plate and cultured with growth medium (GM) which consists of Dulbecco's Minimal Essential Medium (DMEM) (Sigma-Aldrich, St. Louis, MO, USA) supplemented with 10% (v/v) FBS and routine antibiotics (penicillin/ streptomycin). To conduct osteogenic differentiation studies, three SCP-c scaffolds were placed in transwell inserts in 6-well plates (Sigma-Aldrich, Corning, NY, USA) and *ah*MSCs were seeded on the bottom of the wells at a density of 5×10^3 cells cm^{-2} and cultured with GM. Cells seeded onto tissue culture-treated polystyrene (TCPS) culture plate (Sigma-Aldrich, Corning, NY, USA) served as a positive control.

Plates were incubated at 37 °C in a humidified atmosphere consisting of 95% air and 7.5% CO_2. Some of the *ah*MSCs cell cultures were also induced to osteogenic differentiation replacing the GM by osteogenic differentiation medium (OM) from the 21st day, which consisted of the GM supplemented with l-ascorbic acid-2-phosphate (0.2 mM; Sigma-Aldrich, St Louis, MO, USA), dexamethasone (10 nM; Sigma-Aldrich, Corning, NY, USA), and β-glycerolphospathe (10 nM; Merck, Darmstadt, Germany).

2.3. Field Emission Scanning Electron Microscopy (FESEM)

After 7, 14, 21 and 28 days of seeding, FESEM was used to examine cell attachment and proliferation. After fixing with glutaraldehyde (Sigma-Aldrich, Corning, NY, USA), scaffolds were dehydrated with ethanol, critical point dried with liquid CO_2 and then examined by FESEM Microscopy (Merlin™ VP Compact, Carl Zeiss Microscopy S. L., Oberkochen, Germany) after coating with gold.

2.4. Cellular Metabolic Activity Assay

Alamar Blue (Invitrogen, Carlsbad, CA, USA) was used to assess the metabolic activity of the *ah*MSCs at 7, 14, 21 and 28 days after the seeding. Fresh medium (200 µL) containing 10% (v/v) of Alamar Blue reagent was added to each well for 4 h at 37 °C in darkness. The fluorescence was read directly in a Synergy MX ultraviolet visible (UV-Vis) spectrophotometer (Bio Tek Instruments Inc., Winooski, VT, USA) at excitation and emission wavelengths of 560 and 590 nm, respectively.

2.5. Osteogenic Differentiation Assays

The ability of *ah*MSCs to differentiate into osteoblastic lineage cells was studied at 7, 14, 21 and 28 days by inmunofluorescence staining (heparin sulphate, osteocalcin and collagen type I), expression of representative *ah*MSCs surface markers (CD73, CD90 and CD105) and quantitative real-time polymerase chain reaction (qRT-PCR) assay for osteogenic markers.

2.5.1. Immunofluorescence Staining Assay: Heparan Sulphate (HS), Osteocalcin (OCN), Osteopontin (OPN) and Collagen Type I (Col I) Expression

For inmunofluorescence staining of HS, OCN, OPN and Col I, cells were fixed with 4% formaldehyde at 4 °C, and permeabilized with cooled Methanol–Acetone solution (1:1) (Sigma-Aldrich,

St. Louis, MO, USA) at 20 °C for 10 min. Labelling and visualization were performed as previously described [14].

2.5.2. Surface Markers Cluster Differentiation (CD)

The cells were detached from the culture flasks and centrifuged. Then, they were resuspended in buffer (2% FBS, 0.1% NaN_3 in PBS 1X (Sigma-Aldrich, Corning, NY, USA)) and counted. Aliquots of 1×10^5 cells were made in 25 µL of buffer into 3 tubes. Antibodies (CD90-FITC, CD73-PE and CD105-Alexa Fluor 647 and isotypes as negative controls) (Becton Dickinson Co., Franklin Lakes, NJ, USA.) were added at the dilution standardised by our laboratory and incubated at 4 °C for 30 min darkness. Cells were washed, and kept at 4 °C, before analysis by FACSCanto (Becton-Dickinson, Franklin Lakes, NJ, USA).

2.5.3. Osteogenic Gene Expression: Quantitative Real-Time Polymerase Chain Reaction (qRT-PCR) Assay

qRT-PCR assay was performed to analyse the expression of integrin-binding sialoprotein (IBSP), osteocalcin (BGLAP), alkaline phosphatase(ALPL), osteopontin (SPP1), osteonectin (SPARC), runt-related transcription factor 2 (RUNX2) and collagen type I (COL1A1). Total RNA was extracted from cells using a RNAqueous Micro Kit (Invitrogen by Thermo Fisher Scientific, Waltham, MA, USA) according to the manufacturer's instruction, followed by reverse transcription of mRNA with the iScript cDNA Synthesis kit (Bio-Rad). Quantitative PCR was carried out by using the mix SYBR Premix ExTaq (Takara) in an iCycler MyiQ thermocycler (Bio-Rad). Specific primers for mRNA were purchased from Qiagen (QuantiTech Primer Assays, Hilden, Germany).

For each primer set, the efficiency was >95%, and a single product was observed using melt curve analysis. Samples were run in duplicate, and the presented relative gene expression levels were calculated using the $2^{-\Delta Ct}$ method by normalizing to glyceraldehyde-3-phosphate dehydrogenase (GAPDH) (Qiagen, Hilden, Germany).

3. Calculation

All assays were performed at least in triplicate. Student's t-test was used to determine significant differences between groups (p-value < 0.05). All data are reported as mean ± standard deviation (SD).

4. Results

4.1. Field Emission Scanning Electron Microscopy (FESEM)

In order to evaluate adhesion and morphology of *ah*MSCs growing on SCP-c, the scaffolds cultured were examined by FESEM at days 7, 14, 21 and 28 after the seeding in GM and just at 28 days in OM.

By day 7 after the seeding (Figure 1A), the cells showed an initial spreading and the majority of the cells were stretched, but still exhibited some spherical forms.

After 14 days (Figure 1B), *ah*MSCs seeded on the material covered much of the surface and showed a fibroblastic appearance. At 28 days (Figure 1D,E), the cells occupied the entire surface, forming a monolayer. There are not cytotoxicity signals or morphological alterations throughout the study. Morphological differences were observed between cells cultivated with GM (Figure 1D) and OM (Figure 1E). The appearance of the cells treated with OM showed polygonal shapes like osteoblastic cells.

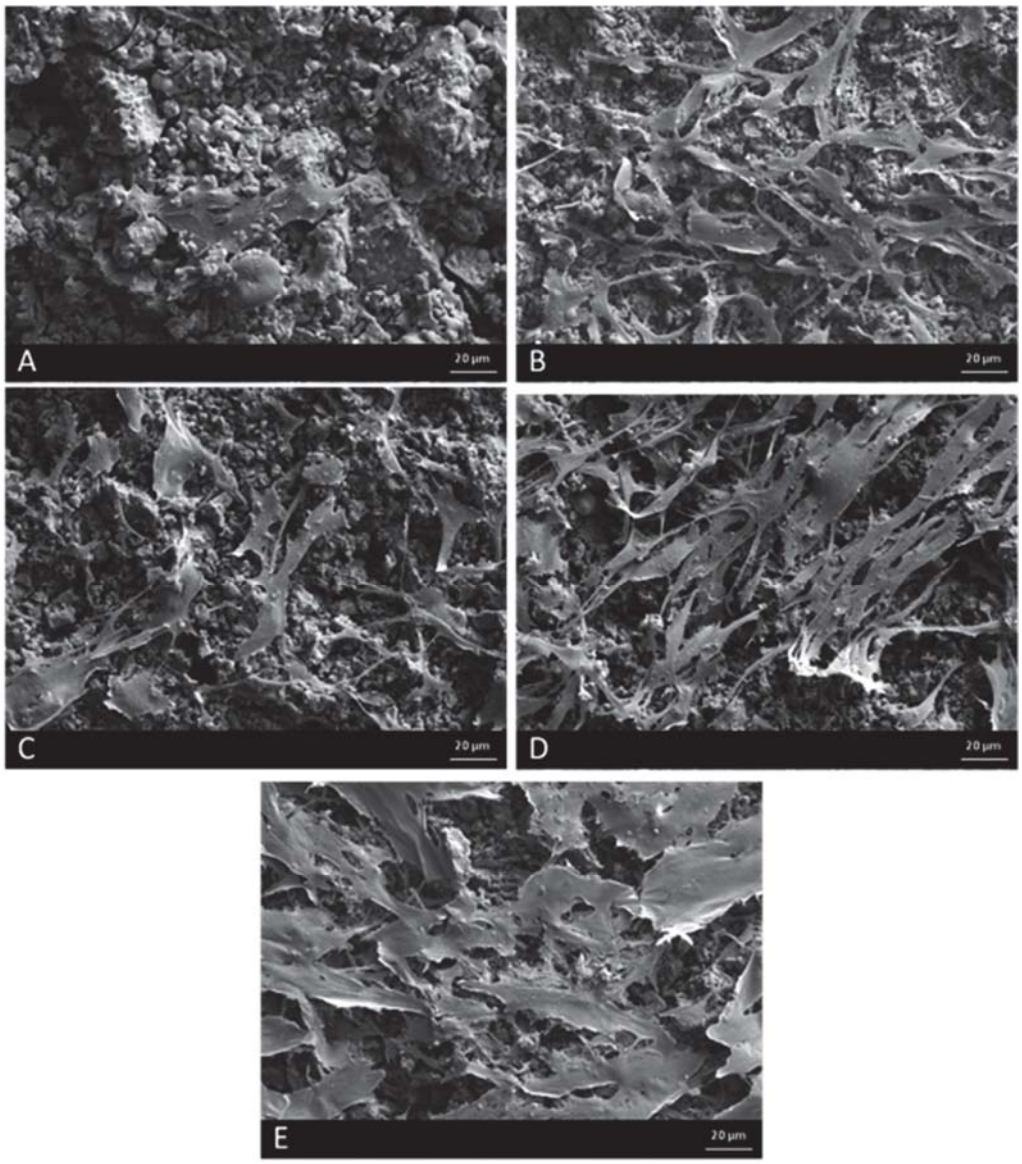

Figure 1. Representative FESEM images of the *ah*MSCs cells grown on ceramic surfaces at 7 days (**A**), 14 days (**B**), 21 days (**C**), 28 days (**D**) in GM and at 28 days in OM (**E**) (Original magnification: bar 20 µm).

4.2. Cellular Metabolic Activity Assay

Figure 2 shows results of cellular metabolic activity as fluorescence arbitrary units (a.u.). The cells seeded on plastic (control) showed higher metabolic activity than *ah*MSCs cultured on SCP-c. Cell proliferation in the presence of SCP-c was inhibited for the first 2 weeks.

On day 21, significantly higher metabolic activity (*t*-test, $p < 0.05$) was observed compared with previous measurements. Remarkably, *ah*MSCs cultured on SCP-c with OM showed major metabolic activity than cells cultured with GM (*t*-test, $p < 0.05$).

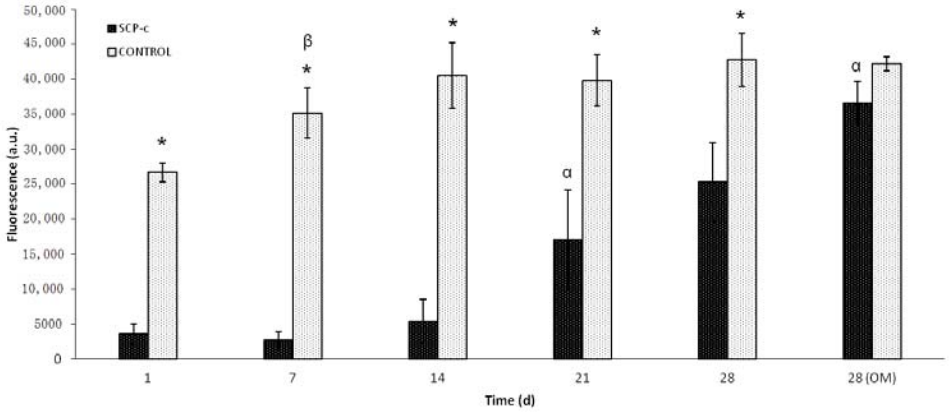

Figure 2. Cellular metabolic activity of the cells seeded on the SCP-c scaffolds compared to cell cultures on plastic (positive controls) obtained by means of Alamar Blue Assay. (*) denotes significant differences ($p < 0.05$) between SCP-c and the control for the same experimental time; (α) denotes significant differences ($p < 0.05$) between different experimental times obtained for cells growing on SCP-c scaffolds; (β) denotes significant differences ($p < 0.05$) between different experimental times obtained for control samples.

4.3. Differentiation Assays

4.3.1. Immunofluorescence Staining Assay: Heparan Sulphate (HS), Osteocalcin (OCN), Osteopontin (OPN) and Collagen Type I (Col I) Expression

Figure 3 shows immunofluorescence staining of HS, OCN, OPN and Col I from the extracellular matrix produced by *ah*MSCs at the end of the experiment (28 days) and 28 days under a week of influence of OM. After 28 days of culture, the cells cultured as control (left column of each chart) without any stimulus emit lower fluorescence in the Col I and HS staining than the cells seeded in indirect contact with SCP-c scaffolds. Moreover, the cells seeded in indirect contact with SCP-c scaffolds (right column of each chart) showed increasing fluorescence intensity in the HS, OCN, OPN and Col I staining with the addition of OM, being especially intense in the labeling of OPN. In addition, the cells acquired a rounded shape after incorporating OM.

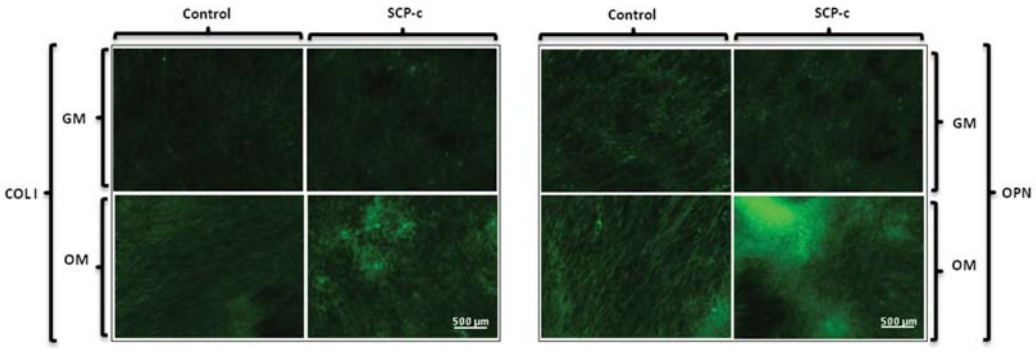

Figure 3. *Cont.*

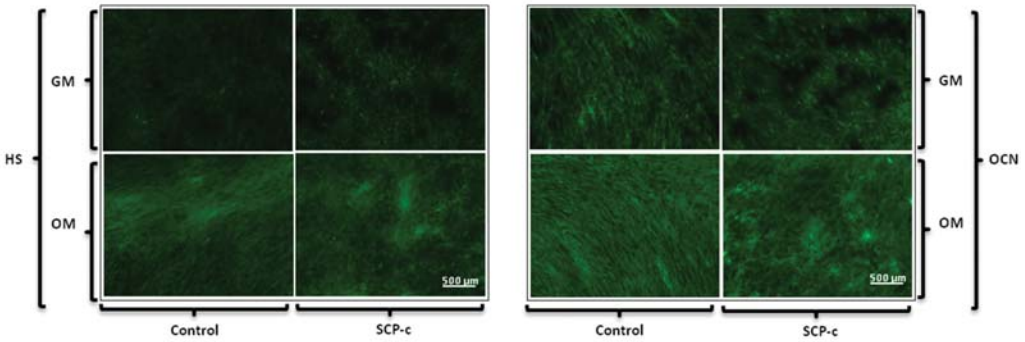

Figure 3. Representative immunofluorescence staining of Collagen I (Col I), Osteopontin (OPN), Heparan Sulphate (HS) and Osteocalcin (OCN) images (magnification: bar 500 µm) of the *ah*MSCs seeded in plastic (control) and cells growing in indirect contact with a Porous Si-Ca-P Monophasic Ceramic (SCP-c) at 28 days with growth medium (GM) or osteogenic medium (OM).

4.3.2. Surface Markers CD

Flow cytometric analysis was used in order to examine the presence of CD90, CD73 and CD105 surface antigens on *ah*MSCs (Figure 4). A total of 8.56% of the *ah*MSCs seeded in indirect contact with SCP-c lost CD90 antigen after 28 days in culture with OM, whereas only 3.94% of the cells cultured in plastic lost this marker (Figure 4A,D). Similarly, there were differences in the loss of the cell marker CD 105 at 28 days after adding OM (Figure 4B,E). Over 16% of the cells grown in indirect contact with the material did not express CD105, being significantly higher ($p < 0.05$) than the loss of the cell marker CD105 in the cells seeded in plastic.

On the other hand, there were no differences in the expression of CD 73 (Figure 4C,F) between treatment (SCP-c) and control (plastic) during the studied experimental times.

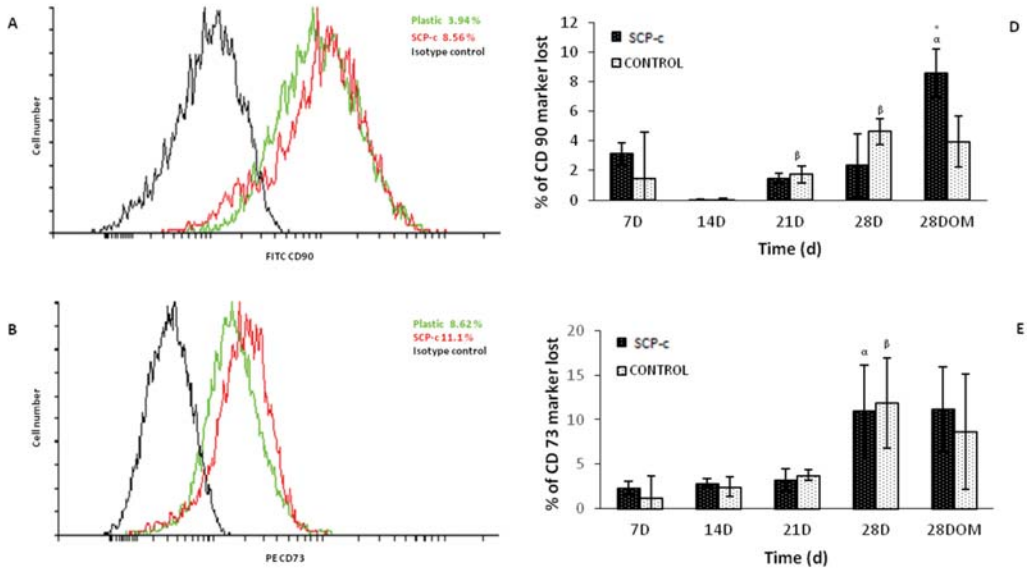

Figure 4. *Cont.*

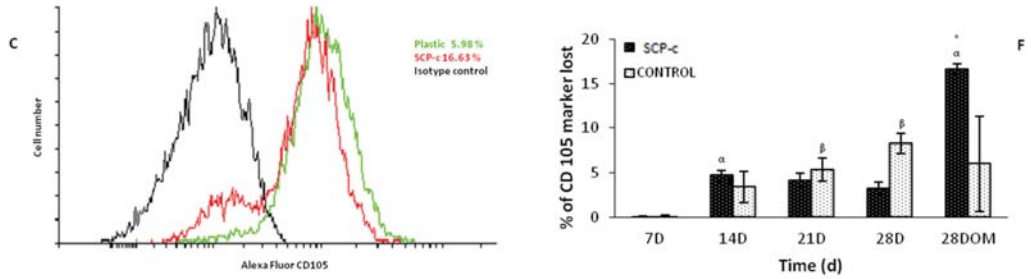

Figure 4. (**A**–**C**) Flow cytometry analysis of the expression of cell surface markers related to *ah*MSCs seeded on the SCP-c scaffolds compared to cell cultures on plastic and isotype control. (**D**–**F**) Percentage of surface marker lost with respect to the isotype control. (*) denotes significant differences ($p < 0.05$) between SCP-c and control at the same experimental time; (α) denotes significant differences ($p < 0.05$) between different experimental times obtained for cells growing on SCP-c scaffolds; (β) denotes significant differences ($p < 0.05$) between different experimental times obtained for control samples.

4.3.3. Quantitative Real-Time Polymerase Chain Reaction (qRT-PCR) Assay

The Pro-osteogenic effect on osteoblasts was further examined with respect to gene expression of IBSP, BGLAP, ALPL, SPP1, SPARC, RUNX2 and COL1A after 7, 14, 21 and 28 days in GM and 28 days of culture after replacing the GM by OM at 21 days. Figure 5 shows that genes associated with osteogenic differentiation including IBSP, ALPL, SPARC, SPP1 and COLI, were all significantly up-regulated in the SCP-c treatment ($p < 0.05$). In all groups, the osteogenic-related gene expression, except BGLAP and RUNX2, increased in a time-dependent manner.

The expression of gene RUNX2 seemed to increase at 28 days, but it was not significantly higher ($p > 0.05$). However, there were no differences between the expression of gene RUNX2 in control cells and *ah*MSCs in contact with SCP-c. In contrast to the other genes, BGLAP showed a continuous decrease from the 14th day in culture.

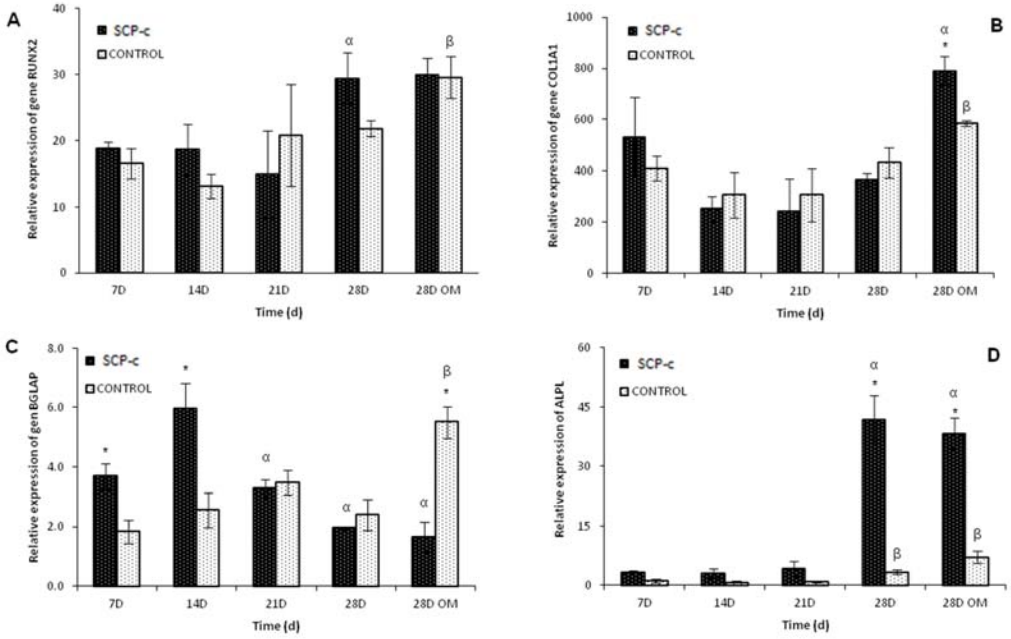

Figure 5. *Cont.*

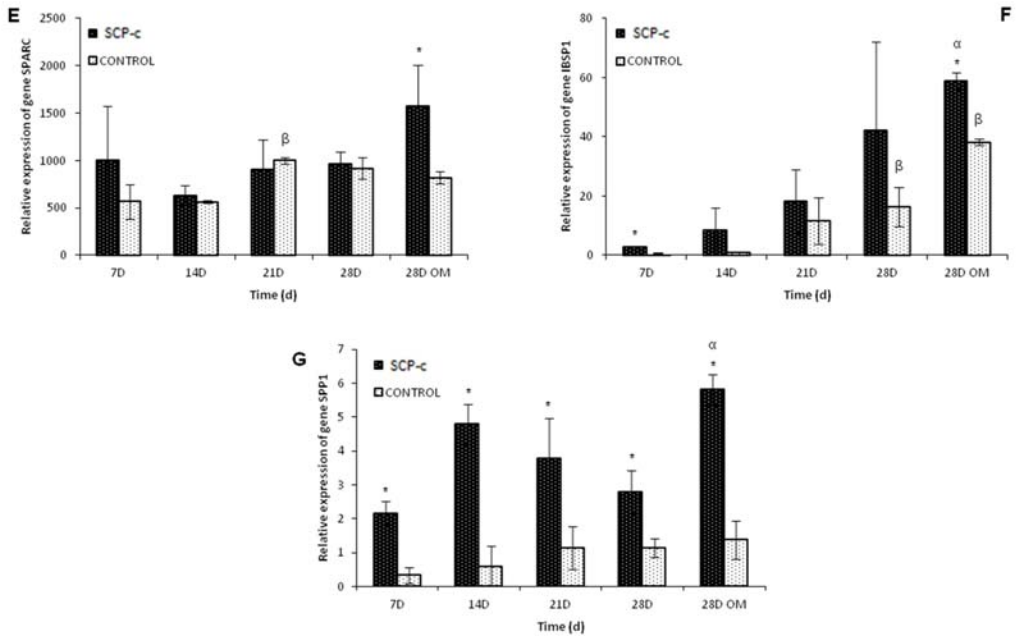

Figure 5. Real-time polymerase chain reaction (RT-PCR) was used to analyze the expression of genes RUNX2 (**A**), COL1A1 (**B**), BGLAP (**C**), ALPL (**D**), SPARC (**E**), IBSP1 (**F**) and SPP1 (**G**) in the cells seeded on the SCP-c scaffolds compared to cells cultured on plastic (positive controls). (*) denotes significant differences ($p < 0.05$) between SCP-c and the control for the same experimental time; (α) denotes significant differences ($p < 0.05$) between different experimental times obtained for cells growing on SCP-c scaffolds; (β) denotes significant differences ($p < 0.05$) between different experimental times obtained for control samples.

5. Discussion

Current treatment strategies for the repair or replacement of bone with synthetic implants and stem cells are a new approach to treat different conditions occurring in the medical field. The fabrication of ceramic scaffolds adding the use of autologous *ah*MSCs is aimed at transplantation to a large bone defect site observed in some clinical conditions such as tumour surgery, infections, implant rescue in orthopaedic and oral surgery [2]. An ideal biomaterial scaffold designed for bone tissue engineering must be degraded over time into non-toxic products and requires osteoconductive, osteoinductive and osteogenic properties.

Adding inorganic elements to scaffolds could significantly improve the bioactivity of materials as previously seen with bioglass, bioceramics that contain CaO, SiO_2 and P_2O_5 or glass-ceramic [19,20]. Also, these constructs could include additional growth factors or incorporate undifferentiated MSCs [21].

The osteoinduction of the materials was tested in this study, verifying their ability to lead *ah*MSCs toward an osteoblastic lineage differentiation.

Firstly, we examined the shape of the cells cultured on SCP-c by FESEM and their metabolic activity. Theoretically, cells will be spherical initially, then flatten and later sufficiently spread out so that the nucleus becomes prominent [17,22]. In our experiments, cells attached and adhered on SCP-c were found to be more spread out when they were cultured with OM. It has been noted that changes in expression of integrins, cadherins, and cytoskeletal proteins that occurs in the differentiation of stem cells produce cell morpholical changes [23]. Moreover, previous studies have suggested that changes in cell shape can regulate the degree of development of lineage-specific markers, or differentiation, in precommitted preadipocytes or preosteoblasts [24,25]. For all this, it is possible the morphological

changes observed are related to the differentiation of cells. Remarkably, *ah*MSCs cultured on SCP-c with OM showed major metabolic activity than cells cultured with GM after 28 days. Upon osteogenic induction, the copy number of mitochondrial DNA, protein subunits of the respiratory enzymes, oxygen consumption rate and intracellular ATP content are increased, indicating the upregulation of aerobic mitochondrial metabolism [26]. Therefore, a greater metabolic activity could be related to cellular differentiation mechanisms.

The presence of the surface markers CD 105, 90, and 73 is considered as fundamental during the characterization and isolation of *ah*MSCs [27]; these markers were previously used by our research group to characterize *ah*MSCs from mononucleated fraction obtained by SEPAX isolation. The analysis of the cell surface markers showed that cells seeded in indirect contact with SCP-c exhibited a reduction of the expression of CD 105 and CD 90; this fact can be considered a consequence of the differentiation program activation [28].

A common method to evaluate the potential osteoinductivity of a novel biomaterial is to establish genetic expression profiles related to differentiation. In this case, the genes of interest are those implicated in osteogenic differentiation, from the first stages, such as APL or Col I [29], to those expressed in the late phase of this process and considered markers of osteoblastic cell differentiation [30], for example OCN.

Among these genes, the RUNX2 transcription factor is known to play a key role in osteoblastic differentiation [31] because it can directly stimulate transcription of OCN, Col I, OPN and collagenase III genes binding to the sequence PuCCPuCA. Beyond this, the molecular mechanism of RUNX2 action is still unknown. Although RUNX2 is expressed exclusively in mineralized tissues and their precursors, in many cases there may be no correlation between their expression and the expression of osteoblast-related genes. It has been demonstrated that inconsistencies between Runx2 mRNA or protein levels and its transcriptional activity suggests that posttranslational modification and/or protein-protein interactions may regulate this factor [32].

The results of the qRT-PCR experiments show that the RUNX2 gene is not upregulated in cells seeded on SCP-c materials or the control. The addition of the OM does not increase RUNX2 expression, but OPN or IBSP expression increases in samples incubated with the materials, indicating the participation of RUNX2 in guiding the expression of these markers. RUNX2 mRNA variations are not correlated with OPN or IBSP levels, probably because the RUNX2 protein is active after post-transcriptional or post-translational modifications [33,34].

ALP activity increased in cells incubated with SCP-c materials 28 days after the seeding with GM and OM, which is concordant with the maximum release of silicon to the medium previously stated by our group [14]. It has been widely proved that silicon plays an important role promoting cell proliferation [11], ALP expression and mineralization [35]. On the other hand, ALP activity can be influenced by calcium levels, which in small amounts cause the increase of ALP activity and cell differentiation. Moreover, osteogenic supplements, like ascorbic acid and β-glycerophosphate, up-regulate ALP gene expression [36]. Osteogenic supplements in OM, low concentrations of Ca and increasing levels of Si from 21 days to 28 days may create a synergistic effect on the stimulation of ALP activity.

The formation and maturation of the extracellular matrix (ECM) are also studied as markers of osteoblastic differentiation. Col I and SPARC are both markers of early osteoblastic differentiation [37]. Their mRNA expression seemed to be influenced by the Si-Ca-P monophasic ceramic in this study from first week to the last week by adding OM at 28 days. *ah*MSCs express high levels of Col I in their in vivo natural environment [38]. qRT-PCR results for Col I were confirmed by Col I immunofluorescence images. In fact, Col I seemed to be synthesized since the first stages of ECM deposition in all the samples considered, and it increased after adding OM at 28 days.

During the fourth week, SCP-c also was able to upregulate the markers of a more mature extracellular matrix, such as OPN and IBSP1, whose role is to influence and regulate mineralization processes. The qRT-PCR results showed that cells seeded under the influence of SCP-c reached the

maximum expression of these mRNA markers during the fourth week with the best performance in presence of the OM. These data are in accordance with the results stated by Kulterer B et al. [39] in the genetic expression profiles obtained for *ah*MSCs during osteoblastic differentiation studies. OPN qRT-PCR results are confirmed by the results of the immunofluorescence study. During the last week of culture, OPN proteins are highly expressed in the samples incubated with the material, demonstrating that the ECM is maturing, as expected.

HA and β-TCP are highly biocompatible, but differ in their biological response at the implantation site. While HA does not significantly degrade, and remains permanent over time, β-TCP has been shown to be a reabsorbable and osteoconductive material [40,41]. For decades, β-TCP has been widely used for repairing small bone defects, proving an environment where osteoblasts and MSCs are able to proliferate, providing an adequate matrix for bone formation [41–44]. Based on its gradually reabsortion and its proven osteoinduction properties, we think that the SCP-c material could be used as an alternative to natural bone.

6. Conclusions

Differentiation osteogenic markers were more intense in cells growing under the influence of SCP-c material, but specially after adding OM. All these results could indicate that the ceramic will be able to induce cell differentiation in the presence of other osteogenic supplements that we can find naturally in organisms.

Future studies will be focused on determining the in vivo properties of this bioceramic and improvements of its composition by adding different molecules such growth factors, drugs or coatings.

Acknowledgments: Part of this work was supported by the Spanish Ministry of Economy and Competitiveness (MINECO) contract grant number: MAT2013-48426-C2-2-R.

Author Contributions: Meseguer-Olmo Luis. and De Aza Piedad N. conceived and designed the experiments; Rabadan-Ros Ruben and Revilla-Nuin Beatriz performed the experiments; Mazón Patricia and Ros-Tarraga Patricia performed the preparation of the ceramics; Rabadan-Ros Ruben, Aznar-Cervantes Salvador, De Aza Piedad N. and Meseguer-Olmo Luis. wrote the paper. All authors contributed to the analyses and discussion of the results.

Conflicts of Interest: The authors declare no conflict of interest.

References

1. Boyan, B.D.; Hummert, T.W.; Dean, D.D.; Schwartz, Z. Role of material surfaces in regulating bone and cartilage cell response. *Biomaterials* **1996**, *17*, 137–146. [CrossRef]
2. Bosetti, M.; Cannas, M. The effect of bioactive glasses on bone marrow stromal cells differentiation. *Biomaterials* **2005**, *26*, 3873–3879. [CrossRef] [PubMed]
3. Lugo, G.; Mazón, P.; De Aza, P. Phase transitions in single phase Si–Ca–P-based ceramic under thermal treatment. *J. Eur. Ceram. Soc.* **2015**, *35*, 3693–3700. [CrossRef]
4. Puppi, D.; Chiellini, F.; Piras, A.; Chiellini, E. Polymeric materials for bone and cartilage repair. *Prog. Polym. Sci.* **2010**, *35*, 403–440. [CrossRef]
5. Hild, N.; Schneider, O.D.; Mohn, D.; Luechinger, N.A.; Koehler, F.M.; Hofmann, S.; Vetsch, J.R.; Thimm, B.W.; Müller, R.; Stark, W.J. Two-layer membranes of calcium phosphate/collagen/plga nanofibres: In vitro biomineralisation and osteogenic differentiation of human mesenchymal stem cells. *Nanoscale* **2011**, *3*, 401–409. [CrossRef] [PubMed]
6. Duan, Y.; Zhang, Z.; Wang, C.; Chen, J.; Zhang, X. Dynamic study of calcium phosphate formation on porous HA/TCP ceramics. *J. Mater. Sci. Mater. Med.* **2004**, *15*, 1205–1211. [CrossRef] [PubMed]
7. Pan, H.; Zhao, X.; Darvell, B.W.; Lu, W.W. Apatite-formation ability–predictor of "bioactivity"? *Acta Biomater.* **2010**, *6*, 4181–4188. [CrossRef] [PubMed]
8. Jonasova, L.; Müller, F.A.; Helebrant, A.; Strnad, J.; Greil, P. Hydroxyapatite formation on alkali-treated titanium with different content of Na+ in the surface layer. *Biomaterials* **2002**, *23*, 3095–3101. [CrossRef]
9. Hoppe, A.; Güldal, N.S.; Boccaccini, A.R. A review of the biological response to ionic dissolution products from bioactive glasses and glass-ceramics. *Biomaterials* **2011**, *32*, 2757–2774. [CrossRef] [PubMed]

10. Valerio, P.; Pereira, M.M.; Goes, A.M.; Leite, M.F. The effect of ionic products from bioactive glass dissolution on osteoblast proliferation and collagen production. *Biomaterials* **2004**, *25*, 2941–2948. [CrossRef] [PubMed]
11. Shie, M.-Y.; Ding, S.-J.; Chang, H.-C. The role of silicon in osteoblast-like cell proliferation and apoptosis. *Acta Biomater.* **2011**, *7*, 2604–2614. [CrossRef] [PubMed]
12. Rabadan-Ros, R.; Mazón, P.; Serena, S.; Sainz, M.; Meseguer-Olmo, L.; De Aza, P. In vitro behaviour of nurse's a ss-phase: A new calcium silicophosphate ceramic. *J. Eur. Ceram. Soc.* **2017**, *37*, 2943–2952. [CrossRef]
13. Rabadan-Ros, R.; Velásquez, P.A.; Meseguer-Olmo, L.; De Aza, P.N. Morphological and structural study of a novel porous nurse's a ceramic with osteoconductive properties for tissue engineering. *Materials* **2016**, *9*, 474. [CrossRef] [PubMed]
14. Rabadan-Ros, R.; Aznar-Cervantes, S.; Mazón, P.; Ros-Tarraga, P.; De Aza, P.N.; Meseguer-Olmo, L. Nurse's a-phase material enhance adhesion, growth and differentiation of human bone marrow-derived stromal mesenchymal stem cells. *Materials* **2017**, *10*, 347. [CrossRef] [PubMed]
15. Lugo, G.J.; Mazón, P.; Piedad, N. Material processing of a new calcium silicophosphate ceramic. *Ceram. Int.* **2016**, *42*, 673–680. [CrossRef]
16. Lugo, G.J.; Mazón, P.; Baudin, C.; De Aza, P.N. Nurse′ s a-phase: Synthesis and characterization in the binary system ca2sio4–ca3 (po4) 2. *J. Am. Ceram. Soc.* **2015**, *98*, 3042–3046. [CrossRef]
17. De Aza, P.N.; García-Bernal, D.; Cragnolini, F.; Velasquez, P.; Meseguer-Olmo, L. The effects of ca2sio4-ca3 (po4) 2 ceramics on adult human mesenchymal stem cell viability, adhesion, proliferation, differentiation and function. *Mater. Sci. Eng. C Mater. Biol. Appl.* **2013**, *33*, 4009–4020. [CrossRef] [PubMed]
18. Dominici, M.; Le Blanc, K.; Mueller, I.; Slaper-Cortenbach, I.; Marini, F.; Krause, D.; Deans, R.; Keating, A.; Prockop, D.; Horwitz, E. Minimal criteria for defining multipotent mesenchymal stromal cells. The international society for cellular therapy position statement. *Cytotherapy* **2006**, *8*, 315–317. [CrossRef] [PubMed]
19. García-Páez, I.H.; Carrodeguas, R.G.; Antonio, H.; Baudín, C.; Pena, P. Effect of mg and si co-substitution on microstructure and strength of tricalcium phosphate ceramics. *J. Mech. Behav. Biomed. Mater.* **2014**, *30*, 1–15. [CrossRef] [PubMed]
20. Taherkhani, S.; Moztarzadeh, F. Influence of strontium on the structure and biological properties of sol–gel-derived mesoporous bioactive glass (MBG) powder. *J. Sol-Gel Sci. Technol.* **2016**, *78*, 539–549. [CrossRef]
21. Giannoudis, P.V.; Dinopoulos, H.; Tsiridis, E. Bone substitutes: An update. *Injury* **2005**, *36*, S20–S27. [CrossRef] [PubMed]
22. Nair, M.B.; Varma, H.; John, A. Triphasic ceramic coated hydroxyapatite as a niche for goat stem cell-derived osteoblasts for bone regeneration and repair. *J. Mater. Sci. Mater. Med.* **2009**, *20*, 251–258. [CrossRef] [PubMed]
23. McBeath, R.; Pirone, D.M.; Nelson, C.M.; Bhadriraju, K.; Chen, C.S. Cell shape, cytoskeletal tension, and rhoa regulate stem cell lineage commitment. *Dev. Cell* **2004**, *6*, 483–495. [CrossRef]
24. Sordella, R.; Jiang, W.; Chen, G.-C.; Curto, M.; Settleman, J. Modulation of rho gtpase signaling regulates a switch between adipogenesis and myogenesis. *Cell* **2003**, *113*, 147–158. [CrossRef]
25. Thomas, C.H.; Collier, J.H.; Sfeir, C.S.; Healy, K.E. Engineering gene expression and protein synthesis by modulation of nuclear shape. *Proc. Natl. Acad. Sci. USA* **2002**, *99*, 1972–1977. [CrossRef] [PubMed]
26. Chen, C.T.; Shih, Y.R.V.; Kuo, T.K.; Lee, O.K.; Wei, Y.H. Coordinated changes of mitochondrial biogenesis and antioxidant enzymes during osteogenic differentiation of human mesenchymal stem cells. *Stem Cells* **2008**, *26*, 960–968. [CrossRef] [PubMed]
27. Conget, P.A.; Minguell, J.J. Phenotypical and functional properties of human bone marrow mesenchymal progenitor cells. *J. Cell. Physiol.* **1999**, *181*, 67–73. [CrossRef]
28. Mafi, P.; Hindocha, S.; Mafi, R.; Griffin, M.; Khan, W. Adult mesenchymal stem cells and cell surface characterization—A systematic review of the literature. *Open Orthop. J.* **2011**, *5*, 253–260. [CrossRef] [PubMed]
29. Setzer, B.; Bächle, M.; Metzger, M.C.; Kohal, R.J. The gene-expression and phenotypic response of hfob 1.19 osteoblasts to surface-modified titanium and zirconia. *Biomaterials* **2009**, *30*, 979–990. [CrossRef] [PubMed]
30. Harada, S.-I.; Rodan, G.A. Control of osteoblast function and regulation of bone mass. *Nature* **2003**, *423*, 349–355. [CrossRef] [PubMed]

31. Ducy, P.; Zhang, R.; Geoffroy, V.; Ridall, A.L.; Karsenty, G. Osf2/cbfa1: A transcriptional activator of osteoblast differentiation. *Cell* **1997**, *89*, 747–754. [CrossRef]
32. Lee, K.-S.; Kim, H.-J.; Li, Q.-L.; Chi, X.-Z.; Ueta, C.; Komori, T.; Wozney, J.M.; Kim, E.-G.; Choi, J.-Y.; Ryoo, H.-M. Runx2 is a common target of transforming growth factor β1 and bone morphogenetic protein 2, and cooperation between RUNX2 and SMAD5 induces osteoblast-specific gene expression in the pluripotent mesenchymal precursor cell line c2c12. *Mol. Cell. Biol.* **2000**, *20*, 8783–8792. [CrossRef] [PubMed]
33. Franceschi, R.T.; Xiao, G. Regulation of the osteoblast-specific transcription factor, runx2: Responsiveness to multiple signal transduction pathways. *J. Cell. Biochem.* **2003**, *88*, 446–454. [CrossRef] [PubMed]
34. Franceschi, R. The developmental control of osteoblast-specific gene expression: Role of specific transcription factors and the extracellular matrix environment. *Crit. Rev. Oral Biol. Med.* **1999**, *10*, 40–57. [CrossRef] [PubMed]
35. Dong, M.; Jiao, G.; Liu, H.; Wu, W.; Li, S.; Wang, Q.; Xu, D.; Li, X.; Liu, H.; Chen, Y. Biological silicon stimulates collagen type 1 and osteocalcin synthesis in human osteoblast-like cells through the BMP-2/SMAD/RUNX2 signaling pathway. *Biol. Trace Elem. Res.* **2016**, *173*, 306–315. [CrossRef] [PubMed]
36. Cheng, S.-L.; Yang, J.W.; Rifas, L.; Zhang, S.-F.; Avioli, L.V. Differentiation of human bone marrow osteogenic stromal cells in vitro: Induction of the osteoblast phenotype by dexamethasone. *Endocrinology* **1994**, *134*, 277–286. [CrossRef] [PubMed]
37. Jikko, A.; Harris, S.E.; Chen, D.; Mendrick, D.L.; Damsky, C.H. Collagen integrin receptors regulate early osteoblast differentiation induced by BMP-2. *J. Bone Miner. Res.* **1999**, *14*, 1075–1083. [CrossRef] [PubMed]
38. Schipani, E.; Kronenberg, H.M. *Adult Mesenchymal Stem Cells*; Harvard Stem Cell Institute: Cambridge, MA, USA, 2009.
39. Kulterer, B.; Friedl, G.; Jandrositz, A.; Sanchez-Cabo, F.; Prokesch, A.; Paar, C.; Scheideler, M.; Windhager, R.; Preisegger, K.-H.; Trajanoski, Z. Gene expression profiling of human mesenchymal stem cells derived from bone marrow during expansion and osteoblast differentiation. *BMC Genom.* **2007**, *8*, 70. [CrossRef] [PubMed]
40. Allabouch, A.; Colat-Parros, J.; Salmon, R.; Naim, S.; Meunier, J. Biocompatibility of some materials used in dental implantology: Histological study. *Coll. Surf. B Biointerfaces* **1993**, *1*, 323–329. [CrossRef]
41. Aybar, B.; Bilir, A.; Akçakaya, H.; Ceyhan, T. Effects of tricalcium phosphate bone graft materials on primary cultures of osteoblast cells in vitro. *Clin. Oral Implant. Res.* **2004**, *15*, 119–125. [CrossRef]
42. Liu, G.; Zhao, L.; Cui, L.; Liu, W.; Cao, Y. Tissue-engineered bone formation using human bone marrow stromal cells and novel β-tricalcium phosphate. *Biomed. Mater.* **2007**, *2*, 78–86. [CrossRef] [PubMed]
43. Payer, M.; Lohberger, B.; Stadelmeyer, E.; Bartmann, C.; Windhager, R.; Jakse, N. Behaviour of multipotent maxillary bone derived cells on β-tricalcium phosphate and highly porous bovine bone mineral. *Clin. Oral Implant. Res.* **2010**, *21*, 699–708. [CrossRef] [PubMed]
44. Yefang, Z.; Hutmacher, D.; Varawan, S.-L.; Meng, L.T. Comparison of human alveolar osteoblasts cultured on polymer-ceramic composite scaffolds and tissue culture plates. *Int. J. Oral Maxillofac. Surg.* **2007**, *36*, 137–145. [CrossRef] [PubMed]

8. ARTÍCULO 4

materials

MDPI

Article

Morphological and Structural Study of a Novel Porous Nurse's A Ceramic with Osteoconductive Properties for Tissue Engineering

Ruben Rabadan-Ros [1], Pablo A. Velásquez [2], Luis Meseguer-Olmo [3] and Piedad N. De Aza [2,*]

1 Grupo de Investigación en Regeneración y Reparación de Tejidos, UCAM—Universidad Católica San Antonio de Murcia, Guadalupe, Murcia 30107, Spain; rubenrabadanros@gmail.com

2 Instituto de Bioingeniería, Universidad Miguel Hernández Avda, Universidad s/n, Elche, Alicante 03202, Spain; pavelasquez@umh.es

3 Service of Orthopaedic at Arrixaca University Hospital, UCAM—Catholic University of Murcia, Murcia 30120, Spain; lmeseguer.doc@gmail.com

* Correspondence: piedad@umh.es; Tel.: +34-96-6658485

Academic Editor: Alina Maria Holban

Received: 25 May 2016; Accepted: 7 June 2016; Published: 15 June 2016

Abstract: The characterization process of a new porous Nurse's A ceramic and the physico chemical nature of the remodeled interface between the implant and the surrounding bone were studied after *in vivo* implantation. Scaffolds were prepared by a solid-state reaction and implanted in New Zealand rabbits. Animals were sacrificed on days 15, 30, and 60. The porous biomaterial displayed biocompatible, bioresorbable, and osteoconductive capacity. The degradation processes of implants also encouraged osseous tissue ingrowths into the material's pores, and drastically changed the macro- and microstructure of the implants. After 60 healing days, the resorption rates were 52.62% ± 1.12% for the ceramic and 47.38% ± 1.24% for the residual biomaterial. The elemental analysis showed a gradual diffusion of the Ca and Si ions from the materials into the newly forming bone during the biomaterial's resorption process. The energy dispersive spectroscopy (EDS) analysis of the residual ceramic revealed some particle categories with different mean Ca/P ratios according to size, and indicated various resorption process stages. Since osteoconductive capacity was indicated for this material and bone ingrowth was possible, it could be applied to progressively substitute an implant.

Keywords: bioceramics; calcium silicophosphate; scanning electron microscopy; μ-Raman spectroscopy; bone response; biocompatibility

1. Introduction

Nowadays, the demand for replacement materials to fill defects is growing, especially in natural bone tissues. Implants made of synthetic polymers, ceramics, and metals are normally used for tissue repair [1,2], but none of these materials can match the quality of the original tissue they replace. In recent decades, several types of synthetic bone graft substitutes and tissue-engineered hybrids have been developed to take over the role of natural bone grafts [3,4].

Bioceramic has attracted much attention because it is low-cost, easy to produce, and offers good biocompatibility. Bone tissue mineral is a calcium-phosphate (CaP)-based apatite phase. For this reason, CaP ceramics—typically hydroxyapatite (HA) and tricalcium phosphate (TCP)—are widely used for bone tissue replacement in maxillogacial surgery and for filling defects [5–7].

Initial bone defect regeneration is favored by the presence of calcium phosphate in the bone replacement material. Despite interest having been shown in Si- and Mg-containing ceramics to

develop bone implant materials [8–10], some research has indicated silicon to be fundamental in skeletal development [11].

Therefore, materials that contain silicon, calcium, and phosphorus are excellent candidates for preparing biomaterials with improved osteogenic properties. Complicated synthesis processes have been followed to acquire Si-CaP biomaterials. It is well-known that preparing single phases of crystallized Si-HA and Si-TCP materials is no easy task [12–15], which means that the mechanism of silicon-containing and/or silicon-substituted calcium phosphates is no trivial matter [16].

In a previous work, a simple low-cost two-step solid-state reaction process was established for obtaining a new porous Si-Ca-P-single phase ceramic called "*Nurse's A*" in the subsystem Nurse's A-phase—silcocarnotite within dicalcium silicate (Ca_2SiO_4)/tricalcium phosphate ($Ca_3(PO_4)_2$) system [17–19].

The main purpose of the present research was to study the physical, chemical, and biological changes that take place at the implant–bone interface that controls the mechanism of direct bone tissue bonding with the implant *in vivo* by analytical scanning electron microscopy. The microstructure effect (porosity, grain size, and phase composition) on the new ceramic's *in vivo* behavior was also studied.

2. Results

2.1. Biomaterial Characterization

Figure 1 shows the XRD diffraction pattern of Nurse's A powder ceramic. Each diffraction peak can be assigned to the characteristic reflections of $2Ca_2SiO_4 \cdot Ca_3(PO_4)_2$ (JCPDS card No. 11-0676). Figure 2A,B shows the polished surface of the obtained porous ceramic after chemical etching (0.5% acetic acid, 2 s). The figure evidenced that a monophasic material of high porosity was obtained. No critical defect was detected on any surface and a homogeneous microstructure with large spherical pores was observed at low magnification. EDS confirmed that silicon, phosphorous, and calcium were present. Figure 2C illustrates the characteristic fracture surface. The microstructure was made up of high-density aggregates with elongated pores around them. The size of the aggregates—with diameters of around 20–30 μm—allows their identification as coming from aggregates initially present in the green compacts. Such aggregates would come from milling. Fracture appears to occur by the detachment of such aggregates through the coalescence of the elongated pores. There are also cavities close to these aggregates that should be the negative of detached zones in the corresponding fracture surface.

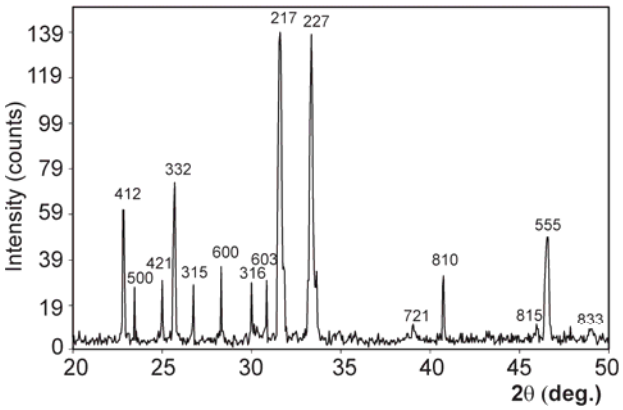

Figure 1. XRD pattern of the Nurse's A powders.

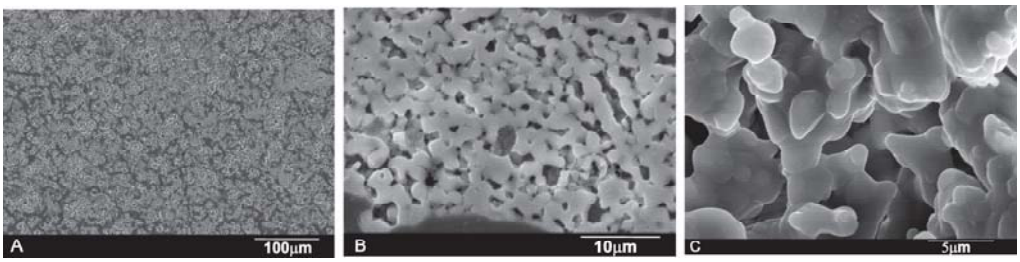

Figure 2. SEM images that depict (**A**,**B**) the polished Nurse's A ceramic microstructure; (**C**) Fracture surface at a high magnification.

When analyzing a material by mercury porosimetry, two kinds of spaces can be detected: those that correspond to the empty spaces between the particles (commonly designated by "interstices" or "interparticle" spaces) and those that correspond to the spaces of the particles themselves (known as "pores" or "intraparticle" spaces). The results obtained for porosity (Figure 3) showed that mercury penetrated to the increasingly smaller pores with increasing pressure. The cumulative curve (Figure 3A) denotes a small intrusion in pores between 300 (upper limit detection) and 12.3 µm, followed by a plateau between 12.3 and 0.86 µm where no intrusion was detected, and then a significant mercury penetration into the pores that are smaller than this value. The initial curve rise corresponded mostly to filling the interparticle spaces, whereas the later curve rise was related to the intraparticle spaces. The range of the intraparticle pores is more obvious in Figure 3B, in which two intense peaks at 0.86 and 0.14 µm are clearly visible. The smaller peak on the left (~100 µm) corresponds to the intrusion of mercury in the interparticle spaces. However, the distinction between the inter- and intraparticle spaces was not always so apparent. This interpretation aimed to elucidate the kind of information that can be extracted from the pore size distribution curves and highlights the importance of always specifying the size range of the measured pores. It should be stressed that the mercury intrusion technique is especially suited to the analysis of intraparticle pores, and is not especially suitable for measuring large spaces (300 µm).

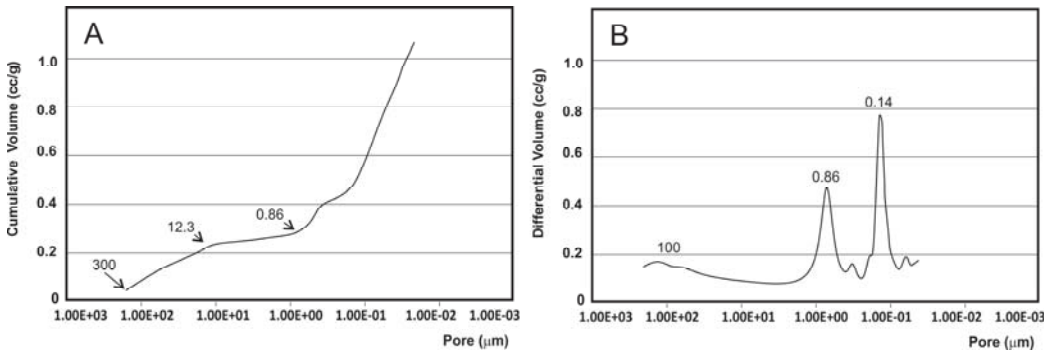

Figure 3. (**A**) Mercury intrusion curves of the ceramic measured by mercury porosimetry: cumulative intruded volume *vs.* pore diameter and (**B**) differential-intruded volume *vs.* pore diameter. The intrusion profiles show a small mercury penetration into pores between 300 and 12.3 µm (interparticle pores) and a significant mercury penetration into pores smaller than 0.86 µm (intraparticle pores).

Microstructural parameters were established to comprehensively characterize the microstructure of the material (Table 1). The obtained strength values for the material were relatively low due to the porosity of the ceramic. The results were directly related to the density of the material.

Table 1. Physical and mechanical properties of Nurse's A phase.

Crystalline Size (Sherrer Å)	Shrinkage (%)	Intruded Volume (cc/g)	Total Porosity (%)	Intraparticle Porosity (%) [a]	Interparticle Porosity (%) [b]	Real Density (g/cm^3)	Apparent Density (g/cm^3)	Strength (MPa)
213	31.99 ± 0.5	0.1127	20.21	15.013	5.1969	2.13	1.72	0.60 ± 0.02

[a] Corresponding to 0.0035 μm < pores < 1 μm; [b] Corresponding to 1 μm < pores < 300 μm.

We can observe in the Raman spectra of Nurse's A material (Figure 4) that the two most intense bands were located at 857 and 961 cm^{-1}. We can also see wide and low intensity bands around 200–650, 1058, and 1084 cm^{-1}. The internal modes of the $SiO_4{}^{-4}$ and $PO_4{}^{-3}$ tetrahedral units dominated the Raman spectra of crystalline silicates and phosphates. The spectra interpretation was not evident because the bands that corresponded to groups $SiO_4{}^{4-}$ and $PO_4{}^{3-}$—which formed the structure—overlapped. Given the similarities of the $SiO_4{}^{4-}$ and $PO_4{}^{3-}$ tetrahedral molecular units, both the silica calcium silicates and the hydroxyapatite crystalline phases share many similarly-spaced vibrational modes [20–23]. The main contribution of phosphate generally fell within a higher wavelength range (955–1115 cm^{-1}), followed by the most intense silicate vibrations (848–879 cm^{-1}), and finally within a narrower range (200–616 cm^{-1}), the phosphate contribution was once again identified.

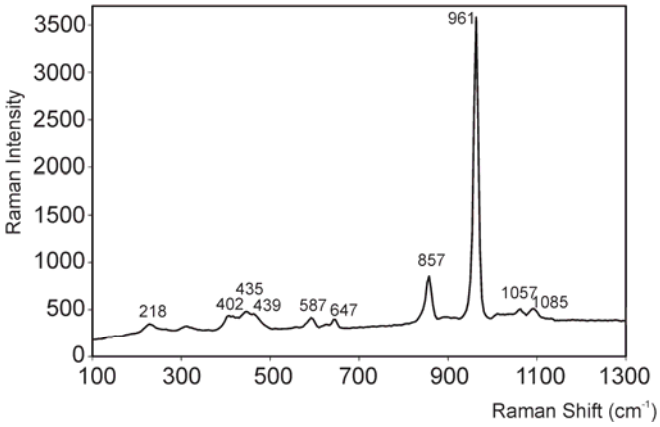

Figure 4. Raman spectra of Nurse's A ceramic.

2.2. Implants Characterization

On day 15 post-implantation, the porous implant was well-integrated into the host tissue and formed an irregular surface boundary caused by the material's gradual degradation (see Figure 5A). The interface between the implant and the surrounding tissue was characterized by the intermittent presence of the calcium phosphate phase and traces of silicon. In structure and morphology terms, it corresponded to new bone tissue. "NB" in Figure 5A denotes new bone, and the EDS analysis supported these findings (Table 2). In many areas, much larger-sized regions contained partly loose and exposed parent Si-Ca-P particles as a result of the material's degradation in the physiological environment. Figure 5A denotes these particles as *. A positive effect was achieved by the formation of a much larger porous structure due to ceramic degradation as it acted as a scaffold for vascular ingrowths and osteoblast activities, which led to new bone growth inside the implanted material.

Figure 5B illustrates the massive bone colonization of the implant via the original pores in the ceramic, owing to progressive structure dissolution. As a result of these advanced processes, free material particles were found in many areas and all over the restructuring implant. An asterisk (*) and NB respectively denote the Si-Ca-P particles and ingrown bone regions in Figure 5B.

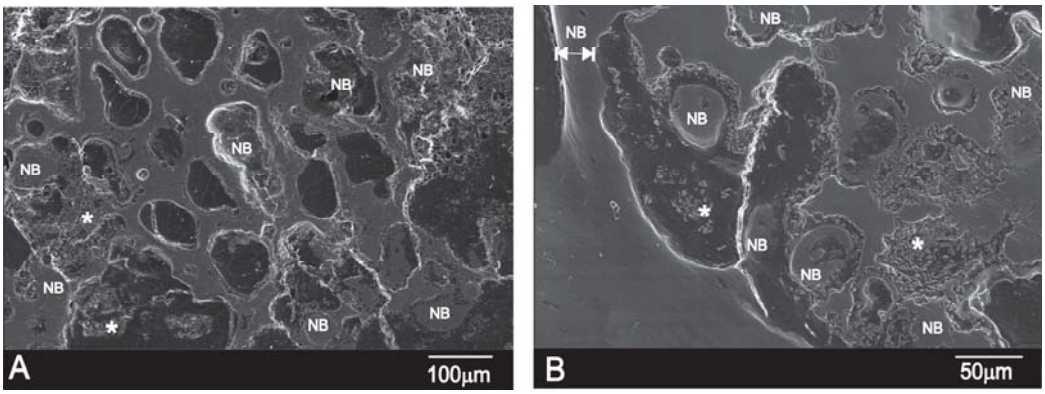

Figure 5. SEM images of the cross-section of Nurse's A implant in bone after (**A**) 15 and (**B**) 30 days of implantation. Letters NB refer to the new bone tissue, while * refers to the Ca-Si-P particles as a result of the degradation process.

Table 2. EDS elemental analysis of the reaction zone 15, 30, and 60 days after implantation. Mean ± SD (Median). Also, EDS elemental analysis of the Nurse' A material and hydroxyapatite (HA) theoretical for comparative purposes.

(wt %)	O	Ca	P	Si
Nurse' A Material				
0 day	39.21 ± 0.50 (39.21)	42.50 ± 0.50 (42.50)	9.70 ± 0.50 (9.70)	8.54 ± 0.03 (8.54)
HA Theoretical				
0 day	41.39	39.90	18.50	-
Implant				
15 days	38.9 ± 1.58 (38.9)	42.12 ± 1.66 (42.12)	10.5 ± 0.57 (10.5)	8.50 ± 1.05 (8.50)
30 days	42.10 ± 1.64 (42.10)	40.30 ± 1.54 (40.30)	9.7 ± 0.53 (9.7)	7.9 ± 0.86 (7.9)
60 days	43.60 ± 1.78 (43.60)	39.7 ± 1.43 (39.7)	9.21 ± 0.40 (9.21)	7.5 ± 0.64 (7.5)
Interphase				
15 days	51.07 ± 1.97 (51.07)	31.46 ± 1.46 (31.46)	15.57 ± 0.96 (15.57)	1.90 ± 1.1 (1.90)
30 days	53.37 ± 1.87 (53.37)	31.27 ± 1.50 (31.27)	14.89 ± 0.87 (14.90)	0.71 ± 1.62 (0.71)
60 days	53.94 ± 1.89 (53.94)	30.94 ± 1.38 (30.94)	14.78 ± 0.84 (14.78)	0.34 ± 0.94 (0.34)
New Bone				
15 days	51.82 ± 1.96 (51.82)	32.56 ± 1.37 (32.56)	15.36 ± 0.98 (15.36)	0.26 ± 1.30 (0.26)
30 days	53.71 ± 1.88 (53.71)	31.92 ± 0.44 (31.92)	14.18 ± 0.96 (14.18)	0.19 ± 1.58 (0.19)
60 days	54.17 ± 0.91 (54.17)	31.57 ± 0.42 (31.57)	14.09 ± 0.87 (14.10)	0.17 ± 1.01 (0.17)

The new bone also filled the implant's central and peripheral porosities on day 60 post-implantation (Figure 6A). The interface characterization demonstrated that the calcium phosphate phase along the implant interface periphery was well-textured since Si-Ca-P material degradation inside the implant continued. The outer product layer comprised phosphorus and calcium elements with an average Ca/P ratio of ≈2.24 (Table 3). Some cracks had readily developed close to the implant surface, and were associated with the drying process. Figure 6B offers a close-up SEM image of the 60-day implant interface. Compared with the 30-day implant (Figure 6B), the surface layer was considerably thicker on day 60. The new bone layer thickness was about 13 ± 10 μm by 15 days, which increased to about 30 ± 7 μm by 30 days, and then to about 50 ± 4 μm by day 60. Figure 6C illustrates a vessel that came into direct contact with the newly formed bone layer around the implant surface on day 60. Granular entities were identified and covered the new bone (refer to *).

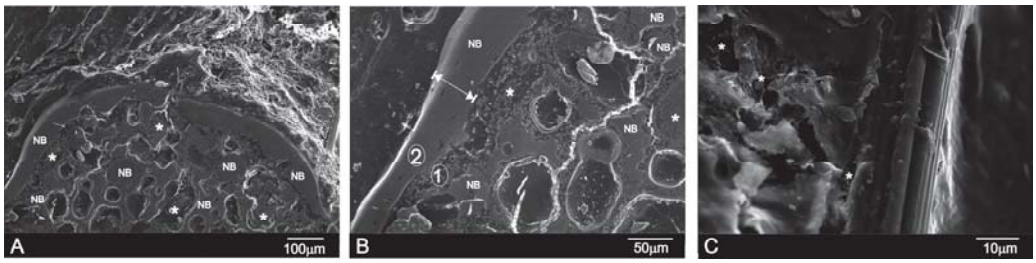

Figure 6. (**A**,**B**) SEM images of the cross-section of Nurse's A implant in bone after 60 days of implantation; (**C**) A vessel present on the surface of the new bone layer in contact with the degraded Si-Ca-P material. Letters NB refer to the new bone tissue, while * refers to the Ca-Si-P particles as a result of the degradation process.

Table 3. Ca/P ratio of the reaction zone 15, 30, and 60 days after implantation. Mean ± SD (Median).

Time of Implantation	Implant	Interphase	New Bone
	Ca/P Ratio	Ca/P Ratio	Ca/P Ratio
15 days	4.01 ± 0.23 (4.01)	2.02 ± 0.54 (2.02)	2.12 ± 0.99 (2.12)
30 days	4.15 ± 0.16 (4.15)	2.10 ± 0.43 (2.10)	2.20 ± 0.67 (2.20)
60 days	4.31 ± 0.64 (4.34)	2.16 ± 0.45 (2.16)	2.24 ± 0.75 (2.24)

According to both the EDS analysis and the high-magnification SEM images of the interface between Nurse's A implant and natural bone, the reaction zone was composed of the Ca-P phase that contained a small quantity of Si, which had almost disappeared a short distance away from the reaction zone (Table 2). No obvious morphological differences were obtained between the newly-formed bone and the old bone into which the implants were inserted.

Table 4 provides information about the residual biomaterial and the resorption rate at different implantation times. Implant volume progressively decreased as bone formation increased along the implant periphery. Filling the central porosities of the implant led to an almost complete cortex closure on day 60. By day 60 post-implant, implantation showed extensive bone resorption (47.38% ± 1.24%). Alterations were not observed during the resorption process of the correct material, nor did any interference take place for the gradual replacement with new bone at the material's implant site.

Table 4. Residual biomaterial and resorption rate 15, 30, and 60 days after implantation. Mean ± SD (Median).

Time of Implantation	Implant Material	
	Residual Biomaterial (%)	Resorption Rate
15 days	73.32 ± 2.04 (73.32)	26.68 ± 1.05 (26.68)
30 days	64.21 ± 1.07 (64.21)	35.79 ± 0.74 (35.80)
60 days	47.38 ± 1.24 (47.39)	52.62 ± 1.12 (52.62)

The Ca-P phase was further identified by examining thin sections under a transmission electron microscope. From a structural and morphological perspective, the present research confirmed that bone was mimicked by the newly-formed phase. Figure 7 displays the implant interface and the bright field image of the stained Ca-P. The micrograph well resolved collagen fibers with the characteristic banding. The selected area diffraction pattern of the unstained thin sections also comprised the new interface phase (Figure 7B), which resulted in typical arcing in the (002) direction given the nano-apatite crystals' preferential orientation in the collagen fiber matrix.

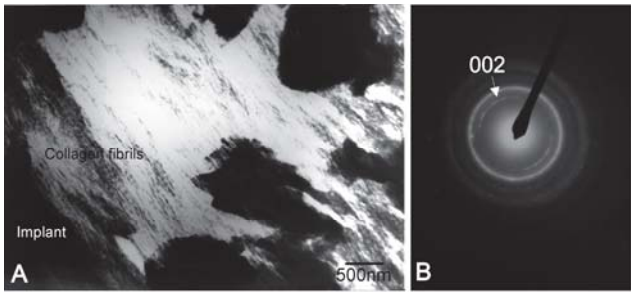

Figure 7. (**A**) Stained interface in a transmission electron micrograph on day 60, where well-resolved collagen fibers are observed in the newly-formed Ca-P phase; (**B**) equivalent selected area diffraction pattern of new bone tissue; thin unstained section.

Figure 8 depicts the μ-Raman spectra from the reaction zone shown in Figure 6B (points 1 and 2) after 60 days of implantation in the 100–1200 cm^{-1} and 3550–3600 cm^{-1} spectral regions. To facilitate comparison, the Raman spectra of pure-Hydroxyapatite (Aldrich) was measured and is represented in Figure 8. Bands were typical of a hydroxyapatite phase [20,23], with the corresponding vibration modes of the PO_4^{3-} group at a wavenumber of around 432 and 443 cm^{-1} (ν_2 symmetric bending mode), 579, 588, and 607 cm^{-1} (ν_4 antisymmetric bending mode), 963 cm^{-1} (ν_1 symmetric stretching mode) and 1029, 1054, and 1074 cm^{-1} (ν_3 antisymmetric stretching mode). An intense Raman peak appeared at 3576 cm^{-1}, and was caused by the O–H stretching mode.

After 60 days of implantation, in reaction area one different bands from those of Nurse's A (Figure 8) can be observed in the Raman spectra. The large line widths of the new bands are typical of non-crystalline materials. Bands were related to the presence of apatite and Nurse's A amorphous phases in the material interphase. The vibrations of the ν_2 and ν_4 modes of the phosphate groups in the apatite phases have been reported to be around 432–450 and 580–617 cm^{-1}, respectively. The presence of two broad bands at 510–600 and 711–715 cm^{-1} can be associated with the CO_3^{2-} groups in the apatite phases [20,23], and/or with the contributions of combining the vibrations of the O–Si–O and O–P–O bonds in the amorphous-like phases [24].

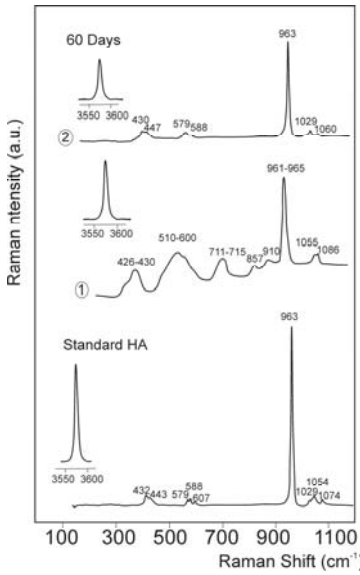

Figure 8. μ-Raman spectra of pure hydroxyapatite and Nurse's A implant–bone interphase. See Figure 6B for the analyzed spots.

Bands of around 440, 540, 590, and 700 cm^{-1} have been assigned in phosphate that contained silicate glasses in relation to the vibrations in phosphorus-oxygen units [24,25]. Bands of around 695 and 780 cm^{-1} have been reported in the Raman spectrum of calcium–phosphate glasses [24,25]. In the present work, a band at 961–965 cm^{-1} was observed close to the most intense peak of Nurse's A ceramic (~961 cm^{-1}, Figure 4) and the principal absorption peak of hydroxyapatite (963 cm^{-1}, Figure 8) [20,23]. At a higher wave number, two bands were observed. The band of around 1055 cm^{-1} was most characteristic of the CO_3^{2-} units in the structure of the carbo-apatite phases [20,23], although the vibrations related to the asymmetric stretching modes of groups Si–O–Si have also been reported in this region [21,22]. The vibrations of groups $–PO_3$ and $–PO_2$ in the phosphate amorphous phases could contribute to this broad band between 1000 and 1300 cm^{-1} [23,24]. An intense Raman peak appeared at 3576 cm^{-1}, which was caused by the O–H stretching mode. It is noteworthy that the bands of Nurse's A in reaction zone two disappeared, and that the intensity and crystallinity of the hydroxyapatite bands increased.

3. Discussion

The obvious sharp peaks and low backgrounds in Figure 1 suggest that the obtained biomaterial powders were highly crystalline. The SEM micrographs and EDS analyses showed that only one homogeneous phase was present in the obtained material. The material's composition, established by the quantitative analysis by EDS at different sample surface points, was around 18.28% SiO_2, 59.49% CaO, and 22.23% P_2O_5 (wt %), and came close to the synthesized material's composition determined by the chemical analysis (around 18.36 wt % SiO_2, 59.96 wt % CaO, and 21.68 wt % P_2O_5).

There is some controversy in the published literature as to the effect of porosity on bone regeneration. Although it has been generally recognized that large pores (>100 μm) enhance new bone formation because they allow the migration and proliferation of osteoblasts and mesenchymal cells, it has also been reported that presence of micro-porosity alters the pattern and dynamics of osteointegration [26], and might enhance ionic exchange with body fluids. It has also been reported that a nanoporous structure improves cell adhesion, proliferation, and differentiation. Nevertheless, pore interconnectivity has been indicated as a major benefit [27].

The measured porosity values (Table 1) showed intra- and inter-particle porosity, as well as total porosity. The majority of studies published in the literature present only total porosity values. However, information about pore size distribution might prove even more relevant to anticipating implant performance. A detailed analysis of the pore size distribution curves that were obtained by mercury intrusion revealed that the major contribution seems to derive from the intraparticle spaces with 15.013% of the total porosity (20.21%).

If we bear in mind the mechanism that several authors have proposed to explain the bioactive response of calcium silicate/phosphate materials [1,5,6,8,16] and the experimental results obtained herein, the reaction of Nurse's A material *in vivo* could be described as a dissolution–transformation process. The SEM and EDS results revealed the preferential dissolution process of Nurse's A material, while the colonization of the implant by newly formed bone on the material surface and into the pores was evidenced by SEM and TEM microscopy. The SEM observation of the cross-section of the sample implanted for 30 and 60 days proved that the process took place not only on the material's surface, but also in the material's internal pores. The Raman results indicated that the newly formed bone was composed of a carbohydroxyapatite phase.

This research demonstrated that Ca, P, and Si ions were released (Table 2), which favored new bone growth. High Ca and P levels could stimulate osteogenesis, given their effects on osteoblast gene expression, as Lazary *et al.* have described [28]. In normal calcified bone, Ca/P molar ratios rise with increased calcification. The presence of silicon is essential for all of these elements because it promotes mineralization processes. The porous Nurse's A material offers biocompatibility, has good mechanical strength (Table 1), and causes no adverse inflammatory reactions at the insertion site. As it is absorbable, its rapid replacement with new bone does not react to foreign bodies, so either

a slight or no inflammatory reaction took place. The same can be stated of the control samples, as their rapid replacement with new bone enabled a bone matrix within the material to be established, which conferred the receiving area similar physical properties to bone.

There may be two reasons for the higher Ca/P ratio obtained. On the one hand, the first important factor is the release of continuous Ca from Nurse's A ceramic. On the other hand, bone can be enriched by carbonate ions, and by producing carbonate-enriched HA. This observation suggests that the material surface could provide an optimal stratum for bone tissue ingrowth. The new bone formation mechanism can be summarized in the following steps:

Dissolution of Nurse's A phase with the release of Ca^{2+} and $HSiO_4{}^-$ as majority ions, and increased Ca^{2+}, $HSiO_4{}^-$, OH^- ionic activities in the neighborhood of the reacting surface until they exceeded the solubility product of HA, led to:

$$Ca_7(PO_4)_2(SiO_4)_2 + 2H_2O \rightarrow 2SiO_4{}^{4-} + 2HPO_4{}^{2-} + 7Ca^{2+} + 2OH^-$$

This reaction started on the material's surface, and progressed deeply into the material in the confined pores as Nurse's A ceramic was dissolved. Apatite layer nucleation occurred through a reaction of phosphate ions with the excess calcium ions released to the medium by the ceramic. The silicate ions released by the ceramic can produce silicon HA. The SEM-EDS data indicated a very small quantity of silicon substitution in the apatite phase: 31.57/14.09/0.17 (Ca/P/Si wt %):

$$(6-x)HPO_4{}^{2-} + ySiO_4{}^{4-} + 10Ca^{2+} + 8OH^- \rightarrow Ca_{10-x}(HPO_4)_x(PO4)_{6-y}(SiO_4)_y(OH)_{2-x} + 6H_2O$$

The silicon that was not implicated in the reaction migrated through the medium away from the interface. Nonetheless, the diffusion of ions across the interface could stop, given the new bone layer's thickness and structure, which was perhaps why we found Si in the new bone layer (Table 2). Bone could be enriched by carbonate ions, could produce the carbonate-enriched HA of variable $CO_3{}^{2-}$ content and lead to variable Ca/P ratios (higher than pure HA) by substituting $PO_4{}^{3-}$ by the $CO_3{}^{2-}$ groups (Table 3 and Figure 8).

What this indicates is that the new bone formation process at the interface and the new bone ingrowths into the implant would continue, provided the ion exchange mechanism between the implant and body fluids took place, assuming that the implant still remained in a biologically healthy environment. We expected this process to come to an end when the supply of Ca, P, and Si ions from the implant part to the surroundings finished. This could occur when the whole implant underwent transformation into the bone phase (and therefore its function as a hard tissue substitute material would be fulfilled), or when the diffusion of the ions across the interface stopped owing to the new bone layer's thickness and structure. These results suggested that Nurse's A ceramic continued to be morphologically active in the natural hard tissue environment, and was bound directly to bone through a Ca-P rich layer with a trace of Si by mimicking natural bone in terms of morphology and composition.

Our study results indicated a strong solution-mediated effect of soluble silicate ions on bone remodeling as silicate ions originated from the dissolution of Nurse's A ceramic. So, they could play a role in accelerating the bone mineralization process around the implant. By means of electron probe microanalysis, the studies of Carlisle have stressed that silicon plays an integral role during bone mineralization processes [29]. Silicon is essential for certain biological tissues to develop and grow—e.g., bone, teeth, and some invertebrate skeletons. Previous research has shown that dietary silicon intake is positively associated with cortical mineral density, which is subject to estrogen availability in humans [11,29,30]. The present research proved that silicon was present at several concentrations in all the phases that formed on the ceramic surface during implantation (Table 2). Although the present paper emphasizes the influence of silicate ions in accelerating the apatite formation process on the surface and inside the implant, it is important to consider the cell- and solution-mediated effects of Ca-P-Si ions on the Nurse's A ceramic osseo-integration processes, because both processes likely occurred in parallel at the implant–tissue interface.

This study also indicated that overall implant colonization was feasible because average pore size was suitable [2]. Such porosity has been reported to allow fibrovascular and bone tissue ingrowth, which have enabled direct integration with neighboring bone [31,32]. Our study also showed that the material was osteoconductive in a physiological environment. The regions with Si-Ca-P particles in the free form were identified near the new bone layer (Figures 5 and 6). Granular entities were also found to cover the new bone more closely to the vessel (Figure 6C). This finding supports the "anchorage-dependence" theory, where cell proliferation, growth and differentiation require a substrate to adhere to it [31–33]. Osteoblasts must react with granular material before growing and proliferating on the HA surface. Granular material may contain proteins from blood, extracellular fluids, products secreted by cells, or glass particles in various stages of degradation [33–36]. When a biomaterial comes into contact with blood, a certain amount of proteins is absorbed prior to cells interacting with the material [33–36]. In particular, proteins preferentially absorb on a given material [36].

This research suggested that Nurse's A ceramic material remained morphologically active in a naturally hard tissue environment, and was bound to bone through a Ca-P layer with traces of Si with dense bone tissue characteristics. The porous implanted material indicated that the observed gradual degradation could be attributed to its components' different solubilities: soluble calcium, phosphate, and silicon, and suitable pore size. A large amount of newly-formed bone tissue was observed in the bone defects treated with Nurse's A ceramic, with a resorption rate of 52.62% $\pm$ 1.12% and of 47.38% $\pm$ 1.24% for the residual biomaterial, after 60 healing days. Other studies have shown that porous HA does not significantly degrade, but remains a permanent fixture susceptible to long-term failure [4,37,38]. Although α- and β-TCP ceramics are degradable at a quicker degradation rate than HA, *in vivo* osteogenesis of sintered α- and β-TCP ceramics is far from optimal [3,5]. Recently, Mate-Sanchez *et al.* [3,5,7,39] found that Si-TCP grafts exhibited better dimensional stability and increased bone-to-implant contact with a reabsorption rate of ~71.5% for α-TCP and ~42.2% for Si-TCP after implanted *in vivo* for 60 days.

Based on these results, we believe that Nurse's A ceramic material could be used as an alternative to natural bone because it gradually reabsorbed and also allowed new bone to grow and remodel over the whole implant volume. Future research should be conducted using standard materials, such as Si-hydroxyapatite or Si-tricalcium phosphate. The ceramic's biological performance should be investigated in different bone defect models, such as those of critical-size or compromised situations (e.g., osteoporosis), and probably with long-term assays, as proposed in International Standard ISO-10993-5.

4. Materials and Methods

4.1. Biomaterial

Porous calcium silicophosphate ceramic was obtained by a solid-state reaction to form a stoichiometric mixture of calcium hydrogen phosphate anhydrous (CaHPO4, Panreac, Castellar del Vallès, Spain), calcium carbonate ($CaCO_3$ > 99.0 wt % Fluka, St. Louis, MO, USA) with an average particle size of 13.8 μm, and silicon oxide (SiO_2 > 99.7 wt %, Strem Chemicals, Inc., Newburyport, MA, USA) with an average particle size <50 μm. Details of this technique can be found in a previous publication [17].

The ceramic's chemical composition was analyzed by X-ray Fluorescence (XRF, Model MagiX Super Q version 3.0 Philips, Eindhoven, The Netherlands) spectrometry. The powder material was mineralogically characterized by XRD (Bruker-AXS D8Advance, Karksruhe, Germany). A comparison was made with the database of the Joint Committee on Powered Diffraction Standards (JCPDS).

The material's microstructure was characterized by SEM-EDS (SEM-Hitachi S-3500N, Ibaraki, Japan) at an accelerating voltage of 20 kV. μ-Raman (Jobin Ivon T64000 spectrometer Edison, Middlesex County, NJ, USA) equipped with a microscope was used to examine the structural characteristics of the obtained ceramic.

Information concerning the sample porosity and pore size distribution was obtained by mercury porosimetry in a Poremaster-60 GT (Quantachrome Instruments, Boyton Beach, FL, USA) within the 5.395 KPa to 410,785.062 KPa pressure range, which corresponds to a range of pore diameters between 300 and 0.0035 μm. Three samples (~0.53 g) were analyzed by this technique. A fourth sample was also used if the measured porosity values differed by more than 5%.

The particle's real density (sample mass/Volume of the solid), excluding empty spaces, was determined by Helium gas pycnometry (Quantachrome Instruments, Boyton Beach, FL, USA). Strength was determined by the Brazilian test or the Diametric Compression of Discs Test (DCDT) [9]. The test was conducted on discs with a diameter of ~18.40 mm (D) and a thickness (t) of ~4.70 mm, (t/D ~0.25). Load was applied at a displacing rate of 0.5 mm/min of the machine frame.

4.2. Animal Experimentation

4.2.1. Principal Protocol

The study protocol was examined and approved by the Institutional Ethic and Animal Experimentation Committee of the University Miguel Hernandez according to Spanish Government Guidelines and European Community Guidelines for animal care (authorized No. 2014/VSC/PEA/00056 tipo2). All surgical procedures, implant insertions, and sacrifices were performed under rigorous aseptic conditions by an experienced surgeon (Dr. L. Meseguer-Olmo, authorized in small animal research). Fifteen male New Zealand rabbits were used, which weighed 3.5–4.5 kg. The ceramic was randomly implanted into critical-size defects in the tibias of these animals.

4.2.2. Surgery

Two circular critical-size defects (6 mm Ø) were created in each tibia. The definition of critical size is a defect with no spontaneous closure by day 60. The surgical procedure affected the proximal-medial area of the tibias some millimeters below frontal tuberosity. Spherical surgical drills (diameter of 6 mm) operated at low rotation speed and constant irrigation to remove bone tissue (Figure 9A,B). Nurse's A ceramic was implanted in the critical size defects created per tibia in the 15 New Zealand rabbits, which totaled 60 defects. They were divided into a ceramic-filled test group (n = 30) and a control group (n = 30) (Figure 9C).

General anesthesia included ketamine plus chlorbutol (5–8 mg/kg intravenously), 0.5–1 mg/kg acepromazine maleate as a coadjutant and 0.05 mg/kg atropine. Amoxicillin (0.1 mL/kg) was administered intramuscularly at the end of surgery.

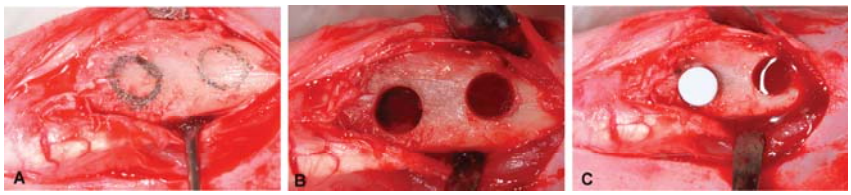

Figure 9. Surgical procedure. (**A**) Tibia after flap removal; (**B**) Preparation of two critical defects of 6 mm diameter located at 4 mm from the top margin with 3 mm of separation between defects; (**C**) biomaterial placement.

4.3. Implant Characterization

Animals were sacrificed with an overdose of anaesthetics in groups of five on post-surgery days 15, 30, and 60. The specimens to undergo SEM examination were prepared from the tibia segments that contained the implant, along with surrounding tissue. Firstly, 10 vol % buffered formaldehyde solution was utilized to fix samples. Samples were then dehydrated in a series of graded alcohol solutions and were hydroxyethyl-methacrylate resin-embedded. All of the undecalcified blocks were polished with

6, 3, and 1 μm diamond pastes. After palladium-coating blocks, scanning secondary electron imaging was performed at 20 keV.

An elemental analysis was run to detect the chemical degradation process and to observe any changes in medullary composition. Thickness measurements of the Ca-P layer were taken on SEM micrographs at a high magnification. Twelve measurements per sample were taken, which gave a total of 60 measurements per implantation period.

Material resorption was assessed by comparing the SEM images before and after implantation. The Image J image analysis program (National Institutes of Health, Bethesda, MD, USA) was used to calculate the resorption rates by demarcating the area of interest as the total biomaterial upon implantation, and then measuring its perimeter and comparing it with the residual material after 15, 30, and 60 days.

The newly-formed Ca-P phase formed at the interface was morphologically and structurally identified by Transmission Electron Microscopy (TEM). Bright field images were studied with Selected Area Diffraction patterns (SAD). The Jeol Jem 2010 microscope (Jeol Ltd., Tokyo, Japan)—which operated at 200 keV and with an 80-cm camera length condition—was used for the SAD patterns.

Raman spectroscopy was used to study the structural characteristics of the newly-formed Ca-P phase that formed at the interface. The μ-Raman microprobe instrument was equipped with a microscope and recorded the spatial resolution on the sample close to 1 μm. The 488-nm line of an Ar+ laser was used as excitation, which centered on a spot with a diameter of ~1 μm. The sample's incident power was ~2 mW.

4.4. Statistical Analysis

The statistical analysis was performed with the PASW Statistics software, v18.0.0 (SPSS Inc., Armonk, NY, USA). Values were recorded as means ± standard deviation.

5. Conclusions

An *in vivo* evaluation of porous Nurse's A ceramic was made by performing an implantation into the tibias of adult New Zealand rabbits. Despite the limitations of this animal study, we can state that Nurse's A ceramic is a bioactive osteoconductive biocompatible material. Ceramic material favors bone regeneration at the implantation site, does not interfere with normal healing processes, and acts as an ideal matrix for new bone formation.

The mechanism of bone bonding to the implant was the result of the dissolution and transformation of Nurse's A implant, which brought about the formation of a new Ca-P layer at the implant interface, and the entire implanted material was transformed into a bone-like phase. From a morphological and structural viewpoint, this phase mimicked natural bone. So, we expect Nurse's A ceramic to be satisfactorily used for repairing or substituting living bone.

Acknowledgments: Part of this work has been supported by Spanish Ministry of Economy and Competitiveness (MINECO) contract grant number: MAT2013-48426-C2-2-R.

Author Contributions: Ruben Rabadan-Ros and Pablo Velasquez performed the implant characterization; Luis Meseguer-Olmo conducted the surgeon and together with Piedad N. De Aza designed and performed the experiments, contributed to the analyses and discussion of the results and prepared the manuscript.

Conflicts of Interest: The authors declare no conflicts of interest.

References

1. Bohner, M. Silicon-substituted calcium phosphates—A critical view. *Biomaterials* **2009**, *30*, 6403–6406. [CrossRef] [PubMed]
2. Chevalier, J.; Gremillard, L. Ceramics for medical applications: A picture for the next 20 years. *J. Eur. Ceram. Soc.* **2009**, *29*, 1245–1255. [CrossRef]

3. Mate-Sanchez de Val, J.E.; Calvo-Guirado, J.L.; Delgado-Ruiz, R.A.; Ramirez-Fernandez, M.P.; Negri, B.; Abboud, M.; Martinez, I.M.; de Aza, P.N. Physical properties, mechanical behavior, and electron microscopy study of a new α-tcp block graft with silicon in an animal model. *J. Biomed. Mater. Res. A* **2012**, *100*, 3446–3454. [CrossRef] [PubMed]
4. Calvo-Guirado, J.L.; Ramirez-Fernandez, M.P.; Mate-Sanchez de Val, J.E.; Negri, B.; Velasquez, P.; de Aza, P.N. Enhanced bone regeneration with a novel synthetic bone substitute in combination with a new natural cross-linked collagen membrane: Radiographic and histomorphometric study. *Clin. Oral Implant. Res.* **2015**, *26*, 154–164. [CrossRef] [PubMed]
5. De Aza, P.N.; Luklinska, Z.B.; Mate-Sanchez de Val, J.E.; Calvo-Guirado, J.L. Biodegradation process of α-tricalcium phosphate and α-tricalcium phosphate solid solution bioceramics *in vivo*: A comparative study. *Microsc. Microanal.* **2013**, *19*, 1350–1357. [CrossRef] [PubMed]
6. Velasquez, P.; Luklinska, Z.B.; Meseguer-Olmo, L.; Mate-Sanchez de Val, J.E.; Delgado-Ruiz, R.A.; Calvo-Guirado, J.L.; Ramirez-Fernandez, M.P.; de Aza, P.N. αTCP ceramic doped with Dicalcium Silicate for bone regeneration applications prepared by powder metallurgy method. *In vitro* and *in vivo* studies. *J. Biomed. Mater. Res. A* **2013**, *101*, 1943–1954. [CrossRef] [PubMed]
7. Calvo-Guirado, J.L.; Ramirez-Fernandez, M.P.; Delgado-Ruiz, R.A.; Mate-Sanchez de Val, J.E.; Velasquez, P.; de Aza, P.N. Influence of biphasic α-TCP with and without the use of collagen membranes on bone healing of surgically critical size defects. A radiological, histological and histomorphometric study. *Clin. Oral Implant. Res.* **2014**, *25*, 1228–1238. [CrossRef] [PubMed]
8. Serena, S.; Caballero, A.; de Aza, P.N.; Sainz, M.A. New evaluation of the *in vitro* response of silicocarnotite monophasic material. *Ceram. Int.* **2015**, *41*, 9411–9419. [CrossRef]
9. García-Paez, I.H.; Garcıa Carrodeguas, R.; de Aza, A.H.; Baudin, C.; Pena, P. Effect of Mg and Si co-substitution on microstructure and strength of tricalcium phosphate ceramics. *J. Mech. Behav. Biomed. Mater.* **2014**, *30*, 1–15. [CrossRef] [PubMed]
10. Lugo, G.J.; Mazón, P.; de Aza, P.N. Phase transitions in single phase Si–Ca–P-based ceramic under thermal treatment. *J. Eur. Ceram. Soc.* **2015**, *35*, 3693–3700. [CrossRef]
11. Jugdaohsingh, R.; Tucker, K.L.; Qiao, N.; Cupples, L.A.; Kiel, D.P.; Powell, J.J. Dietary silicon intake is positively associated with bone mineral density in men and premenopausal women of the framingham offspring cohort. *J. Bone Miner. Res.* **2004**, *19*, 297–307. [CrossRef] [PubMed]
12. Sayer, M.; Stratilatov, A.D.; Reid, J.; Calderin, L.; Stott, M.J.; Yin, X.; MacKenzie, M.; Smith, T.J.N.; Hendry, J.A.; Langstaff, S.D. Structure and composition of silicon-stabilized tricalcium phosphate. *Biomaterials* **2003**, *24*, 369–382. [CrossRef]
13. Reid, J.W.; Tuc, L.K.; Sayer, M.; Fargo, K.; Hendry, J.A. Synthesis and characterization of single-phase silicon-substituted α-tricalcium phosphate. *Biomaterials* **2006**, *27*, 2916–2925. [CrossRef] [PubMed]
14. Martinez, I.M.; Velasquez, P.A.; Meseguer-Olmo, L.; Bernabeu-Esclapez, A.; de Aza, P.N. Preparation and characterization of novel bioactive α-Tricalcium Phosphate doped with Dicalcium Silicate ceramics. *Mater. Sci. Eng. C* **2012**, *32*, 878–886. [CrossRef]
15. Martinez, I.M.; Velasquez, P.A.; Meseguer-Olmo, L.; de Aza, P.N. Production and study of *in vitro* behaviour of monolithic α-Tricalcium Phosphate based ceramics in the system $Ca_3(PO_4)_2$–Ca_2SiO_4. *Ceram. Int.* **2011**, *37*, 2527–2535. [CrossRef]
16. Carrodeguas, R.G.; de Aza, A.H.; Jimenez, J.; de Aza, P.N.; Pena, P.; López-Bravo, A.; de Aza, S. Preparation and *in vitro* characterization of wollastonite doped tricalcium phosphate bioceramics. *Key Eng. Mater.* **2008**, *361–363*, 237–240. [CrossRef]
17. Lugo, G.J.; Mazón, P.; de Aza, P.N. Material processing of a new calcium silicophosphate ceramic. *Ceram. Int.* **2016**, *42*, 673–680. [CrossRef]
18. Ros-Tarraga, P.; Mazón, P.; Meseguer-Olmo, L.; de Aza, P.N. Revising the subsystem nurse's A–phase-silicocarnotite within the system $Ca_3(PO_4)_2$–Ca_2SiO_4. *Materials* **2016**. [CrossRef]
19. Rubio, V.; de la Casa-Lillo, M.A.; de Aza, S.; de Aza, P.N. The system $Ca_3(PO_4)_2$–Ca_2SiO_4: The sub-system Ca_2SiO_4–$7CaOP_2O_5 \cdot 2SiO_2$. *J. Am. Ceram. Soc.* **2011**, *94*, 4459–4462. [CrossRef]
20. De Aza, P.N.; Guitian, F.; Santos, C.; de Aza, S.; Cusco, R.; Artus, L. Vibrational properties of calcium phosphare compounds. II Comparation between hydroxyapatite and β-tricalcium phosphate. *Chem. Mater.* **1997**, *9*, 916–922. [CrossRef]

21. Remy, C.; Reynard, B.; Madon, M. Raman spectroscopic investigations of Dicalcium Silicate: Polymorphs and high-temperature phase transformations. *J. Am. Ceram. Soc.* **1997**, *80*, 413–423. [CrossRef]
22. Ibáñez, J.; Artús, L.; Cuscó, R.; López, A.; Menéndez, E.; Andrade, M.C. Hydration and carbonation of monoclinic Ca_2SiO_4 and Ca_3SiO_5 studied by Raman spectroscopy. *J. Raman Spectrosc.* **2001**, *38*, 61–67. [CrossRef]
23. Antonakos, A.; Liarokapis, E.; Leventouri, T. Micro-Raman and FTIR studies of synthetic and natural apatites. *Biomaterials* **2007**, *28*, 3043–3054. [CrossRef] [PubMed]
24. Bonino, F.; Damin, A.; Aina, V.; Miola, M.; Vernè, E.; Bretcanu, O.; Bordiga, S.; Zecchina, A.; Morterra, C. *In situ* Raman study to monitor bioactive glasses reactivity. *J. Raman Spectrosc.* **2008**, *39*, 260–264. [CrossRef]
25. Aguiar, H.; Solla, E.L.; Serra, J.; González, P.; León, B.; Malz, F.; Jäger, C. Raman and NMR study of bioactive Na_2O–MgO–CaO–P_2O_5–SiO_2 glasses. *J. Non Cryst. Solids* **2008**, *354*, 5004–5008. [CrossRef]
26. Hadjicharalambous, C.; Prymak, O.; Loza, K.; Buyakov, A.; Kulkov, S.; Chatzinikolaidou, M. Effect of porosity of alumina and zirconia ceramics toward pre-osteoblast response. *Front. Bioeng. Biotechnol.* **2015**, *3*, 175–180. [CrossRef] [PubMed]
27. Kumar, A.; Akkineni, A.R.; Basu, B.; Gelinsky, M. Three-dimensional plotted hydroxyapatite scaffolds with predefined architecture: Comparison of stabilization by alginate cross-linking *versus* sintering. *J. Appl. Biomater. Funct. Mater.* **2015**, *30*, 1168–1181. [CrossRef] [PubMed]
28. Lazáry, A.; Balla, B.; Kósa, J.P.; Bácsi, K.; Nagy, Z.; Takács, I.; Varga, P.P.; Speer, G.; Lakatos, P. Effect of gypsum on proliferation and differentiation of MC3T3-E1 mouse osteoblastic cells. *Biomaterials* **2007**, *28*, 393–399. [CrossRef] [PubMed]
29. Carlisle, E.M. Silicon: A possible factor in bone calcification. *Science* **1970**, *167*, 279–280. [CrossRef] [PubMed]
30. Schwarz, K.A. Bound form of silicon in glycosaminoglycans and polyuronides. *Proc. Natl. Acad. Sci. USA* **1973**, *70*, 1608–1612. [CrossRef] [PubMed]
31. De Aza, P.N.; Mate-Sanchez de Val, J.E.; Baudin, C.; Perez Albacete-Martinez, C.; Armijo-Salto, A.; Calvo-Guirado, J.L. Bone neoformation of a novel porous resorbable Si-Ca-P-based ceramic with osteocondutive properties: Physical and mechanical characterization, histological and histomorphometric study. *Clin. Oral Implant. Res.* **2016**. [CrossRef] [PubMed]
32. De Aza, P.N.; Peña, J.I.; Luklinska, Z.B.; Meseguer-Olmo, L. Bioeutectic® ceramics for biomedical application obtained by Laser Floating Zone Method: *In vivo* evaluation. *Materials* **2014**, *7*, 2395–2410. [CrossRef]
33. Baier, R.E. The organisation of blood components near interface. *Ann. N. Y. Acad. Sci.* **1977**, *283*, 17–36. [CrossRef]
34. Kochwa, S.; Litwak, R.S.; Rosenfield, R.E.; Leonard, E.F. Blood elements at foreign surfaces: A biochemical approach to the study of the adsorption of plasma proteins. *Ann. N. Y. Acad. Sci.* **1977**, *283*, 37–49. [CrossRef]
35. Breemhaar, W.; Brinkman, E.; Ellens, D.J.; Beugeling, T.; Bantjes, A. Preferential adsorption of high-density lipoprotein form blood plasma onto biomaterial surfaces. *Biomaterials* **1984**, *5*, 269–274. [CrossRef]
36. Xynos, I.D.; Edgar, A.J.; Buttery, L.D.K.; Hench, L.L.; Polak, J.M. Ionic products of bioactive glass dissolution increase proliferation of human osteoblasts and induce insulin-like growth factor II mRNA expression and protein synthesis. *Biomed. Biophys. Res. Commun.* **2000**, *276*, 461–465. [CrossRef] [PubMed]
37. Beltrame, F.; Cancedda, R.; Canesi, B.; Crovace, A.; Mastrogiacomo, M.; Quarto, R.; Scaglione, S.; Valastro, C.; Viti, F. A simple non invasive computerized method for the assessment of bone repair within osteoconductive porous bioceramic grafts. *Biotechnol. Bioeng.* **2005**, *92*, 189–198. [CrossRef] [PubMed]
38. Mate-Sanchez de Val, J.E.; Calvo-Guirado, J.L.; Gomez Moreno, G.; Perez Albacete-Martinez, C.; Mazón, P.; de Aza, P.N. Influence of hydroxyapatite granule size, porosity and crystallinity on tissue reaction *in vivo*. Part A: Synthesis, characterization of the materials and SEM analysis. *Clin. Oral Implant. Res.* **2016**. [CrossRef] [PubMed]
39. Mate-Sanchez de Val, J.E.; Calvo-Guirado, J.L.; Delgado-Ruiz, R.A.; Ramirez-Fernandez, M.P.; Martinez, I.M.; Granero-Marin, J.M.; Negri, B.; Chiva-Garcia, F.; Martinez-Gonzalez, J.M.; de Aza, P.N. New block graft of α-TCP with silicon in critical size defects in rabbits: Chemical characterization, histological, histomorphometric and micro-CT study. *Ceram. Int.* **2012**, *38*, 1563–1570. [CrossRef]

9. RESULTADOS Y DISCUSIÓN

En la presente Tesis Doctoral se ha evaluado la bioactividad, biofuncionalidad, y la respuesta celular *in vitro* de la cerámica monofásica Fase A de Nurse, además de su comportamiento biológico *in vivo* después de ser implantada en tejido óseo de conejos Nueva Zelanda (NZ). La interpretación de los resultados alcanzados han evidenciado que el biomaterial en el transcurso del estudio es bioactivo y reabsorbible y, al mismo tiempo, posee el potencial de estimular la proliferación de *ah*MSCs y su diferenciación a células de estirpe osteoblástica, responsables directas de la síntesis de la matriz ósea extracelular.

Para verificar la hipótesis de trabajo, se ha tratado de dar respuesta en el primer artículo ***"In vitro behaviour of Nurse´s Ass – phase: A new calcium silicophosphate ceramic"*** a los dos primeros objetivos propuestos en esta Tesis. Para ello se ha estudiado la bioactividad de la cerámica Fase A de Nurse *in vitro* utilizando SFA con el fin de determinar la capacidad de mineralización, la velocidad de disolución y la liberación iónica al medio de la biocerámica. Los resultados obtenidos ponen de manifiesto claramente que después de la inmersión en SFA, se forman dos capas bien diferenciadas. La más externa corresponde a una capa densa de hidroxiapatita deficiente en calcio (HADC) bien cristalizado, similar a los apatitos naturales, tal como se ha puesto de manifiesto por Microscopía Electrónica de Barrido - Espectrometría de Dispersión de Energías de Rayos X (MEB-EDX), Microscopía Electrónica de Transmisión – Difracción de Electrones en el Área Seleccionada (MET-DAS) y se ha confirmado por micro-Raman. La otra capa intermedia está formada por HADC porosa tal y como se ha podido establecer por MEB-EDX, debido a una a transformación

pseudomórfica de Si-Ca-P (Fase A de Nurse) en HADC. Así mismo, se ha detectado la presencia de partículas de sílice amorfa mediante MET-DAS debido a la disolución del material y confirmado por confirmado por Espectrometría de Masas con Plasma Acoplado Inductivamente (ICP-MS) mediante un incremento de la concentración de Si (de 0 a 1.14 mmol), un aumento de la concentración de Ca (de 2.5 a 5.2 mmol) y una disminución en la concentración de P (de 1 a 0.1 mmol) a lo largo de todo el experimento.

Los resultados alcanzados por medio de Microscopía de Fuerza Atómica (MFA) han revelado que el proceso de precipitación/transformación comienza con la formación de partículas nanométricas de forma redondeada en una matriz amorfa. Posteriormente, estos precipitados evolucionan a partículas de forma redonda con una estructura granulada que finalmente cubre por completo la superficie del material cerámico. Estos precipitados han sido identificados por MET y por Espectroscopía de Raman como carbohidroxiapatita (CHA) y la fase amorfa de Ca-Si-P-O-H.

La formación de ambas capas está en consonancia con los resultados previamente descritos por otros investigadores (66, 67, 77, 78) para explicar la respuesta bioactiva de las cerámicas de C_2S. Los hechos expuestos pueden explicarse en principio, por un mecanismo complejo que se desarrolla siguiendo fases consecutivas y en ocasiones solapadas en el tiempo. Así, durante los primeros estadios de inmersión de las muestras en SFA, se ha constatado que tiene lugar un incremento apreciable en la concentración de calcio y silicio en el suero, cuya procedencia únicamente se puede atribuir a la disolución parcial del

material durante el tiempo que estuvo sumergido. De este modo, la Fase A de Nurse en contacto con el SFA, da comienzo a una reacción de intercambio iónico de H_3O^+/H^+ formando grupos silanol (Si-OH^+) en la interfase material-SFA.

Seguidamente hay una disolución parcial de Fase A de Nurse en el SFA liberando iones de SiO_4^{4-}, HPO_4^{2-} y Ca^{2+} conforme a la siguiente reacción:

$$Ca_7(PO_4)_2(SiO_4)_2 + 2H_2O \rightarrow 2SiO_4^{4-} + 2HPO_4^{2-} + 7Ca^{2+} + 2OH^-$$

Posteriormente, se produce una repolimerización de los grupos silanol que llevan a la formación de partículas de sílice amorfa que se distribuyen aleatoriamente por la superficie del material, tal como se ha constatado mediante TEM y MFA). Seguidamente, los grupos $3HPO_4^{2-}$ y Ca^{2+} migran a la superficie del material a través de partículas ricas en SiO_2 y se produce la precipitación de partículas de Ca-P de aspecto redondeado. La presencia de partículas de SiO_2, induce la nucleación y posterior crecimiento de HA según la reacción:

$$3HPO_4^{2-} + 5Ca^{2+} + H_2O \rightarrow Ca_5(PO_4)_3OH + 4H^+$$

Finalmente, tiene lugar la cristalización del $CaO\text{-}P_2O_5$ amorfo mediante la incorporación de iones OH y/o $CO^{3=}$ procedentes de la solución. Como resultado, la superficie del material queda recubierta por un precipitado poli-cristalino de CHA y fase amorfa Ca-Si-P-O-H, datos confirmados mediante los análisis de μ-Raman y MET.

Ahora bien, considerando todas las posibles reacciones de disolución de la Fase A de Nurse también puede precipitarse una fase de Si-HA según la siguiente reacción:

$$(6\text{-}x)HPO_4^{2-} + ySiO_4^{4-} + 10Ca^{2+} + 8OH^- \rightarrow Ca_{10-x}(HPO_4)_x(PO4)_{6-y}(SiO_4)_y(OH)_{2-x} + 6H_2O,$$

tal y como sugieren los resultados obtenidos por medio de MEB-EDX.

Resumiendo, esta secuencia de reacciones químicas comienzan en la superficie de la biocerámica Fase A de Nurse, y progresa hacia el interior del material en los poros confinados formados al disolverse el material. Una vez que los núcleos de apatita se han formado en la superficie de la capa porosa, crecen espontáneamente al consumir los iones calcio y fosfato de la solución de SFA circundante, produciendo como consecuencia la capa externa densa de HA.

En el segundo artículo, ***"Nurse´s A-phase material enhance Adhesion, Growth and Differentiation of Human Bone Marrow-Derived Stromal Mesenchymal Stem Cells"*** se ha evaluado la respuesta celular *in vitro* provocada por la cerámica monofásica Fase A de Nurse, dando respuesta al tercer objetivo. En este estudio, se desarrollan y exponen los primeros pasos para precisar la propiedades osteopromotoras de la biocerámica mediante el uso de técnicas clásicas como la tinción de Alizarin Red (AR-s) o la medición de la actividad Fosfatasa Alcalina (ALP), abordando el cuarto objetivo junto al tercer artículo "***Impact of a porous Si-Ca-P monophasic ceramic on variation of osteogenesis-related gene expression of adult human mesenchymal stem cells***", en el que hemos aplicado técnicas más complejas, precisas y específicas con el propósito de discernir los mecanismos moleculares por los que es estimulada la diferenciación osteogénica de las *ah*MSCs por parte de la biocerámica.

Pese a disponer de resultados previos de liberación iónica del material en SFA, se han realizado nuevos estudios a más largo plazo mediante ICP-MS, esta vez utilizando un medio básico de cultivo celular (DMEM). En esta ocasión, se observó un comportamiento similar excepto en la liberación de Ca, que disminuye a partir de 7 días, y que intuimos sea consecuencia de un proceso de precipitación.

Un aspecto importante a tener en cuenta en el diseño de un dispositivo o material para potencial uso en clínica, es el relacionado con su citotoxicidad o biocompatibilidad. En nuestro estudio, hemos seguido las directrices de la International Standard Organitation (ISO-10993-5) (79) para la evaluación de la citotoxicidad in vitro. Para ello hemos seleccionado, dentro de las tres categorías propuestas por este organismo, los ensayos de contacto directo para evaluar la biocompatibilidad de la cerámica Fase A de Nurse. De los diferentes métodos de medición existentes nos hemos centrado en la medición del crecimiento celular sobre el material mediante técnicas de fluorescencia midiendo la actividad metabólica celular (Alamar Blue), y la observación directa de la superficie del material sembrado mediante Microscopía Electrónica de Barrido de Emisión de Campo Claro (FESEM).

De entre los hallazgos más relevantes apreciados, destacamos que tras un período inicial de inactividad correspondiente a la fase de adaptación al entorno, las *ah*MSCs adheridas proliferan llegando a tapizar toda la superficie del biomaterial formando una monocapa de células alargadas y fusiformes con aspecto fibroblástico. El ensayo Alamar Blue ha demostrado el aumento de la

actividad metabólica de las células a medida que recubrían la superficie del biomaterial, observándose un pico de actividad máxima después de cambiar el medio básico de crecimiento (GM) por medio osteogénico (OM). De forma simultánea, las células fueron adquiriendo una morfología poligonal típica de *ah*MSCs cuando están experimentando diferenciación osteogénica. Estos hechos hacen recapacitar en que el aumento de la actividad metabólica pudiera estar relacionado con cambios en la expresión de integrinas, cadherinas y proteínas del citoesqueleto, así como un aumento del metabolismo aeróbico mitocondrial, que ocurren cuando las *ah*MSCs experimentan cambios morfológicos durante su diferenciación, tal como sugieren otros estudios (80).

La presencia de los marcadores de superficie CD 105, 90 y 73 se considera fundamental durante la caracterización y aislamiento de *ah*MSCs (81). Hemos verificado mediante citometría de flujo que las células sembradas en contacto indirecto con la biocerámica han reducido la expresión de CD105 y CD90, pudiendo considerar este hecho como una consecuencia de la activación del programa de diferenciación (82).

En *ah*MSCs, altos niveles de ALP y producción de Col I están asociados a procesos de diferenciación osteogénica, siendo considerados marcadores osteogénicos tempranos (83). Por otro lado, la formación de nódulos de calcio o la expresión de OCN están asociadas a estadios tardíos de diferenciación osteogénica (84).

En nuestros ensayos hemos comprobado por distintos métodos como la Fase A de Nurse parece inhibir inicialmente la actividad fosfatasa alcalina. Sin

embargo, transcurridos 28 días tras la siembra, las células en contacto directo con la bioceramica han incrementado su actividad ALP. Los estudios genéticos llevamos a cabo mediante análisis de la cuantificación de la reacción en cadena de la polimerasa con transcriptasa inversa (qRT-PCR) han mostrado un aumento en la expresión de los genes que codifican ALP, además de los que codifican Col I, ON, OPN y sialoproteina ósea (BSP), principalmente al final del periodo de estudio y tras sustituir el GM por OM. El marcaje inmunofluorescente ha puesto de manifiesto como la expresión de COLI, OCN, OPN y heparán sulfato (HS) en la matriz extracelular MEx ha aumentado de forma progresiva.

La formación de nódulos de Ca evaluada mediante tinción de Alizarin Red (AR-s) ha sido observada en los cultivos de *ah*MSCs en contacto indirecto con el material transcurridos 28 días desde la siembra y, principalmente, en aquellas que han crecido con OM, mientras que las células control no mostraron tinción alguna en ese periodo.

En resumen, la expresión de los marcadores osteogénicos estudiados ha sido siempre más intensa en las células que han crecido bajo la influencia del biomaterial Fase A de Nurse, especialmente cuando se ha agregado OM a las condiciones del cultivo celular. Probablemente esto se deba al efecto sinérgico de los suplementos incorporados en el OM, la concentración idónea de Ca liberado por la biocerámica (altos niveles de Ca inhiben ALP (85, 86)) y el aumento de los niveles de Si, cuyo papel en la diferenciación osteogénica ha sido ya mencionado (63, 87).

La disponibilidad de Ca y P proporcionada por el biomaterial podría explicar la observación de nódulos o depositos de calcio al mismo tiempo que las células han mostrado actividad fosfatasa alcalina, debido a que éstas dispondrían de todos los elementos necesarios para llevar a cabo el proceso de mineralización de la MEx (86). Además, la unión de los iones de Ca liberados al medio por la biocerámica a receptores de Ca induce la expresión de marcadores típicos de diferenciación como Col I.

Por el contrario, los niveles de OCN hallados han sido bajos, esta circunstancia podría tener su justificación en el hecho de que se trata de un marcador tardío en la diferenciación osteogénica de *ah*MSCs y que no hubiera comenzado a producirse en el periodo estudiado.

Finalmente, en el cuarto artículo "**Morphological and Structural Study of a Novel Porous Nurse´s A Ceramic with Osteoconductive Properties for Tissue Engineering**" se han determinado *in vivo* los cambios experimentados por el material en el transcurso del experimento, así como la naturaleza de los acontecimientos biológicos que acontecen en la interfase biomaterial-hueso huésped tras la implantación intraósea en tibias de conejo de la raza Nueva Zelanda durante 15, 30 y 60 días.

En este estudio, la biocerámica Fase A de Nurse ha actuado como un biomaterial biocompatible, bioreabsorbible y con capacidad osteogénica. Se han detectado cambios en la macro- y micro-estructura de los implantes, tanto en la interfase biomaterial-hueso como en el interior del mismo.

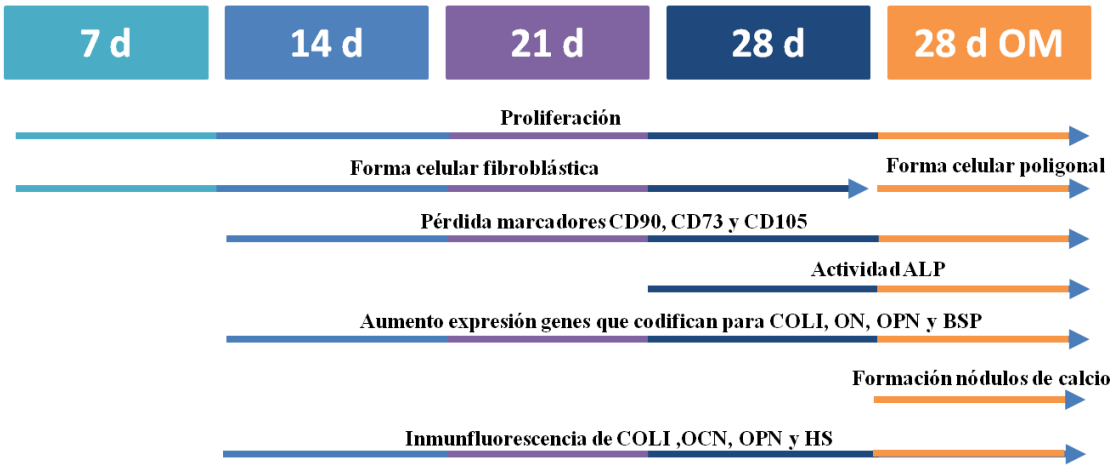

Figura 14. Gráfico que resume la respuesta celular in vitro en términos de biocompatibilidad, proliferación y diferenciación osteogénica de las *ah*MSCs frente a la cerámica monofásica Fase A de Nurse.

En relación con la porosidad del material, se ha determinado la presencia de porosidad inter- e intra-particular mediante porosimetría por inyección de mercurio, determinándose que la mayor contribución de la porosidad del material (20.21 %) corresponde a los espacios intraparticulares menores de 0.86 μm (15.013%).

El análisis elemental EDX ha mostrado una difusión gradual de iones Ca y Si de la biocerámica al hueso neoformado durante los procesos de reabsorción del biomaterial. Se ha comprobado que existen distintas zonas en el biomaterial atendiendo a la relación Ca/P y la proporción de Si, indicando distintos estadios

de reabsorción. Transcurridos 60 días de la implantación, el porcentaje de biomaterial que conserva la composición inicial de la Fase A de Nurse; es decir, el biomaterial residual, es de 47.38% ±1.24%. La interfase biomaterial-hueso huésped se ha caracterizado por mostrar una proporción de Ca/P (≈2.10) menor que el implante original, con una disminución de los niveles de Si respecto al biomaterial inicial. Tanto alrededor del implante como en distintas zonas del interior se han distinguido áreas que, en términos de composición y morfología observada mediante MEB, podrían corresponder con tejido óseo neoformado. Estas zonas han presentado similar proporción Ca/P (≈2.24) que el hidroxiapatito original del hueso, comparten el mismo espectro de Raman que la HA pura, pudiéndose observar, en algunos casos, pequeñas oquedades que podrían corresponder con las lagunas osteocíticas. Por otro lado, como resultado de los procesos de reabsorción, se han encontrado numerosos gránulos en distintas zonas en todo el implante correspondientes a precipitados de CaP.

Así mismo, se ha detectado mediante MET-DAS la presencia de fibras de aspecto estriado en la interfase implante-hueso huésped que podrían corresponder a fibras de colágeno, y la aparición de nano cristales de apatita en la matriz donde se encuentran estas fibras de colágeno.

Atendiendo a los estudios acerca de la bioactividad de los silicofosfatos cálcicos (68, 88, 89) y los resultados obtenidos, la reacción del biomaterial Fase A de Nurse *in vivo* podría definirse como un proceso de disolución-transformación. La continua liberación de Ca por parte de la biocerámica, así como el aporte de carbonato por parte del hueso, propicia un ambiente óptimo para el crecimiento

de tejido óseo. Como ya se ha discutido previamente, la liberación de Ca y P podría estimular la osteogénesis (57, 90), además, ha de tenerse en cuenta la importancia de la presencia de Si debido a su carácter promotor de los procesos de mineralización (59, 63, 67, 87).

10. CONCLUSIONES

1. La biocerámica Fase de Nurse A, tras los ensayos de inmersión en SFA, se comporta como un biomaterial ***bioactivo.*** Facilita la formación de una doble capa de apatita en la superficie, una capa externa que corresponde a una capa densa de HADC y una capa intermedia formada por HADC poroso, que recuerdan a la estructura mineralógica de los huesos.
2. Esta cerámica experimental muestra propiedades biológicas apropiadas proporcionando un microentorno óptimo para la proliferación de *ah*MSCs y su diferenciación osteogénica.
3. Los resultados obtenidos en términos de biocompatibilidad, adhesión y proliferación de *ah*MSCs, mediante ensayos directos e indirectos, demuestran que la cerámica Fase A de Nurse no ha provocado ningún efecto citotóxico, como se demuestra por la adhesión y crecimiento celular sobre el material, comparándolas con *ah*MSCs crecidas sobre plástico y usadas como control.
4. Las *ah*MSCs, bajo la influencia de la biocerámica Fase A de Nurse, pierden marcadores de superficie típicos de células madre mesenquimales como CD73, CD90 y CD105, al mismo tiempo que comienzan a expresar los marcadores típicos osteogénicos Col I, ALP, OCN, ON, OPN y BSP. La expresión estos últimos, es significativamente más intensa en las células que crecen bajo la influencia de la biocerámica respecto al control, y particularmente cuando se incluye suplemento osteogénico en el medio de cultivo.
5. A pesar de las limitaciones de este estudio en animales, podemos afirmar que la biocerámica Fase A de Nurse es un material biocompatible y bioactivo. La

biocerámica favorece la regeneración ósea en el sitio de implantación, no interfiere en los procesos de curación normales, y actúa como una matriz ideal para la neoformación de hueso.

6. El material Fase A de Nurse se une directamente con el tejido óseo circundante después de ser implantado en defectos óseos experimentales contenidos en metáfisis de tibias de conejo NZ.
7. El material se comporta como una estructura conductora facilitando la colonización centrípeta del mismo por el tejido óseo neoformado, y simultáneamente es progresivamente reabsorbido o degradado y sustituido por tejido óseo neoformado.
8. El mecanismo de unión ósea al implante es el resultado de la disolución y transformación del implante Fase A de Nurse, que provoca la formación de una nueva capa de Ca-P en la interfase del implante, y gran parte del material implantado se transforma en una fase similar al hueso desde un punto de vista morfológico y estructural.
9. En definitiva, el material Fase A de Nurse constituye un biomaterial biocompatible con propiedades osteoconductoras, osteoinductoras y biodegradable, alcanzando las propiedades o características exigidas a los materiales destinados a la regeneración del tejido óseo, bien sea como materiales de relleno o como sustratos-scaffolds para ingeniería tisular.

11. BIBLIOGRAFÍA

1. Navarro M, Michiardi A, Castano O, Planell J. Biomaterials in orthopaedics. Journal of the Royal Society Interface. 2008;5(27):1137-58.
2. Jones JR, Lee PD, Hench LL. Hierarchical porous materials for tissue engineering. Philosophical Transactions of the Royal Society of London A: Mathematical, Physical and Engineering Sciences. 2006;364(1838):263-81.
3. Agarwal R, García AJ. Biomaterial strategies for engineering implants for enhanced osseointegration and bone repair. Advanced drug delivery reviews. 2015;94:53-62.
4. Goldberg VM. Natural history of autografts and allografts. Bone implant grafting: Springer; 1992. p. 9-12.
5. Denry I, Kuhn LT. Design and characterization of calcium phosphate ceramic scaffolds for bone tissue engineering. Dental Materials. 2016;32(1):43-53.
6. Henkel J, Woodruff MA, Epari DR, Steck R, Glatt V, Dickinson IC, et al. Bone regeneration based on tissue engineering conceptions—a 21st century perspective. Bone research. 2013;1(3):216.
7. Açil Y, Terheyden H, Dunsche A, Fleiner B, Jepsen S. Three-dimensional cultivation of human osteoblast-like cells on highly porous natural bone mineral. Journal of Biomedical Materials Research Part A. 2000;51(4):703-10.
8. Buckwalter J, Glimcher M, Cooper R, Recker R. Bone biology. I: Structure, blood supply, cells, matrix, and mineralization. Instructional course lectures. 1996;45:371.
9. Boskey A, Posner A. Bone structure, composition, and mineralization. The Orthopedic clinics of North America. 1984;15(4):597-612.
10. Planeta Saber www.espasa.planetasaber.com: Editorial Planeta S.A.; 2003.
11. Glimcher MJ. The nature of the mineral component of bone and the mechanism of calcification. Instructional course lectures. 1987;36:49-69.
12. Ecarot-Charrier B, Glorieux FH, Van Der Rest M, Pereira G. Osteoblasts isolated from mouse calvaria initiate matrix mineralization in culture. The Journal of Cell Biology. 1983;96(3):639-43.
13. Blair HC, Teitelbaum SL, Ghiselli R, Gluck S. Osteoclastic bone resorption by a polarized vacuolar proton pump. Science. 1989;245(4920):855-8.
14. Curso de Fisiología. Sistema ósea: estructura y función www.iqb.es/cbasicas/fisio/cap06/cap6_3.htm#osteoclastos.
15. http://www.writeopinions.com/bone-remodeling: writeopinions.com; 2011.
16. Ritchie RO, Buehler MJ, Hansma P. Plasticity and toughness in bone. 2009.
17. Laurencin CT, Ambrosio A, Borden M, Cooper Jr J. Tissue engineering: orthopedic applications. Annual review of biomedical engineering. 1999;1(1):19-46.
18. Giannoudis PV, Dinopoulos H, Tsiridis E. Bone substitutes: an update. Injury. 2005;36(3):S20-S7.
19. Cornell CN. Osteoconductive materials and their role as substitutes for autogenous bone grafts. Orthopedic Clinics. 1999;30(4):591-8.
20. Kumar G, Narayan B. Morbidity at bone graft donor sites. Classic Papers in Orthopaedics: Springer; 2014. p. 503-5.
21. Greenwald AS, Boden SD, Goldberg VM, Khan Y, Laurencin CT, Rosier RN. Bone-graft substitutes: facts, fictions, and applications. JBJS. 2001;83(2_suppl_2):S98-103.

22. Navarro M, Michiardi A, Castano O, Planell J. Biomaterials in orthopaedics. JR Soc Interface 2008; 5: 1137-58. 2008.
23. El-Ghannam A. Bone reconstruction: from bioceramics to tissue engineering. Expert review of medical devices. 2005;2(1):87-101.
24. Hench LL, Polak JM. Third-generation biomedical materials. Science. 2002;295(5557):1014-7.
25. Agrawal C, Ray RB. Biodegradable polymeric scaffolds for musculoskeletal tissue engineering. Journal of Biomedical Materials Research Part A. 2001;55(2):141-50.
26. Williams DF. On the nature of biomaterials. Biomaterials. 2009;30(30):5897-909.
27. Finkemeier CG. Bone-grafting and bone-graft substitutes. J Bone Joint Surg Am. 2002;84(3):454-64.
28. Hutmacher DW, Schantz JT, Lam CXF, Tan KC, Lim TC. State of the art and future directions of scaffold-based bone engineering from a biomaterials perspective. Journal of tissue engineering and regenerative medicine. 2007;1(4):245-60.
29. Aubin JE. Bone stem cells. Journal of Cellular Biochemistry. 1998;72(S30–31):73-82.
30. Hench LL. An introduction to bioceramics: World Scientific Publishing Co Inc; 2013.
31. Verfaillie CM. Adult stem cells: assessing the case for pluripotency. Trends in cell biology. 2002;12(11):502-8.
32. Bruder SP, Jaiswal N, Haynesworth SE. Growth kinetics, self-renewal, and the osteogenic potential of purified human mesenchymal stem cells during extensive subcultivation and following cryopreservation. Journal of cellular biochemistry. 1997;64(2):278-94.
33. Bianco P, Robey PG, Simmons PJ. Mesenchymal stem cells: revisiting history, concepts, and assays. Cell stem cell. 2008;2(4):313-9.
34. Dominici M, Le Blanc K, Mueller I, Slaper-Cortenbach I, Marini F, Krause D, et al. Minimal criteria for defining multipotent mesenchymal stromal cells. The International Society for Cellular Therapy position statement. Cytotherapy. 2006;8(4):315-7.
35. Enam S, Jin S. Substrates for clinical applicability of stem cells. World journal of stem cells. 2015;7(2):243.
36. Kon E, Muraglia A, Corsi A, Bianco P, Marcacci M, Martin I, et al. Autologous bone marrow stromal cells loaded onto porous hydroxyapatite ceramic accelerate bone repair in critical-size defects of sheep long bones. Journal of biomedical materials research. 2000;49(3):328-37.
37. Albee FH. Studies in bone growth: triple calcium phosphate as a stimulus to osteogenesis. Annals of surgery. 1920;71(1):32.
38. Brauer DS. Bioactive glasses—structure and properties. Angewandte Chemie International Edition. 2015;54(14):4160-81.
39. Kaur G, Pandey OP, Singh K, Homa D, Scott B, Pickrell G. A review of bioactive glasses: their structure, properties, fabrication and apatite formation. Journal of Biomedical Materials Research Part A. 2014;102(1):254-74.

40. Suchanek W, Yoshimura M. Processing and properties of hydroxyapatite-based biomaterials for use as hard tissue replacement implants. Journal of Materials Research. 1998;13(1):94-117.
41. Bosetti M, Cannas M. The effect of bioactive glasses on bone marrow stromal cells differentiation. Biomaterials. 2005;26(18):3873-9.
42. Hsu Y, Turner I, Miles A. Mechanical characterization of dense calcium phosphate bioceramics with interconnected porosity. Journal of Materials Science: Materials in Medicine. 2007;18(12):2319-29.
43. Hutmacher D, Hürzeler MB, Schliephake H. A review of material properties of biodegradable and bioresorbable polymers and devices for GTR and GBR applications. International Journal of Oral & Maxillofacial Implants. 1996;11(5).
44. Hutmacher DW. Scaffolds in tissue engineering bone and cartilage. Biomaterials. 2000;21(24):2529-43.
45. Hing K, Annaz B, Saeed S, Revell P, Buckland T. Microporosity enhances bioactivity of synthetic bone graft substitutes. Journal of Materials Science: Materials in Medicine. 2005;16(5):467-75.
46. Karageorgiou V, Kaplan D. Porosity of 3D biomaterial scaffolds and osteogenesis. Biomaterials. 2005;26(27):5474-91.
47. Sanzana ES, Navarro M, Ginebra MP, Planell JA, Ojeda AC, Montecinos HA. Role of porosity and pore architecture in the in vivo bone regeneration capacity of biodegradable glass scaffolds. Journal of Biomedical Materials Research Part A. 2014;102(6):1767-73.
48. Merten HA, Wiltfang J, Grohmann U, Hoenig JF. Intraindividual comparative animal study of α-and β-tricalcium phosphate degradation in conjunction with simultaneous insertion of dental implants. Journal of Craniofacial Surgery. 2001;12(1):59-68.
49. Allabouch A, Colat-Parros J, Salmon R, Naim S, Meunier J. Biocompatibility of some materials used in dental implantology: histological study. Colloids and Surfaces B: Biointerfaces. 1993;1(5):323-9.
50. Aybar B, Bilir A, Akçakaya H, Ceyhan T. Effects of tricalcium phosphate bone graft materials on primary cultures of osteoblast cells in vitro. Clinical oral implants research. 2004;15(1):119-25.
51. Liu G, Zhao L, Cui L, Liu W, Cao Y. Tissue-engineered bone formation using human bone marrow stromal cells and novel β-tricalcium phosphate. Biomedical Materials. 2007;2(2):78.
52. Payer M, Lohberger B, Stadelmeyer E, Bartmann C, Windhager R, Jakse N. Behaviour of multipotent maxillary bone-derived cells on β-tricalcium phosphate and highly porous bovine bone mineral. Clinical oral implants research. 2010;21(7):699-708.
53. Yefang Z, Hutmacher D, Varawan S-L, Meng LT. Comparison of human alveolar osteoblasts cultured on polymer-ceramic composite scaffolds and tissue culture plates. International journal of oral and maxillofacial surgery. 2007;36(2):137-45.
54. Puppi D, Chiellini F, Piras A, Chiellini E. Polymeric materials for bone and cartilage repair. Progress in Polymer Science. 2010;35(4):403-40.

55. Hild N, Schneider OD, Mohn D, Luechinger NA, Koehler FM, Hofmann S, et al. Two-layer membranes of calcium phosphate/collagen/PLGA nanofibres: in vitro biomineralisation and osteogenic differentiation of human mesenchymal stem cells. Nanoscale. 2011;3(2):401-9.
56. Sánchez-Salcedo S, Arcos D, Vallet-Regí M, editors. Upgrading calcium phosphate scaffolds for tissue engineering applications. Key Engineering Materials; 2008: Trans Tech Publ.
57. Hoppe A, Güldal NS, Boccaccini AR. A review of the biological response to ionic dissolution products from bioactive glasses and glass-ceramics. Biomaterials. 2011;32(11):2757-74.
58. Porter AE, Patel N, Skepper JN, Best SM, Bonfield W. Effect of sintered silicate-substituted hydroxyapatite on remodelling processes at the bone–implant interface. Biomaterials. 2004;25(16):3303-14.
59. Carlisle EM. Silicon: a possible factor in bone calcification. Science. 1970;167(3916):279-80.
60. Carlisle EM. Silicon: a requirement in bone formation independent of vitamin D 1. Calcified tissue international. 1981;33(1):27-34.
61. Schwarz K, Milne DB. Growth-promoting effects of silicon in rats. Nature. 1972;239(5371):333-4.
62. Valerio P, Pereira MM, Goes AM, Leite MF. The effect of ionic products from bioactive glass dissolution on osteoblast proliferation and collagen production. Biomaterials. 2004;25(15):2941-8.
63. Shie M-Y, Ding S-J, Chang H-C. The role of silicon in osteoblast-like cell proliferation and apoptosis. Acta Biomaterialia. 2011;7(6):2604-14.
64. Liu X, Xie Y, Ding C, Chu PK. Early apatite deposition and osteoblast growth on plasma-sprayed dicalcium silicate coating. Journal of Biomedical Materials Research Part A. 2005;74(3):356-65.
65. Liu X, Morra M, Carpi A, Li B. Bioactive calcium silicate ceramics and coatings. Biomedicine & Pharmacotherapy. 2008;62(8):526-9.
66. Bandyopadhyay A, Bernard S, Xue W, Bose S. Calcium Phosphate-Based Resorbable Ceramics: Influence of MgO, ZnO, and SiO2 Dopants. Journal of the American Ceramic Society. 2006;89(9):2675-88.
67. Dorozhkin SV. In vitro mineralization of silicon containing calcium phosphate bioceramics. Journal of the American Ceramic Society. 2007;90(1):244-9.
68. Serena S, Caballero A, De Aza P, Sainz M. New evaluation of the in vitro response of silicocarnotite monophasic material. Ceramics International. 2015;41(8):9411-9.
69. Frank H, Bredig M, Kanert E. Untersuchungen Über Kalk-Alkali-Phosphate. II. Über Calcium-Kalium-Phosphate. Zeitschrift für anorganische und allgemeine Chemie. 1938;237(1):49-78.
70. Fix W, Heymann H, Heinke R. Subsolidus Relations in the System 2CaO· SiO2-3CaO· P2O5. Journal of the American Ceramic Society. 1969;52(6):346-7.
71. Rubio V, la Casa-Lillo MA, Aza S, Aza PN. The System Ca3 (PO4) 2–Ca2SiO4: The Sub-System Ca2SiO4–7CaOP2O52SiO2. Journal of the American Ceramic Society. 2011;94(12):4459-62.

72. Martinez I, Velasquez P, De Aza P. Synthesis and stability of α-tricalcium phosphate doped with dicalcium silicate in the system Ca 3 (PO 4) 2–Ca 2 SiO 4. Materials Characterization. 2010;61(7):761-7.
73. Ros-Tárraga P, Mazón P, Meseguer-Olmo L, De Aza PN. Revising the Subsystem Nurse's A-Phase-Silicocarnotite within the System Ca3 (PO4) 2–Ca2SiO4. Materials. 2016;9(5):322.
74. Lugo GJ, Mazón P, Baudin C, De Aza PN. Nurse' s A-Phase: Synthesis and Characterization in the Binary System Ca2SiO4–Ca3 (PO4) 2. Journal of the American Ceramic Society. 2015;98(10):3042-6.
75. Lugo GJ, Mazón P, Piedad N. Material processing of a new calcium silicophosphate ceramic. Ceramics International. 2016;42(1):673-80.
76. Kokubo T, Takadama H. How useful is SBF in predicting in vivo bone bioactivity? Biomaterials. 2006;27(15):2907-15.
77. Gibson I, Best S, Bonfield W. Chemical characterization of silicon-substituted hydroxyapatite. Journal of Biomedical Materials Research Part A. 1999;44(4):422-8.
78. Gou Z, Chang J. Synthesis and in vitro bioactivity of dicalcium silicate powders. Journal of the European Ceramic Society. 2004;24(1):93-9.
79. International Organization for Standardization (ISO 10993-5): Tests for cytotoxicity: in vitro methods 1992
80. Cheng S-L, Yang JW, Rifas L, Zhang S-F, Avioli LV. Differentiation of human bone marrow osteogenic stromal cells in vitro: induction of the osteoblast phenotype by dexamethasone. Endocrinology. 1994;134(1):277-86.
81. Conget PA, Minguell JJ. Phenotypical and functional properties of human bone marrow mesenchymal progenitor cells. Journal of cellular physiology. 1999;181(1):67-73.
82. Mafi P, Hindocha S, Mafi R, Griffin M, Khan W. Adult mesenchymal stem cells and cell surface characterization—a systematic review of the literature. Open Orthop. J. 5: 253–260. 2011.
83. Setzer B, Bächle M, Metzger MC, Kohal RJ. The gene-expression and phenotypic response of hFOB 1.19 osteoblasts to surface-modified titanium and zirconia. Biomaterials. 2009;30(6):979-90.
84. Harada S-i, Rodan GA. Control of osteoblast function and regulation of bone mass. Nature. 2003;423(6937):349-55.
85. Golub EE, Boesze-Battaglia K. The role of alkaline phosphatase in mineralization. Current Opinion in Orthopaedics. 2007;18(5):444-8.
86. Orimo H. The mechanism of mineralization and the role of alkaline phosphatase in health and disease. Journal of Nippon Medical School. 2010;77(1):4-12.
87. Dong M, Jiao G, Liu H, Wu W, Li S, Wang Q, et al. Biological silicon stimulates collagen type 1 and osteocalcin synthesis in human osteoblast-like cells through the BMP-2/Smad/RUNX2 signaling pathway. Biological trace element research. 2016:1-10.
88. Bohner M. Silicon-substituted calcium phosphates–a critical view. Biomaterials. 2009;30(32):6403-6.
89. Velasquez P, Luklinska ZB, Meseguer-Olmo L, Mate-Sanchez de Val JE, Delgado-Ruiz RA, Calvo-Guirado JL, et al. αTCP ceramic doped with dicalcium silicate for

bone regeneration applications prepared by powder metallurgy method: in vitro and in vivo studies. Journal of Biomedical Materials Research Part A. 2013;101(7):1943-54.
90. Lazáry Á, Balla B, Kósa JP, Bácsi K, Nagy Z, Takács I, et al. Effect of gypsum on proliferation and differentiation of MC3T3-E1 mouse osteoblastic cells. Biomaterials. 2007;28(3):393-9.

12. ANEXOS

12.1. PRODUCCIÓN CIENTÍFICA RELACIONADA CON LA TESIS

12.1.1. Contribución a congresos de carácter Nacional.

- 8ª Sesión del Ciclo Investigadores de la Región de Murcia, Octubre 2017, Murcia, España. **Comunicación oral** "Respuesta biológica *in vitro* e *in vivo* de materiales cerámicos de silicofosfato cálcico". Rubén Rabadán Ros.

- II Jornadas Científicas del IMIB-Arrixaca, Noviembre 2017, Murcia, España. **Comunicación mediante póster** "Efecto de los elementos iónicos liberados por una nueva cerámica bifásica formada por wollastonita y fosfato tricálcico sobre una población de células madre mesenquimales adultas". Patricia Ros-Tarraga, Patricia Mazon, Ruben Rabadan-Ros, Angel Murciano, Piedad N de Aza, Luis Meseguer-Olmo.

- III Jornadas de Investigación y Doctorado: Reconocimiento de los Doctores en el Mercado Laboral de la EIDUCAM, Junio 2017, Murcia, España. **Comunicación oral *Mi tesis en 3 minutos*** "Nuevos materiales cerámicos reabsorbibles con porosidad controlada como sustratos para ingeniería de tejidos con amplias perspectivas de uso en medicina". Ruben Rabadan-Ros.

- III Jornadas de Investigación y Doctorado: Reconocimiento de los Doctores en el Mercado Laboral de la EIDUCAM, Junio 2017, Murcia, España. **Comunicación oral** "Graphene based scaffolds on stem cells commitment". Ruben Rabadan-Ros.

- III Jornadas de Investigación y Doctorado: Reconocimiento de los Doctores en el Mercado Laboral de la EIDUCAM, Junio 2017, Murcia, España. **Comunicación mediante póster** "Nurse´s A-phase material enhance differentiation of human bone marrow-derived stromal mesenchymal stem cells". Ruben Rabadan-Ros.

- 11 Congreso Nacional INVESCOT – Asociación Española de Investigación en Cirugía Ortopédica y Traumatológica, Febrero 2016, Madrid, España.

Comunicación oral "Estudio in vivo del comportamiento de una matriz tridimensional de silicofosfato cálcico". Patricia Ros-Tarraga, Ruben Rabadan-Ros, Miguel A. Rodríguez, Patricia Mazón, Piedad N. De Aza, Luis Meseguer-Olmo.

- II Jornadas de Investigación y Doctorado: Doctorado Industrial de la EIDUCAM, Junio 2016, Murcia, España. **Comunicación oral** "Behaviour of a primary culture of adult human mesenchymal stem cells (*ah*MSCs) in the presence of a novel Nurse´s (7CaO.P2O5.2SiO2) ceramic". Ruben Rabadan-Ros.

- 32 Jornadas Nacionales de Enfermería en Cirugía Ortopédica y Traumatología, Mayo 2016, Murcia, España. **Comunicación oral** "Medicina Regenerativa en la especialidad de C.O.T.". Ruben Rabadan-Ros, Patricia Ros-Tarraga.

12.1.2. Contribución a congresos de carácter Internacional.

- X Congreso Internacional Enfermedades Raras, Noviembre 2017, Murcia, España. **Comunicación oral** "Biomateriales para regeneración ósea y Bioimpresión 3D". Jose Acosta, Ruben Rabadan-Ros.

- 2nd Annual Conference and Expo on Biomaterials, Marzo 2017, Madrid, España. **Comunicación mediante E-póster** "Nurse´s A-phase material enhance adhesion, growth and differentiation of human bone marrow-derived stromal mesenchymal stem cells". Ruben Rabadan-Ros, Salvador Aznar-Cervantes, Patricia Mazón, Patricia Ros-Tarraga, Piedad N. De Aza, Luis Meseguer-Olmo.

- 18th ESRR Symposium, 2016, Salzburgo, Austria. **Comunicación mediante póster** "In vivo biodistribution of adult human mesenchymal stem cells (*ah*MSCs) labeled with 99MTC-HMPAO administered via intravenous and intra-articular in an animal model. Preliminary results". Alejandra Abella, Teodomiro Fuente, Antonio Jesús Montellano, Teresa Martínez, Ruben Rabadan-Ros y Luis Meseguer-Olmo.

- 5th World Congress on Materials Science and Engineering, Junio 2016, Alicante, España. **E- Póster** "Effect of a new biomaterials in the system

tricalcium phosphate-dicalcium silicate on osteogenic markers expression in human mesenquimal stem cells". Ruben Rabadan-Ros, Patricia Ros-Tarraga, Piedad N de Aza, Francesca Cragnolini, Salvador Aznar, Abel Lozano, Ana Pagan, JL Cenis, Luis Meseguer-Olmo.

- 5th World Congress on Materials Science and Engineering, Junio 2016, Alicante, España. **E- Póster "**Influence of ionic disolution of si-ca-p biphasic ceramics on multipotent stem cells proliferation *and in vitro* mineralization". Patricia Ros-Tárraga, Ruben Rabadán-Ros, Jose Acosta, Piedad N. de Aza, Francesca Cragnolini, Salvador Aznar, Abel Lozano, Ana Pagan, J.L. Cenis, Luis Meseguer-Olmo.

- 3rd International Conference and Expo on Ceramics and Composite Materials, Junio 2016, Madrid, España. **Comunicación mediante póster** "In vitro behavior of Nurse´s A phase$_{ss}$, a new calcium silicophosphate ceramic for bone tissue engineering". Ruben Rabadan-Ros, Patricia Mazón, S Serena,MªA Sainz, Luis Meseguer-Olmo, Piedad N. De Aza.

12.1.3. Registros en propiedad Intelectual y Patentes.

- **Registro Propiedad Intelectual** "Un nuevo biomaterial compuesto (Sulfato cálcico hemihidratado-Silicato dicálcico-fosfato tricálcico) con capacidad optimizada para absorción de proteínas presentes en el suero", 01 de Julio de 2015. Luis Meseguer-Olmo, Ruben Rabadan-Ros, Abel Lozano-Perez, Salvador Aznar-Cervantes, Ana Pagan-Bernabeu, J.L. Cenis-Anadon, Piedad N. de Aza, J.Francisco Abellan-Guillen.

- Presentación solicitud de **Patente** en Oficina Española de Patentes y Marcas, Ministerio de Industria, Energía y Turismo "Procedimiento de obtención de un material para regeneración ósea y material así obtenido", 24 Julio de 2017.

12.1.5. Otras Publicaciones.

- Ros-Tárraga, P., Rabadan-Ros, R., Murciano, A., Meseguer-Olmo, L., & De Aza, P. N. (2016). Assessment of Effects of Si-Ca-P Biphasic Ceramic

the Osteogenic Differentiation of a Population of Multipotent Adult Human Stem Cells. *Materials*, *9*(12), 969.